Title
The Development of Short and Long Term Continuous and Real Time In Situ Medical Pressure Sensors

Author
Tan, Robert

Publication Date
2012

Peer reviewed|Thesis/dissertation

UNIVERSITY OF CALIFORNIA

Los Angeles

The Development of Short and Long Term Continuous and Real Time *In Situ* Medical Pressure Sensors

A dissertation submitted in partial satisfaction of the requirements for the degree Doctor of Philosophy in Bioengineering

by

Robert Nien-Kuo Tan

2012

ABSTRACT OF THE DISSERTATION

The Development of Short and Long Term
Continuous and Real Time *In Situ* Medical Pressure
Sensors

by

Robert Nien-Kuo Tan

Doctor of Philosophy in Bioengineering

University of California, Los Angeles, 2012

Professor Jacob Schmidt, Chair

There has been a push to modernize the technology used in patient monitoring. One area that is being investigated is the use of *in situ* sensors for real time, continuous vital signs monitoring, particularly to measure pressure. We developed two sensors fulfilling different roles. One is fully implantable and wireless for long term urological pressure monitoring using conventional MEMS technology. This sensor required the use of a battery-powered wireless transmitter. The second sensor utilizes an entirely new method of pressure sensing designed to be easily scaled down in size while being extremely cost effective. By using an electrolyte solution-filled elastic tube, the sensor does not require further packaging; also the materials used are easily obtainable commercially, so no custom components are required even when downsizing. Although initially designed and tested as a wired sensor, the new catheter sensor was designed to be integrated with

wireless capability later—to create a truly minimally invasive long term pressure monitor. Both pressure sensing systems were developed by fabricating a pressure sensitive catheter lead, designing the electronics required to amplify and filter the sensor signal, programming the software client that received, stored, graphed, and interpreted the data. Furthermore, both sensors were subjected to extensive *in vitro* testing to characterize sensor performance and lifetime, as well as simulate an *in vivo* environment. Both sensors required the investigation of robust packaging techniques to ensure functionality and survivability while implanted. Last, both sensors demonstrated their potential use as a pressure monitor in animal studies: within the bladder for the wireless implantable sensor and as an intravascular sensor for the new conductometric design.

The dissertation of Robert Nien-Kuo Tan is approved.

Dino DiCarlo

Wentai Liu

Peyman Benharash

Jacob Schmidt, Committee Chair

University of California, Los Angeles

2012

Table of Contents

List of Figures

List of Tables

Acknowledgements

I have been waiting to write this piece for a long time, and this is the only time that I can write with my own voice. Since there won't be an orchestra to play me off, it's going to take a while. There are a lot of people throughout my graduate school career that have influenced my time here, and I'd like to take this opportunity to give them props. First off, I'd like to thank my family. In particular, my parents have supported me throughout my time here and through thick and thin, have stood by me. In the worst of times, they helped me stay strong and focused even when I wanted to quit. Mom and dad, I couldn't have done it without you. I'd like to thank my brother, Roger, for entertaining me every day with our inane banter. We talked about everything: from Cal football, to how to "hoop it up" for crabs, to our gaming adventures. By the way, Roger, you suck at flying helicopters in Saints Row: the Third.

I'd like to thank the people who directly helped me on my project. CK Lin started this project and provided a lot of expertise and wisdom in helping me complete the first part of my thesis. Although he had to leave early in my career here, he took time out of his day to make sure I was on track. The early collaborators: Tim Canan, David Jea, Foad Dabiri, and Tammy Massey were integral in getting all the components working, especially since I didn't know how the hell they worked. The guys at Medtronic, particularly Ed Chernoff and Robert Schaefer, provided me a lot of insight in practical ways to solve manufacturing problems. They taught me a lot of skills that aren't covered in textbooks or academic journals. Robert Schaefer, also, was always a cool guy to talk to, and I always enjoyed our discussions about football. Tim McClure was a urology resident that was assigned to my project. Usually, collaborators are usually a crap shoot in terms of chemistry, but Tim was always a guy that I enjoyed hanging out with. I could always rely on him for sophomoric humor, as well as free medical advice. One time, we had to sign some forms

for the Office of Intellectual Property, so in fitting fashion, we did it at Ohara's, nee Maloney's, over a glass of beer and the waitress as the official witness. Good times. Mike Lee, a MS student in my class, while a good friend, taught me how to wirebond during a time that I was completely lost and didn't know how to do anything. As someone who spent a lot of time in industry, I could always rely on his advice on assembling ICs.

PJ Rezzai, my undergraduate was always receptive when talking to him and he hooked me up with a doctor for my *in vivo* studies. Peyman Benharash, a thoracic surgeon, was that doctor and he was always accommodating in helping me test my sensors both *in vitro* and *in vivo*. He also provided a lot of advice and medical input. Although we ultimately did not finish up our polyaniline project, Julio D'Arcy was a great collaborator and friend. We bounced our crazy ideas off each other in between serious discussions of food, 3D rendered art, beer, and lots of joking around. Finally, my advisor, Jacob Schmidt, was obviously instrumental in my project. I'm grateful for kicking my ass when I needed it and helping me realize my inner strength and fortitude. It's kind of like those old Army commercials: "be all that you can be." Also, "an Army of one" is sort of fitting since I was working solo most of the time. I truly believe that this experience, by forcing me to work alone and solve problems by myself, I ended up a stronger and more skilled person. My other PI, Dr. Pete Schulam, had an infectious optimism and would always pump me up regardless of how many failures I've suffered. Also, his colorful language was always amusing.

I'd like to individually acknowledge my labmates. The people in my lab were the coolest guys to work with, and we were a pretty close knit group. Taejoon Jeon, although I didn't work with him directly, was an avuncular figure in the lab. He'd take me to his eating holes that

nobody else knew about and was always a great guy to share a drink with. I'm grateful for the times he'd randomly call me up to see how I was going all the way from Korea although I'm pretty sure he was drunk for most of those calls. Jason Poulos joined the department the same time I did, so he was always my closest buddy in the lab. He was pretty much my drinking buddy and we shared many adventures together that I'm sure would bite me in the ass if I ever decided to run for president. Robert Purnell was a fellow graduate of UC Berkeley, so I could always talk to him about Cal football and other Cal-related things. I remember going to football viewing parties with Robert at O'brien's. Hyunwoo Bang, a postdoc, always took time to help me learn Rhino and how to create awesome CGI for posters and papers. I could talk to him about what the hottest games were. Kunal Mehta…you went to Stanfurd. Enough said. I do find it funny, though, that he associates himself more with the furd than UCLA. It's supposed to be the opposite!

Shiva Portonovo, my sidekick for the majority of the latter half of my career here, was always dependable when discussing everything during our many lunches and dinners together. I will always remember all the jokes we made about how ghetto we were when clearly, we weren't. I'm still amazed at his encyclopedia-like knowledge about pop culture in the 80s and early 90s. It kind of drops off after that. I thoroughly enjoyed talking to Ahmad El-Arabi, the super undergrad, about really random things: from terrible fashion choices of random people to cooking techniques. He was always willing to participate in my adventures. If you were able to combine Ahmad with Shiva, you'd get Carl Salazar. He was a drinking buddy, a fishing partner, and a shutdown defensive back. Actually, most of his pass defense ability was due to pass interference. Bin Lu, the fellow Asian in the lab, was always useful for when I wanted to talk trash about people in Chinese. Shiv Acharyia was a great sport whenever I would diss him. It

was all in good fun though. Tanuj Thapliyal helped me a lot in learning Labview. He was always patient with me in explaining everything and helped me on developing a program to receive and interpret data from a Bluetooth transmitter. Abha Jeukar was always reliable to share a laugh and many memories, including da Baus. Peter Du was a fun guy to talk to about the UCLA football team and their injuries, as well as gaming and other random things. I loved discussing fishing with Takashi Nisisako, who was just learning how to fish, but was always willing to learn. Finally, there was the army of undergrads: Bryan Myint, Gayane, Alex Portman, Quincy Chen, and others that would participate in our lab antics.

Additionally, I'd like to thank the staff of the Department of Bioengineering: Stacy, Lee, Larry, Apryll, and Laurie for their assistance in graduate school. Larry was especially helpful in giving advice in dealing with the bureaucracy at UCLA and for friendly discussions. Laurie was always down for a friendly game of catch in the hallways or for providing crackers for the squirrels that hung outside my window at Boelter Hall. Apryll was always up for discussions about random things. As was fellow Cal alum Professor Dan Kamei—he was always willing to talk about the state of affairs within the department, as well as sports and gaming.

Next, I'd like to thank all those that made my graduate experience what it was despite not being associated with my lab or my project. Eric Schopf, Jared Frey, Sean Anderson, Alex Shen, and the rest of our men's intramural football team "Death or Glory," "Scissor me Timbers," or "Touch of Gray" were integral in helping me preserve my desire for greatness on the gridiron. I perfected my craft as a cornerback by playing on this team and I still look back fondly at the interceptions and perfect play calls. Of course, when men's football got to be too intense, my season on a coed team, which included Chen, Tiffany, Pertz, Cynthia, and Coral provided a lax

atmosphere while shutting down chicks without much effort. While the DiCarlo lab was generally chill to hang out and drink a beer with, in particular, Danny Gossett and Henry Tse were my compadres in arms when it came to fishing. That is especially important because they could tolerate my endless fishing discussions even when they didn't know what I was talking about. Tight lines guys.

My buddies outside of UCLA kept me entertained throughout graduate school. Just talking to them on a consistent basis kept me grounded and sane. Gary Chung, my floor mate my freshman year in Bowles Hall and classmate, and I had many long conversations and debates over Gchat about live, religion, the terribleness of Apple, as well as random trips to watch football or to Mexico. He'd bravely go boat fishing with me despite being sea sick, and yet somehow manages to outfish me. Andrew Petersen, who went to high school and college with me, was my main source for football discussion. We shared many good moments like Cal versus UCLA and Oregon in 2006 and many bad moments like Tennessee and USC. My other football buddy was Frank Liu, and we watched many Cal games together. One of the best games I've ever witnessed was the Cal and Tennessee game in 2007, which I watched with Frank. Frank was always down to wet a line, but he'd prefer to catch baitfish than go for the big boys that swam. I met Frank through Francis Yoshimoto, whose neurosis provided a welcome distraction from my own drudgery. Also, despite having worked there for one summer, my Navy friends, Kyle Woolrich and Amit Patel, have kept in touch years after we left SPAWAR. My conversations with Tron always made me laugh even in the worst times of grad school. Lastly, there's Jeff Tedford and the Cal football team. The athleticism and highlights of players like Marshawn Lynch, DeSean Jackson, Justin Forsett, Lavelle Hawkins, Craig Stevens, Jahvid Best, Shane

Vereen, Keenan Allen, and others provided something to look forward to during some of the darkest times.

Finally, my roommates over the years, in particular, Linus Lau and Jon Savage, by the virtue of not being in the same field of study, helped expand my horizons. They let me meet their lady friends and were always willing to shoot the shit over some beers. Lastly, Michelle, you're a terrible human being.

Now for some administrative rules that I have to complete…Chapters 2-4 are a version of "Development of a fully implantable wireless pressure monitoring system" authored by me, Timothy McClure MD, CK Lin, David Jea, Foad Dabiri, Tammara Massey, Majid Sarrafzadeh, Mani Srivastava, CD Montemagno, Peter Schulam MD, and Jacob Schmidt (PI) and published by Biomedical Microdevices, which has given permission to reprint the article. Chapters 6-9 will be published in two separate works: "Design and mathematical model of a novel pressure sensor" authored by me and Jacob Schmidt and "Implantable electrolyte conductance-based pressure sensing catheter" by me, Peyman Benharash, and Jacob Schmidt. The following work was mostly funded by the US Army's Telemedicine and Advanced Technology Research Center (TATRC).

VITA

2004	National Science Foundation Research Experience for Undergraduates fellow University of Central Florida, Orlando
2005	B. S., Bioengineering University of California, Berkeley
2006	M. S., Biomedical Engineering University of California, Los Angeles
2006	Naval Research Enterprise Intern Program Space and Naval Warfare Systems Center, San Diego
2008	Teaching Assistant Department of Bioengineering University of California, Los Angeles
2006-2011	Graduate Student Researcher Department of Bioengineering University of California, Los Angeles

PUBLICATIONS AND PRESENTATIONS

- Tan, R., Schmidt, J., Schulam, P., “Implantable sensors for continuous monitoring,” Women and Philanthropy, Center for Advanced Surgical and Interventional Technology (CASIT), UCLA, November 2006 (Poster).
- Lin, C.K., Jea, D., Dabiri, F., Massey, T., Tan, R., Sarrafzadeh, M., Srivastava, M.B., Schulam, P.G., Schmidt, J., Montemagno, C., "The Development of an In-vivo Active Pressure Monitoring System," 4th International Workshop on Wearable and Implantable Body Sensor Networks , March 2007.

- Tan, R., "Development of an implantable, wireless vital signs sensor suite," 16th Medicine Meets Virtual Reality Conference, Long Beach, CA, January 2008 (Oral).
- McClure, T., Tan, R., Breda, A., Lin, C.K., Schmidt, J., Schulam, P., "Development of a microelectromechanical system (MEMS) pressure sensor for intraperitoneal, bladder, and detrusor pressures," *Journal of Endourology,* 22, 11, 2008, p. 2583
- Tan, R., McClure, T., Schmidt, J., Schulam, P., "Development of an implantable, wireless, and continuous pressure monitoring system," Joint Symposium on Nano-Scale Research into Biosensors, Biomaterials, and Nanotoxicology, California NanoSystems Institute, UCLA, March 2008 (Poster).
- Tan, R., "Development of an implantable, wireless vital signs sensor suite," 9th Annual UC Bioengineering Symposium, Riverside, CA, June 2008 (Oral).
- Tan, R., "Minimally Invasive Implantable Wireless Vital Signs Sensor Platform," 17th Medicine Meets Virtual Reality Conference, Long Beach, CA, January 2009 (Oral).
- Dabiri, F., Massey, T., Noshadi, H., Hagopian, H., Lin, C.K., Tan, R., Schmidt, J., Sarrafzadeh, M., "A Telehealth Architecture for Networked Embedded Systems: A Case Study in *In Vivo* Health Monitoring," *IEEE Transactions on Information Technology in Biomedicine,* 13, 3, 2009, p. 351-359
- Tan, R., McClure, T., Lin, C.K., Jea, D., Dabiri, F., Massey, T., Sarrafzadeh, M., Srivastava, M., Montemagno, C.D., Schulam, P., Schmidt, J., "Development of a fully implantable wireless pressure monitoring system," *Biomedical Microdevices*, 11, 1, 2009, p. 259-264
- Tan, R., McClure, T., Schulam, P., Schmidt, J., "Minimally Invasive Implantable Wireless Vital Signs Sensor Platform," *Medicine Meets Virtual Reality 17*, 2009, p. 380-385
- Tan, R., Schulam, P., Schmidt, J., "Conductometric Catheter-Mounted Pressure Sensor", *Medicine Meets Virtual Reality 19,* 2012, p. 512-514
- Tan, R., "Conductometric Catheter-Mounted Pressure Sensor," 19th Medicine Meets Virtual Reality Conference, Newport Beach, CA February 2012 (Poster).

Chapter 1 Introduction

In the United States, an estimate of 44,000 to 98,000 patients die every year due to errors in diagnosis or treatment [1]. There are several reasons for this, such as human errors, lacking of diagnostic information. While there is little technology can do about human mistakes, avoiding misdiagnosis can be aided by technology that provides a wealth of information previously inaccessible to clinicians. Diagnosis typically occurs after a patient complains about symptoms. The physician, like a detective, must piece together clues based on the patient's qualitative descriptions and from quantitative data at his disposal. Unfortunately, in healthcare, clinicians cannot afford the luxury of extended time to obtain accurate and quick diagnoses as the patients' condition could worsen over time. Misdiagnosis is compounded when the patient cannot effectively communicate with the physician. Furthermore, certain parameters, like pain, are based completely on a subjective scale reported by the patient, and thus, there is no standard metric to compare with—making the metric unreliable.

To accurately understand a patient's physiology and pathology, it's clear enough that medical personnel must rely on quantitative data of vital signs to make correct diagnoses. Many conditions are underlying and go undetected before the patient seeks treatment, which complicate matters further. Sometimes patients have experienced severe episodic or transient events, such as a myocardial infarction or stroke; by the time correct treatment is given, irreparable damage has already occurred. This heightens the need for reliable physiological data. Unfortunately, vital signs are typically measured discretely, which only gives a snapshot in time, and trends in physiological data are difficult to detect and interpret. Although there are continuous sensors have already been used, like arterial lines, swan-ganz catheters,

electrocardiograms, and pulse oximeters, many of these patient monitors are tethered to the patient and impractical to use outside of the bedside in the hospital.

Continuous monitoring devices, the states of the art of each are discussed in further detail later, can be separated into two categories: short-term and long-term. Briefly, short-term sensors are designed to be used only in the hospital and are typically used in critical care units or in the emergency rooms. As mentioned before, to get a better picture of the patient's physiology at one moment, a variety of sensors need to be used, which tether the patient to the bedside. For hemodynamic monitoring, patients often need to be catheterized with a various catheters to monitor different cardiac parameters, such as arterial pressure, venous pressure, and cardiac output. The technological trend is to combine sensing modalities into one sensor; for example, cardiac output can be inferred by measuring arterial pressure, thus it eliminates the need for a separate pulmonary artery catheter [2]. However, the current arterial blood pressure monitors still rely on *ex vivo* measurements. Sensing artifacts relating to tube kinking, tube resonance, bubble formation, and body position may occur [3]. Moreover, the tubing and sensors need to be periodically flushed or perfused with heparin solution to prevent thrombogenesis. *In situ* sensors measure blood pressure directly within the blood stream; therefore, they are advantageous since they are not plagued by the same motion artifacts and can produce more accurate data. They are also as invasive as current arterial lines since they can utilize current catheter ports, which are already used for arterial lines. However, their high costs preclude them from being broadly used. This thesis addresses the concern by using novel sensing and fabrication techniques that are easily scalable to small size while keeping costs low.

Long-term patient monitoring is used when a physician needs to keep track of a patient's various physiological parameters over a period of time spanning months and even years. It would be impractical to keep the patient in the hospital for that long, so the patient is required to wear the monitor while being ambulatory at home. A physician may be interested in the progression of a previously diagnosed disease, the effectiveness of therapy, the use of an early warning system for crisis events in high risk patients, or an automated closed-loop disease management system. Also there have been studies, which show that physiological data measured in a hospital differs from the data collected in a normal ambulatory setting due to psychological or physical factors, such as being tethered to a patient monitor or artificial stimulation [4, 5]. In fact, the literature has extensively documented the effects of restraining an animal on its core temperature, heart rate, blood pressure, and hormone levels [6-8]. By monitoring physiology in ambulatory settings, the patient is in a relatively stress-free environment, yielding results more typical of that particular patient's physiology. However, the condition of being stress-free depends on the patient's monitor being less restrictive to patients' movements. The Holter monitor, a continuous, wearable, portable electrocardiogram, represents one of the first long-term patient monitors, but its bulkiness, hassle, short lifetime, lack of telemetry capability, and susceptibility to motion artifacts limit its use. Other systems that continuously monitor blood glucose levels, such as Medtronic's Guardian, have been developed and even integrated with insulin pumps to form a closed-loop diabetes management system. However, blood pressure is a parameter widely tracked in critical care situations, but it is not measured in typical home monitoring. Several companies have developed various wireless blood pressure monitors, the details of each of them are discussed later. Typically, they rely on radio frequency induction to power the sensor and transmit its data; therefore, unless the patient stands next to the patient monitor, continuous data

for a prolonged period of time is difficult to obtain. This thesis addresses this issue by developing an active powered pressure sensor capable of transmitting data every second.

This thesis addresses the development of two different pressure sensors. Chapter 2 to 4 focuses on a long-term urological pressure monitoring system, which consists of a catheter-mounted microfabricated pressure die connected to an internal battery and wireless transmitter. Chapter 5 to 9 covers a short term solution that focused only on the design, characterization, and

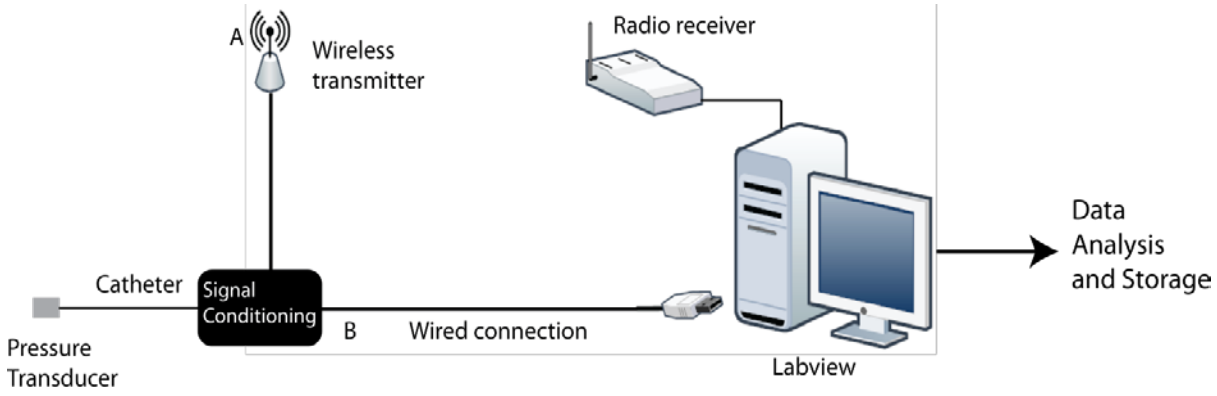

Figure 1.1. A block diagram of both a short-term and long-term continuous pressure monitoring system. The pressure transducer is mounted at the end of a catheter that is connected to a signal conditioning circuit that amplifies and filters the data. The sensors communicate with a LabVIEW station through A) wireless communication for the long-term sensor or B) a wired connection for the short-term sensor. The data is then analyzed and stored.

implementation of a novel arterial blood pressure sensitive catheter. Furthermore, the signal processing, data amplification, data analysis, and communication between the sensor and monitor are discussed (Figure 1.1). At the end, the thesis discusses improvements and future developments needed to integrate the sensor into a sensor network within a hospital or as a standalone home monitoring device.

Chapter 2 Fully Implantable Pressure Monitor

2.1 The Need for Wireless Pressure Monitoring

In the medical community, there has been significant interest in telemedicine and remote patient monitoring at home and in the hospital [9]. Current patient monitoring instrumentation and practices can be cumbersome and restrictive. For example, in the intensive care unit, blood pressure can be monitored continuously with an arterial line. This is a catheter that is placed in the artery, and an external transducer detects the pressure. The limitations of this are that the accuracy is highly variable, and the patient is often sedated to prevent injury from movement. On the other hand, in standard care, while completely non-invasive and burden-free to the patient, standard blood pressure measurements with a cuff are non-continuous point measurements typically taken every 2-12 hours. The development of critical vital signs between measurements could be missed. Currently, there is no device which provides clinicians with continuous monitoring of vital signs without being extremely invasive and/or cumbersome.

A device capable of continuous and real-time monitoring without significantly reducing the patient's comfort or restricting his/her movement would fill the gaps in performance and comfort between intensive and standard care. A simple and cost- effective solution is to use implantable microsystems utilizing wireless telemetry. Wireless telemetry frees the patient from being tethered to large hospital monitors and can participate in a hospital sensor network, which could increase monitoring efficiency by minimizing staff work load, increasing the amount of data obtained, and streamlining its storage and processing. Micromachined pressure sensors are readily available and have been explored for use in blood pressure measurement, either in

intravascular systems or implantable pressure cuffs [10-16]. Sensors are also being developed for sensing intraocular pressure, intracranial and spinal pressure, and orthopedic stresses [17-23]. In urology, a field in which the etiology of disease is often times secondary to abnormalities in pressure, there have been only a few pressure sensors developed for this purpose, but based on information available in the market place, none have been tested successfully *in vivo* [24, 25]. The diagnosis and management of urologic diseases could be benefitted from these sensors.

For the most part, wireless implantable pressure sensor development has been focused on devices powered by radio frequency (RF) induction, which enables indefinite implantation and operation without the need for subsequent surgeries to change batteries; besides, the total device volume is minimized, as the battery is typically the largest component. Several groups have developed and tested devices that detect dynamic blood pressure in the femoral artery or aorta of animal models [11, 13]. Two systems are commercially available: the Savacor HeartPod and CardioMEMS EndoSure for implantation in the left atrium and aortic aneurysm, respectively [10, 15, 26]. However, the transmission range is often limited to centimeters [11, 13], and the sensor can only transmit data when it is exposed to RF energy. This circumstance often limits the measurements to discrete points in time or tethers the patient to an antenna at all times for continuous measurements [15, 26].

Here a different approach is presented to monitor ambulatory pressures, which consists of a micromachined pressure die, amplifying electronics, microcontroller, wireless transmitter, and battery that is implanted into the body and communicates with a personal digital assistant (PDA) or computer. Because the RF energy involved does not need to power the device, the frequency can be chosen to maximize transmission range. Therefore, the PDA or computer can be located

relatively far away, and the patient is free to move around without fear of losing data. Monitoring can be done during normal activity levels of the patient as opposed to being bedridden and immobile as is currently required.

2.2 Ureteropelvic-junction Obstructions

The ureteropelvic junction connects the kidney to the ureter. Obstruction of the junction leads to abnormally and chronically high renal pressures, and if left untreated, renal deterioration and kidney failure can result. Ureteropelvic junction obstructions (UPJO) are not common in adults with an incidence rate of 3.8% [27] and more prevalent in children. UPJO is caused by kidney stones, blood clots, retroperitoneal fibrosis, congenital defects, or even pregnancy [28]. Typical diagnosis occurs when a patient complains of flank pain, vomiting, and fatigue. A typical blood analysis would show impaired kidney functionality, such as elevated urea and creatinine, hyponatremia, hyperchloremia, and metabolic acidosis. A clinician suspecting hydronephrosis or an accumulation of water in the kidney may order a pyelogram, a radiological imaging of the urinary tract with a perfusion of imaging contrast at a rate of 5-10 ml/min into the renal pelvis [29] to differentiate between obstructive and non-obstructive uropathy. However, pyelogram may not always diagnose UPJO [30], so a more comprehensive test, the Whitaker test, may be used.

The Whitaker test requires perfused fluid into the bladder over the course of 30 to 90 minutes. Pressure transducers connected to catheters, which are inserted into the rectum and urethra collect pressure data for later analysis. By directly measuring renal pressure, UPJO can be diagnosed [31]. However, variability in data can be produced by differences in patient positioning, transducer brands, and catheter placement [32-34].

There is clearly a need for continual monitoring at home for patients with chronic UPJO. However, an invasive and time-consuming procedure like the Whitaker test is impractical for this purpose. For continual monitoring, patients that may not be able to communicate effectively with their physicians complicate matters. In addition, the diagnosis and therapy of patients with UPJO still remains a mystery [35], and further research is needed in studying the exact pathophysiology of UPJO, as well as effective treatment techniques. The pressure sensor developed in this research can help directly tracking renal pressures long-term in a minimally invasive package. Any changes in pressure resulting from renal blood flow and urinary tract drainage can be detected, which would usher in a new paradigm in UPJO diagnosis. Lastly, multiple sensors can be used to map pressure changes in different locations, providing a more thorough picture of the disease.

Chapter 3 Fully Implantable Wireless Pressure Monitor Design

3.1 Catheter Fabrication, Packaging, and Characterization

The work described below was detailed in previously published works [36, 37]. The catheter lead houses the pressure sensor assembly and connects it to the sensor node. It consists of a piezoresistive pressure sensor (Silicon Microstructures 5108) measuring 0.65 mm x 0.65 mm affixed onto a ceramic printed circuit board (PCB) with UV epoxy (Masterbond UV10). The die was chosen for its size, sensing range, and precision with a sensitivity of 1.6 mV/psi/V. The strain gauges on the die are configured in a temperature-compensated Wheatstone bridge. As shown in Figure 3.1A, the chip was then wirebonded (West Bond 7402C) to contact pads on the substrate board. Four individually insulated platinum-iridium (Pt-Ir) wires threaded through a 7.5 French (2.5 mm) catheter were soldered to leads on the board connected to the contact pads. UV epoxy was applied over all contact and solder pads on the substrate board and chip and then cured for eight minutes to prevent any of the Pt-Ir wires or wirebonds from breaking contact. A gold cap with four wedge-shaped holes cut out of the side was affixed with UV epoxy onto the PCB over the pressure die to protect the chip. The four Pt-Ir wires are wound around a high-tensile insulating Dacron core and threaded through Tygon tubing. This assembly was threaded through silicone tubing prior to soldering.

The packaging is depicted in Figure 3.1B: 44.5 μm-thick cellophane film (3M) was wrapped around the substrate board and gold cap. The film was sealed with 5 minute epoxy (Devcon). Once cured, the tip of the catheter lead was compression-molded in medical-grade

polydimethylsiloxane (PDMS) silicone (Nusil Med-4011), which is FDA-approved for short-term implantation [38].

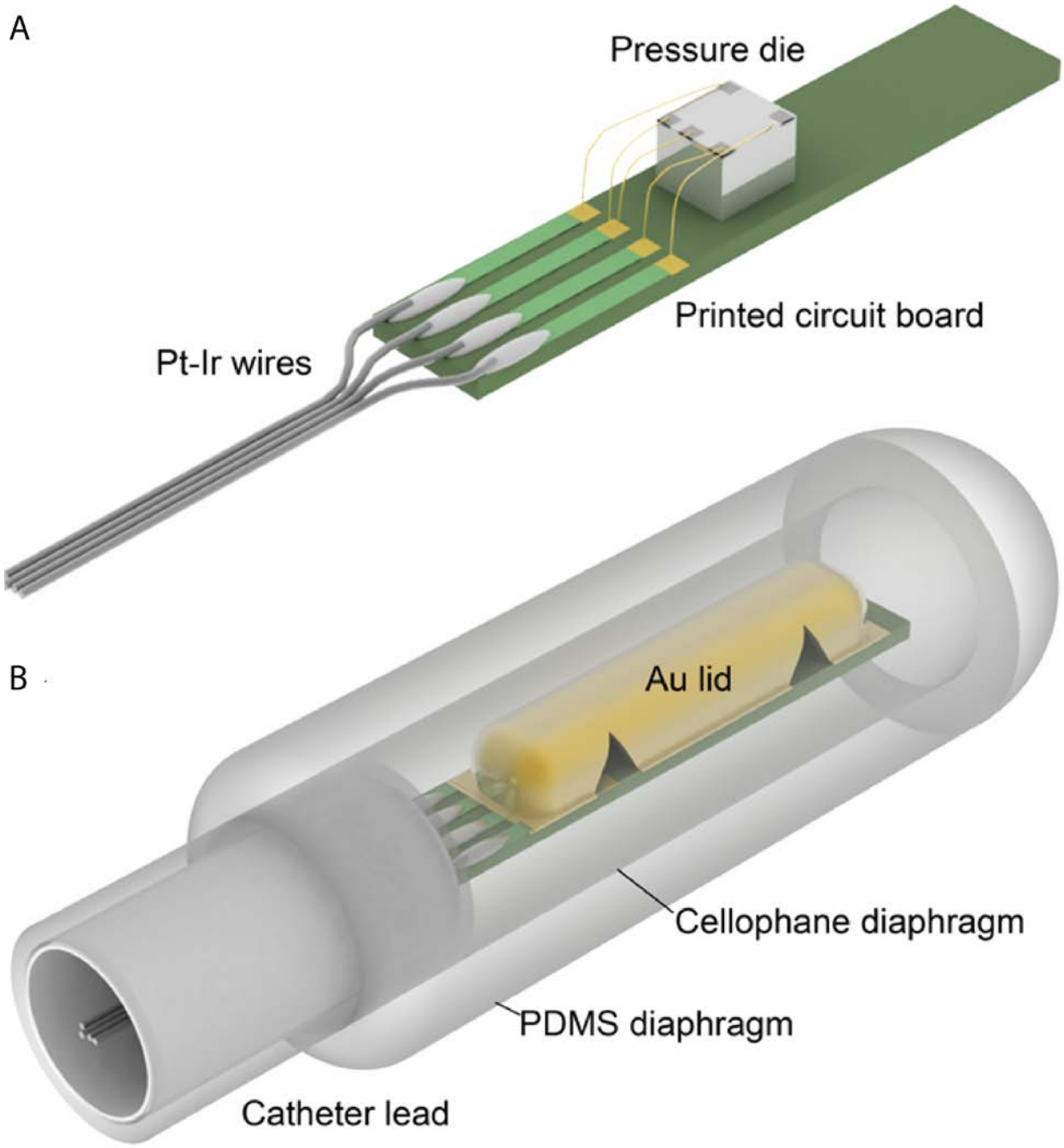

Figure 3.1. Artist's rendition of catheter lead tip. A) shows the lead tip unpackaged. A commercial pressure die is affixed and wirebonded onto a PCB substrate. Four Pt-Ir wires fed through the catheter are soldered onto the PCB. B) depicts the lead after packaging. A gold lid covers and protects the chip and wirebonds. Cellophane is wrapped around the lead; PDMS is molded around it to make it biocompatible.

The PDMS was mixed in a 10:1 elastomer base to curing agent ratio and degassed under vacuum. Once in the mold, the PDMS was allowed to cure for ~24 hours at room temperature. The final diameter of the molded tip of the catheter lead measured about 12 French (4 mm).

3.2 Sensor Node

The sensor node consists of three components: amplifying electronics, a microcontroller with a built-in wireless transmitter, and a battery. The other end of the catheter lead is soldered onto a custom-designed circuit board. On this circuit board, there are a quad micro-power, single supply operational amplifier (Texas Instruments TLV2764), a 2.5 V voltage regulator chip (Analog Devices REF192), and a single pole, double-throw (SPDT) magnetic reed switch to turn the device on and off (Hamlin) [39]. The voltage regulator chip sets the supply voltage powering the device and other electronics to 2.5 V to prevent any variations in signal from the pressure die due to variations in battery voltage. The operational amplifiers were configured to null any offset from the sensor bridge and amplify the bridge voltage by a factor of 300. The physiologically relevant pressure measurement range was 1.5 psi gauge pressure, and with the device sensitivity, supply voltage, and amplification, the device output was 1.2V/psi and 1.8 V for the physiological pressure range.

The output of the amplifying circuit was connected to the microcontroller with a wireless transmitter (Mica2Dot Crossbow MPR510CA), hereafter referred to as the dot mote) built in. The microcontroller is an Atmel ATmega 128L microprocessor plus analog-to-digital converter (ADC). The internal wireless transmitter operates at a carrier frequency of 433 MHz. The microcontroller was programmed to acquire and transmit data while battery life was maximized in three ways: first, the microcontroller pulses the sensor for only 30 μs each measurement cycle,

after which the entire device goes into sleep mode. Second, the measurements are taken only once per second. Last, since the greatest power draw comes from transmission, the sampled data is stored locally on the dot mote and is transmitted every 30 measurements [40]. These techniques reduce the energy consumption from 3 mJ per measurement to 625 μJ [39, 40]. The battery used in the design is a 3.7 V, 850 mAH lithium-polymer battery (Batteries America). The device was observed to have a lifetime of 387,300 measurements or >4 days at this sampling rate before the battery voltage dropped below the operating level.

Once fully fabricated, the sensor node was first wrapped in 25 μm-thick low density polyethylene (LDPE, Plastic Sheeting Supply) and then compression-molded in PDMS. Afterwards, the device was dipped into PDMS for a second silicone layer to seal any holes in the first PDMS layer.

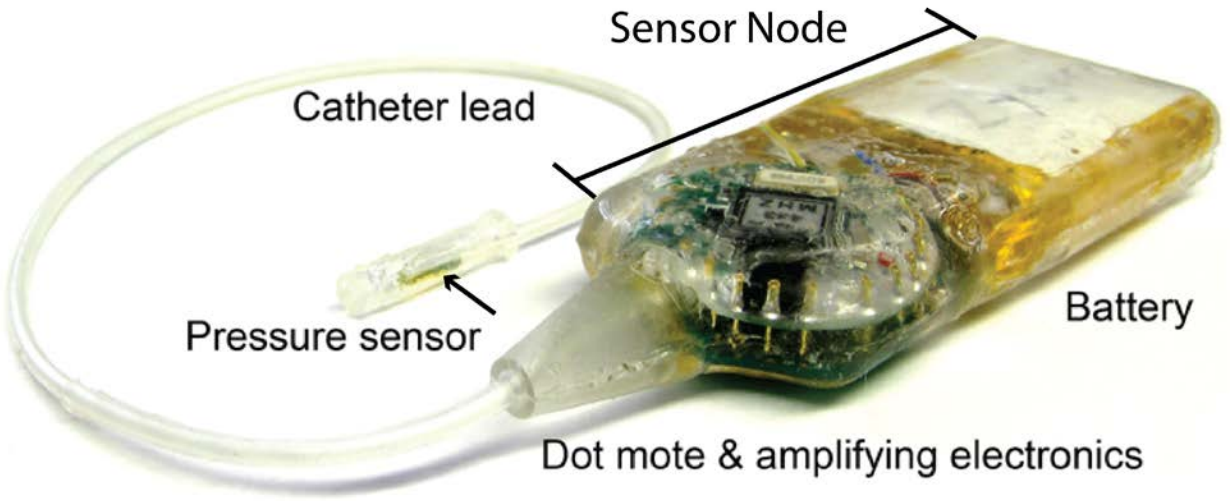

Figure 3.2. The implanted device after being fully packaged. The pressure sensor is housed at the end of a 7.5 French catheter, which is implanted directly into the bladder or peritoneal cavity. The other end of the catheter is connected into the sensor node, which consists of the dot mote (microcontroller and wireless transmitter), the amplifying electronics, and battery. The device is wrapped in LDPE film and molded in medical-grade PDMS

3.3 Data Collection and Storage

During and after the packaging process, the battery cannot be charged or replaced, so neodymium magnets were stacked on top of the mold to activate the magnetic switch and turn off the power while the PDMS was being cured and in storage awaiting animal testing. The completed sensor is depicted in Figure 3.2. The data processing, transmission, collection, and storage were previously described by Dabiri, *et al.* [41]. A collaborative effort with Majid Sarrafzadeh and Mani Srivastava in the Department of Computer Science and Department of Electrical Engineering, respectively at UCLA was set up to develop the wireless data transmission protocol. Briefly, the dot mote transmitted a data point every second to a radio receiver connected to a personal computer in hex format via a serial cable. By using LabVIEW to communicate through the computer's serial port, the data was retrieved, converted into decimal, and stored in a temporary buffer. Each hex data packet contained timing data and voltage data from each of the 6 ADCs found in the microprocessor of the dot mote, and thus LabVIEW was required to properly interpret the hex string to separate each value. Once the buffer was filled, the data was plotted and stored in a permanent file. A moving average was applied to the data in order to smooth it out. In addition to the sensor data, LabVIEW kept tracking of the time and date the program was started, the internal battery voltage, both raw and smoothed data sets, and the number of transmission errors encountered, as well as featured rudimentary calibration control. Figure 3.3 shows the front panel of the LabVIEW program.

Unfortunately, the integrity of the wireless transmission was not always 100% received, and the data would be corrupted occasionally. Typically, one or more bits in a hex string would be missing. Since the data is interpreted in LabVIEW by the position of each hex string in the data packet, the data corruption can cause misinterpretation of each subsequent hex string after the missing bits. The result would contain false information.

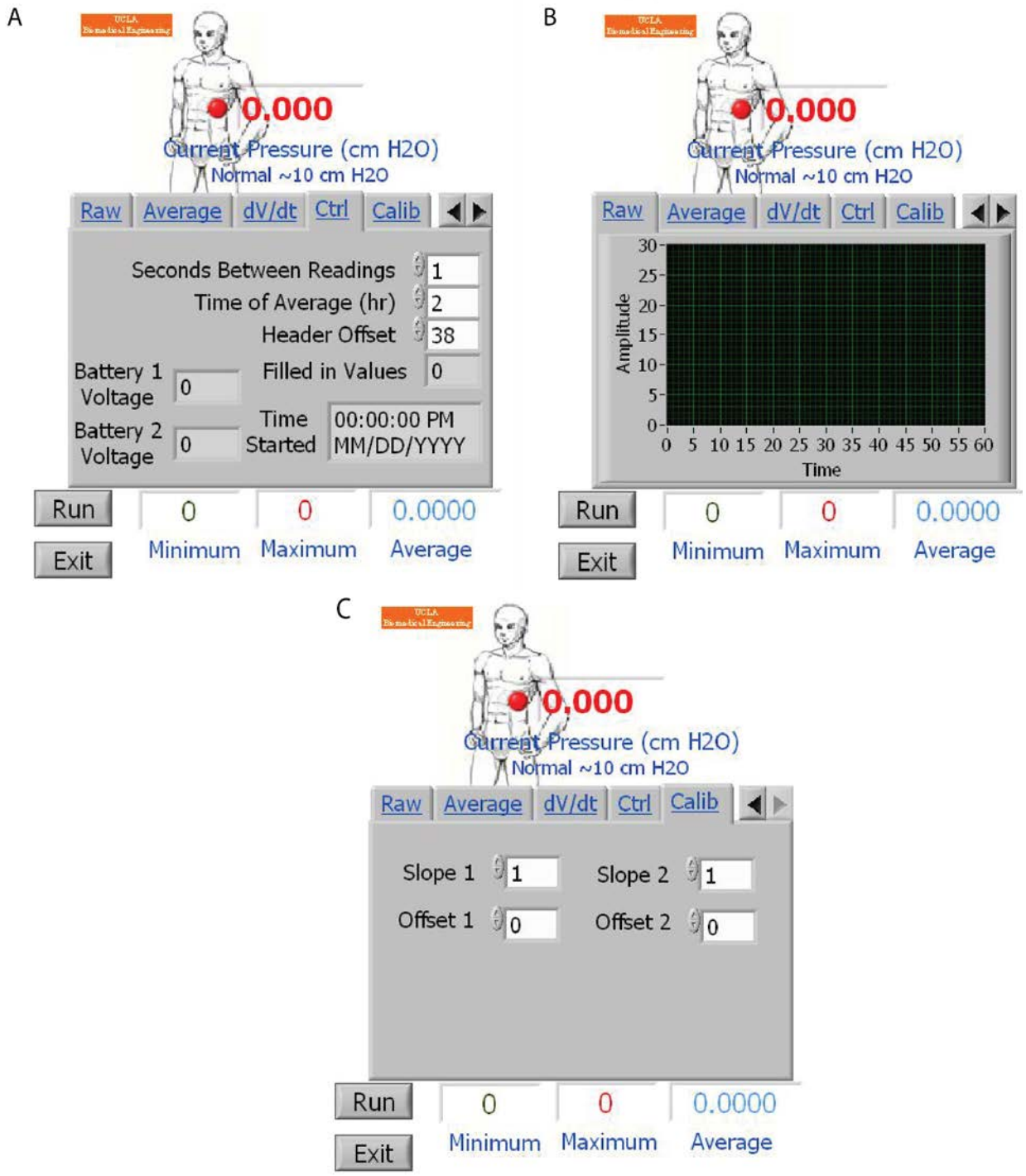

Figure 3.3. Three of the five tabs on the front panel of the LabVIEW program used to read and record the pressure sensor data: A) the system measurement settings, B) the raw data graph, C) the calibration settings.

When this occurred, LabVIEW recorded random peaks in the data set if the sensor was left on for a prolonged period of time. These events of data loss were typically short lived, lasting only a

few seconds at a time, so it was determined that a software fix would clean the data up. If the pressure recorded exceeded a threshold that was deemed physiologically impossible, that particular packet was ignored, and the closest previously accepted value was recorded and displayed in its stead.

Chapter 4 Full Sensor Testing and Animal Study

4.1 Sensor Node *In Vitro* Testing

Once fabrication of each catheter lead was completed, the lead alone was tested and characterized by placing it in a sealed pressure chamber (Binks). It was electrically connected to wires threaded through the lid of the pressure chamber. The lead was externally powered (Agilent E3630A), and the output voltage was read by a high precision multimeter (Keithley 2000). The pressure was held constant at atmospheric pressure for 30 minutes while the device output and pressure readings from a NIST-calibrated pressure gauge (Omega DPG5600B-30A) were being recorded every five minutes. The chamber was connected to a cylinder of compressed nitrogen through a pressure regulator, and the pressure was raised in 1.0 or 1.5 psi increments and held for 30 minutes. For the first 10 minutes, pressure and voltage readings were taken every minute and every five minutes for the following 20 minutes. At the conclusion of the calibration, the pressure vessel was vented back to atmospheric pressure, and the voltage and pressure were again read every minute for 10 minutes and every five minutes for the following 20 minutes. The calibration was performed three times for each lead to test the effects of the environment on the lead and its packaging. It was tested in air first as a control, and then the tip of the lead was placed in a beaker of water inside the chamber. It was left submerged for four days before it was tested again. If the output magnitude and temporal response stayed consistent after the fourth day, it was paired with a sensor node.

After a sensor node was paired to a catheter lead, the entire device was tested again before packaging. The lead was placed in water within the sealed pressure vessel.

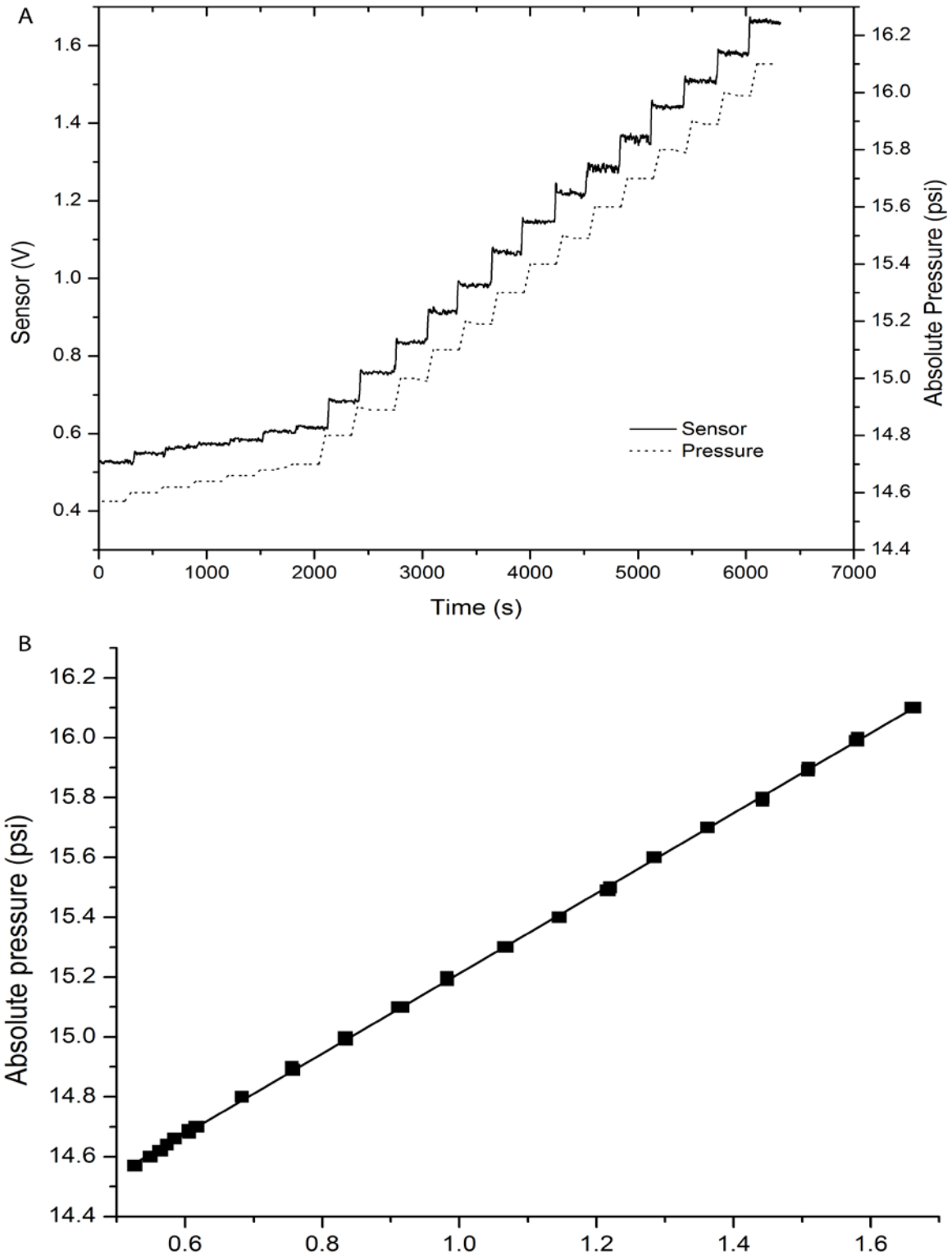

Figure 4.1. Typical results of in vitro testing. A) is the temporal response of the measured voltage and the pressure input. Each small increment is 0.02 psi; each large increment is 0.1 psi. The pressure range is from 0-1.5 psi gauge. B) shows the high linearity between the measured voltage and the pressure. The equation of the best fit line is $P = 1.3393 \cdot V_{out} + 13.873$ (R^2 = 0.9998).

The sensor node was connected to the lead outside the pressure chamber and powered either by the battery or DC power source. The LabVIEW program ran on the computer and stored the wireless pressure data. The pressure was incrementally stepped up from 0-1.5 psi to test the required pressure range and held at each step for five minutes with pressure readings taken every two minutes. To test the resolution of the device, the incremental pressure changes were 0.02 psi from 0-0.1 psi and 0.1 psi from 0.1-1.5 psi. At the conclusion of each test, a calibration curve was generated that related the voltage recorded on the computer to the pressure inside the chamber.

Testing of the fully assembled lead and sensor node showed a rapid and linear response (1.34 psi/V) of the sensor (Fig 4.1). When the device was disassembled and reassembled following the initial tests, the offset was observed to change slightly. Once the device was fully packaged and ready to be implanted, this change was compensated by comparing the calculated pressure from the calibration curve with the actual pressure from a pressure gauge and then adjusting the offset value on the calibration curve.

4.2 *In Vivo* Rat Rectum Testing

The pressure sensor was tested inside a rat rectum to verify the functionality of the sensor in an *in vivo* environment. Although the waterproofing of the sensor lead packaging was previously vetted by being submerged in water, it was believed that insertion into the rectum of a rat would better replicate the conditions encountered in surgery. Namely, the insertion process into a tight orifice would test how the packaging withstood the physical demands of surgery. The rat would also provide some insight into the pressures encountered inside a body cavity as well.

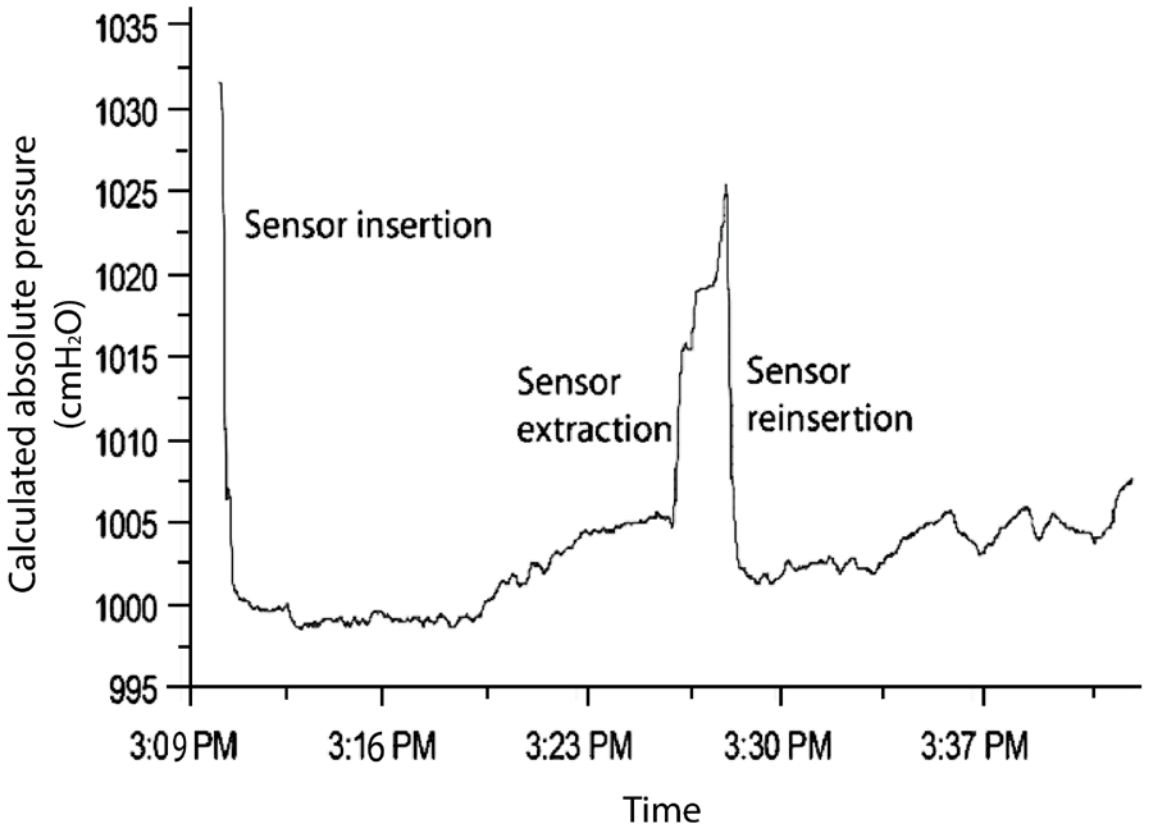

Figure 4.2. Pressure trace from sensor inserted into a rat rectum.

An adult rat was anesthetized prior to sensor insertion. The sensor was turned on and recorded during the insertion process. During insertion, the belly of the sensor was compressed by hand under constant force and in pulses. In the middle of the experiment, the sensor was extracted and reinserted while being read. The data from the study is shown in Figure 4.2. The sensor behaved as expected when a medical doctor compressed on the abdominal cavity. The packaging stayed intact, and the pressure sensor die continued to function after the experiment was concluded. However, a curious phenomenon was detected: the rectum of the rat was at a lower pressure than atmospheric conditions. This was confirmed as the pressure signal was decreased by a noticeable amount upon insertion. However, as the sensor was extracted, the detected pressure increased back to nearly the original value at atmospheric conditions. The

pressure again dropped after immediate reinsertion of the sensor. This drop in pressure had been previously seen in porcine implantations that are described later.

4.3 *In Vivo* Porcine Implantation

Adult female swines were used for *in vivo* testing as approved by the UCLA Medical Center IRB #2004-185-11. One device was implanted into the bladder and another was placed inside the peritoneal cavity as a reference. The tips of the catheter leads were placed in those spaces while the sensor nodes were placed in a subcutaneous pocket. Following surgery, the pigs were kept in a holding pen in a vivarium while the computer and radio receiver were set up outside the pen to collect the data. At this point, the pigs were fully conscious and ambulatory. After 2-4 days, the pigs were sacrificed and the devices were explanted. A brief necropsy was performed to look for tissue inflammation or any immune response to the silicone packaging. The devices were later inspected for any damage, leaking, or any other failure points if necessary.

When the pressure from the peritoneal sensor is subtracted from the pressure of the bladder sensor, the detrusor (bladder muscle) pressure is obtained. Therefore, any pressure change can be attributable from activities within the bladder or from other sources, such as abdominal contractions, peristalsis, movement, etc. Pressure changes of the detrusor possibly due to bladder contractions were observed (Figure 4.3) during the animal studies. This data shows that the detrusor pressure stayed relatively constant as the bladder filled as the bladder wall is highly compliant. The detrusor pressure increased sharply followed by a sudden decrease in detrusor pressure, which is representative of a bladder void. Figure 4.3 is demonstrative of known pressure graphs of voiding.

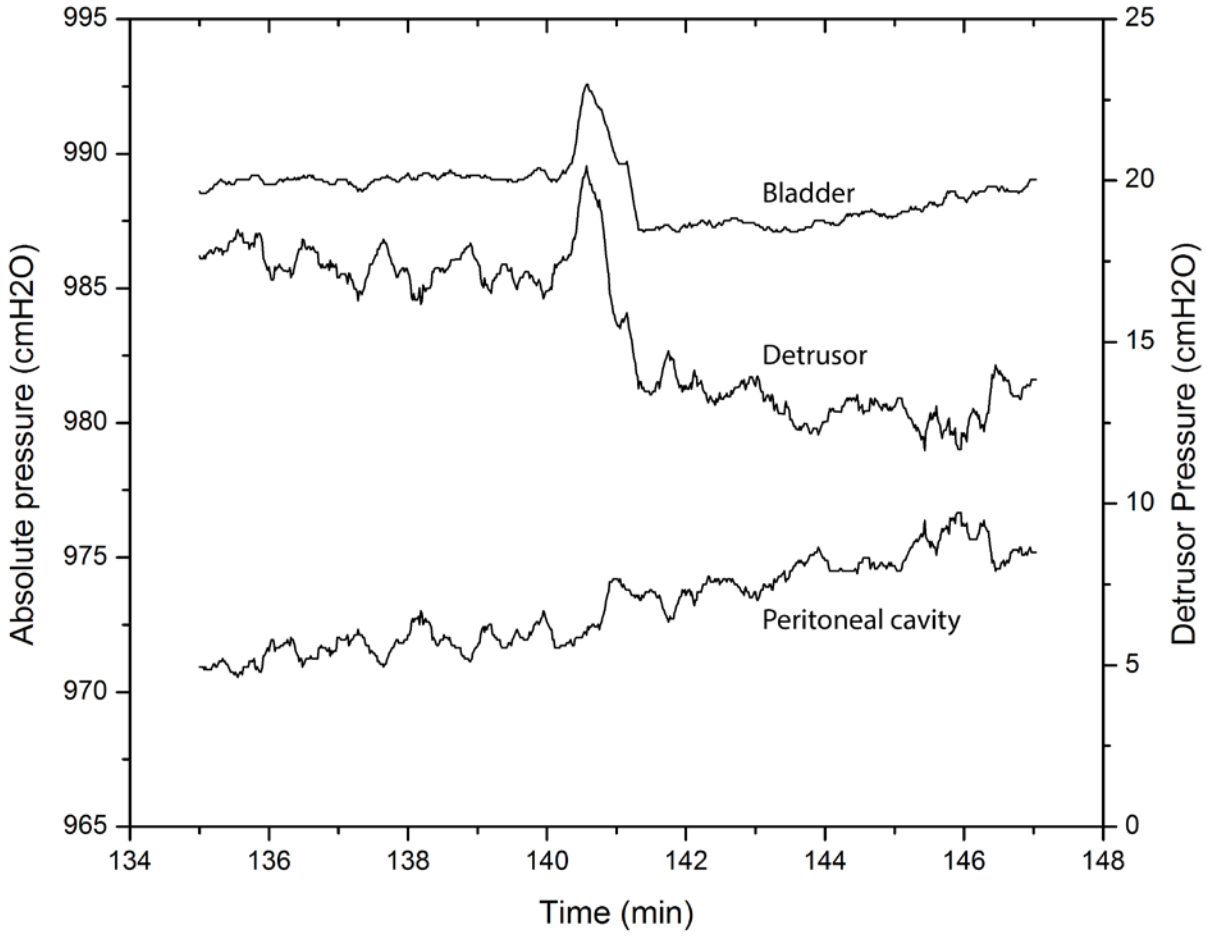

Figure 4.3. The results of a urination event during an in vivo test. The peritoneal cavity pressure is subtracted from the bladder pressure to calculate the detrusor pressure.

The devices in this test transmitted data for more than four days *in vivo* until the batteries drained out. Furthermore, they were able to transmit data to the computer more than 20 feet away while implanted. Neither device showed signs of fluid leaks; however, the device implanted into the peritoneal cavity had a damaged catheter lead tip. In fact, the gold lid protecting the pressure die was flattened along the back half of the substrate board. Despite the damage, the chip remained functional throughout the test. Analysis of the data revealed the data obtained for the first 2.5 days had several urination events. The pressure data from the peritoneal cavity had many

discontinuities: the baseline pressure suddenly jumped to a higher level before falling back down. This may be due to the sensor contacting various internal structures as the animal moves (Figure 4.4). These discontinuities are not seen in the bladder trace possibly since the sensor was placed in a bag of fluid and thus would not encounter these phenomena. Towards the end of the study, the data became unreadable and was characterized by high loss of data packets and many sudden spikes. This may be due to a combination of a draining battery and the hostile environment for transmission as it was known that the radio receiver had difficulty picking up the wireless signals at the beginning of each in vivo study.

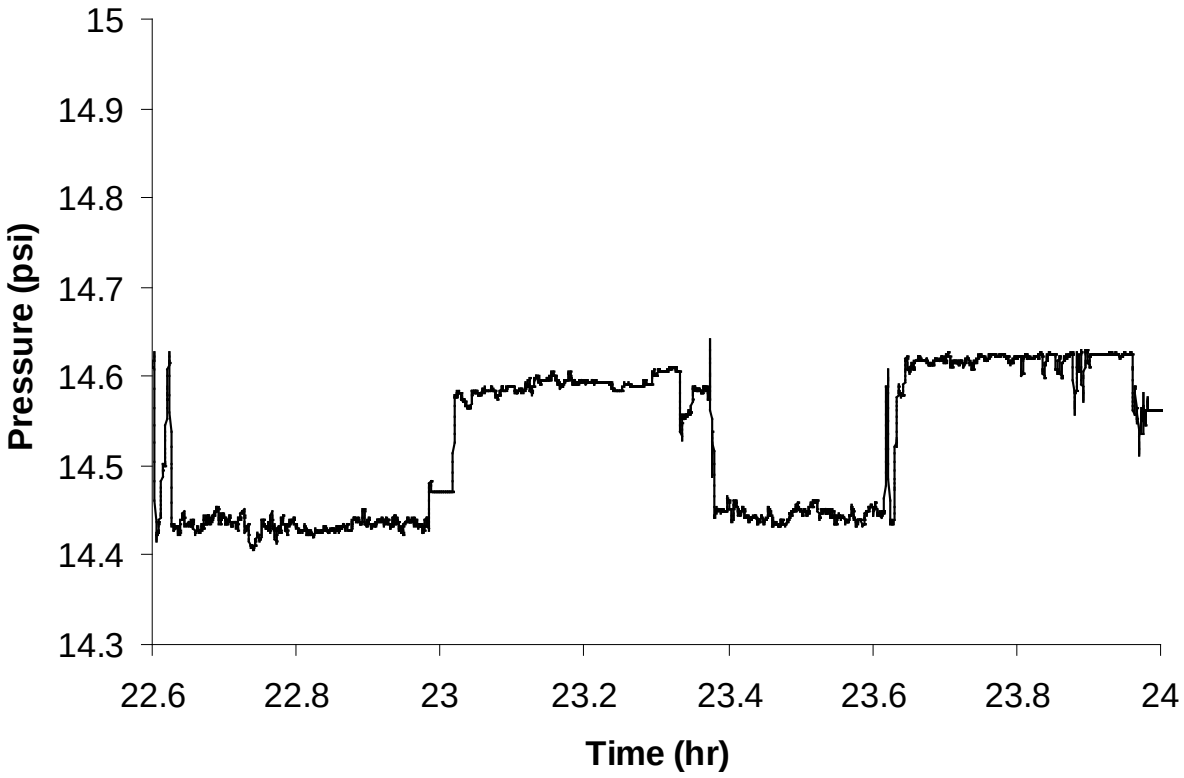

Figure 4.4. Pressure measurements from the sensor located within the peritoneal cavity. The discontinuous changes in measured pressure may be a result of intermittent contact with abdominal organs in the mobile animal.

4.4 Conclusion

In summary, a fully implantable wireless *in vivo* pressure sensor was designed for use in short-term urological studies and patient monitoring has been constructed. With better battery technology, this solution can be used to monitor pressure for extended periods of time. In vitro testing demonstrates its quick temporal response and its high linearity. Through in vivo tests in the bladder and peritoneal cavity of porcine models, the pressure-sensing system was able to successfully record medically relevant data, which contained physiological events like urination.

Although the previously described pressure sensor was a demonstration of a long-term, fully implantable, wireless pressure sensor for home monitoring, there were a few drawbacks with the design. One feature of the sensor that made it different from other continuous monitors was the use of a battery as a power source. There must be a compromise between the capacity of the battery and the temporal resolution the sensor can provide: a longer time between transmissions would obviously prolong battery life. However, for the ultimate goal of hemodynamic monitoring, a loss in temporal resolution simply is not an option. An ability to recharge the battery while implanted would mitigate the problem, and the conversion of kinetic energy into electrical energy would reduce the need for the user to actively recharge the battery. Another issue encountered was the packaging. It was required to isolate the electronics from bodily fluids and protect the fragile electrical connections, which made the pressure sensitive lead too bulky to fit into an artery.

Chapter 5 Introduction to Blood Pressure Monitoring

Currently, in the intensive care unit (ICU) or operating room, continuous pressure monitoring is done by using an arterial line, which indirectly measures blood pressure through a length of tubing connected to an *ex vivo* pressure transducer. This low-tech method is plagued with artifacts, such as bubbles in the catheter, kinking, and motion artifacts [3]. Furthermore, the patient must be tethered to the bedside pressure transducer. In contrast, patients undergoing standard floor care have their blood pressure taken every 2-12 hours at discrete intervals using a sphygmomanometer, which is a pressure cuff that surrounds a limb and inflates until the patient's arteries occlude before slowly venting. A microphone or nurse listens to the Korotkoff sounds associated with diastolic and systolic pressures and records those values. Aside from the obvious disadvantage of not providing continuous pressure measurements that can lead to undetected critical conditions, the pressure measurement is indirect—the pressure value is determined by detecting certain sounds, which can be obscured background noise or requires a trained ear if pressure is taken manually. Also, operator error can lead to injury from burstblood vessels by overinflating the cuff.

Ideally, pressure is measured *in situ* and directly, so this avoids many sensing artifacts and can free patients from tethered monitors. Many groups have created fully implantable pressure sensors that wirelessly transmit data to the patient monitor that are designed to be used in many applications, such as urological, spinal, ocular, as well as intravascular uses [10, 12-24, 42, 43]. The advantage of doing so allows the patient to be free to move around since they are no longer tethered to a bedside transducer. However, implantation of these devices often requires open surgery, which limits their deployment to a smaller selected group of patients. Recently,

catheter-mounted pressure sensors have been developed [44-46]. Implantation is easily performed by using standard catheterization techniques; thus the deployment of these pressure sensors is extended to a larger group of patients. While most arterial *in situ* pressure sensors are made using MEMS technology, microfabricated transducers require extensive packaging to protect them from the hostile environment in the body, which adds to the size and bulk of a device. In order for the device to fit inside an artery, the chip and packaging needs to be extremely small, such construction can be very expensive. Moreover, the size of the catheter lead can only be reduced to the size of the pressure die itself. The Silicon Microstructures 5108 was the smallest commercially available pressure die at the time, and that chip was already 0.6 mm in each dimension, which meant the smallest possible catheter would be 2 French. To fabricate an even smaller catheter would require a large amount of capital just in the development of a smaller chip. Furthermore, the assembly of each catheter lead is typically done by hand, increasing cost considerably. The high cost of each sensor often precludes them from widespread use—often limited to be reused in the operating room or ICU or for research use only. Table 5.1 compares various pressure-sensing catheters with the proposed sensor design.

Company	**RADI [47]**	**Millar [11]**	**OPSENS [48]**	**Proposed Sensor**
Model	Pressure wire	SPC320	OPP-M	CRISP
Mode of operation	Piezoresistance	Piezoresistance	Interferometry	Fluid conductance
Size	1F	2F	1F	2-6F

Table 5.1. A comparison of existing catheter-based pressure sensors with the proposed design in terms of operating mode, and size.

The experimental sensor, hereby known as the Catheter, Real-time, *In Situ*, Pressure (CRISP) sensor, on the other hand, requires minimal packaging, which does not add bulk over any of the functional components; therefore, the overall size is reduced. Besides, scalability to smaller sensors is trivial due to the wide availability of components and easy construction. The

proposed sensor works by measuring the dimension change of an electrolyte-filled elastomeric tube. The change in diameter in the tube translates to a change in electrical resistance, which is easily measured. By using a reference volume and due to the incompressibility of liquids, the sensor compresses in the region exposed to pressure, but expands within the reference volume. Wu, et al. created a pressure sensor on a similar concept [49]. However, their device used a microfluidic chip on the centimeter scale, making it too large for arterial implantation. Also, the conductive solution used was an ionic solution, which is toxic [50] if the device leaked. On the other hand, the CRISP sensor is tailor-made for *in vivo* use: the small footprint allows for arterial implantation via catheterization and all the materials are non-toxic and safe for the patient. Last, while sensor described in chapters 2-4 was an integrated wireless system, this part of the research focused on developing solely the new sensor design with the idea of adapting an existing wireless communication to the CRISP sensor.

Chapter 6 CRISP Sensor Design and Theory

6.1 Overview of Sensor Design

A schematic of a catheter implementation of an electrolyte-based CRISP sensor is shown in Figure 6.1. As discussed in a previously published work [49], a flexible chamber containing a conductive electrolyte deforms after pressure exposure, changing the electrolyte dimensions and enabling electrical detection. This system left one side of the chamber to the environment to allow fluid to displace. However, the experimental catheter is completely sealed to prevent the fluid from exiting in response to an increase in applied pressure. By encapsulating half of the tube in an inflexible jacket, a reference volume is created in the space between the elastic tube and the jacket.

By bifurcating the elastomer tube with the metal jacket, it creates two distinct regions. If the sensor is placed in a medium at a higher pressure than that of the reference volume, the elastomer tube will get compressed in the exposed region. Due to the incompressibility of water, the elastomer tube within the jacketed region expands as water flows from the exposed region into the jacketed region to equalize the pressure inside the tube.

The changes in dimension of the jacketed and un-jacketed portions of the tube are measured by the change in electrical conductance of the electrolyte fluid in the tube. By placing wires in the electrolyte at each end of the tube and at the jacket boundary, the conductance of the jacketed and un-jacketed portions of the tube may be measured. From the analysis in the preceding paragraph, it was expected that the resistance of the electrolyte would increase in the unjacketed portion of the tube and the resistance of the jacketed region would decrease.

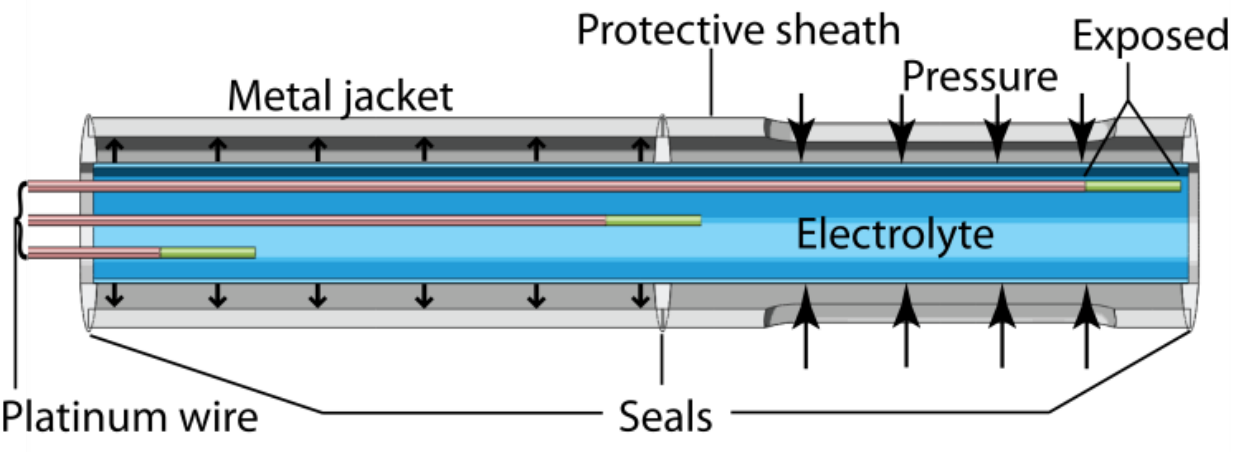

Figure 6.1. Cross-sectional schematic of the CRISP sensor.

6.2 Mathematical Model

In order to mathematically model the sensor performance, the sensor can be considered as a thick walled tube since the wall thickness of the elastic tube exceeds the one-tenth criterion for thin walled tubes [51]. Most elastomers follow Hookean behavior (linear stress-strain relation) under very small strains [52], which is applicable for the experimental sensor. The radial and hoop stresses of a thick walled tube [53, 54] with isotropic Hookean elasticity give the inner radial displacement, *U*, as a function of pressure (Eq. 1),

$$U = \frac{a}{E}\left\{\frac{2P_o b^2(\nu^2-1)+P_i[a^2(1-\nu-2\nu^2)+b^2(1+\nu)]}{b^2-a^2}\right\} \qquad \textbf{Eq. 1}$$

where a is the inner radius of the tube, b is the outer radius of the tube, E is the Young's modulus, P_o is the external pressure, which is assumed to be atmospheric pressure, P_i is the pressure within the elastic tube, and ν is the Poisson's ratio. Highly elastic materials have a Poisson's ratio of 0.5 [55], which reduces Eq. 1 to a simpler form:

$$U = \frac{a}{E}\left\{\frac{\frac{3}{2}b^2(P_i-P_o)}{b^2-a^2}\right\} \qquad \textbf{Eq. 2}$$

The CRISP sensor design has two regions with different P_o, but since they are connected and filled with a fluid electrolyte, under the steady state, the inner pressure of a static fluid, P_i must be equal for both regions. Furthermore, since the tube interiors are connected to each other and filled entirely with an incompressible fluid, the tube inner volume is conserved, and any inner volume change of the exposed tube must be compensated by an opposite inner volume change of the jacketed tube. Because the ends of the elastic tube are affixed to rigid components, the length cannot change. Eq. 2 can be rearranged to solve for the pressure within the elastic tube as a function of displacement (Eq. 3). Since the two regions are connected to each other, and fluid can freely flow from one region to another, P_i remains constant.

$$P_i = \frac{2U_{exposed}E}{3ab^2}(b^2 - a^2) + P_0 + P_{app} = \frac{2U_{jacket}E}{3ab^2}(b^2 - a^2) + P_0 \qquad \textbf{Eq. 3}$$

The displacements of the exposed and jacketed regions can now be solved as a function of each other (Eq. 4). Besides, because the fluid is incompressible, the total volume within the entire length of the elastic tube must remain constant (Eq. 6), assuming Li and Lo are the lengths of the jacketed and exposed tubes, respectively.

$$U_{exposed} = U_{jacket} - A \qquad \textbf{Eq. 4}$$

$$A \equiv \frac{3ab^2P_{app}}{2E(b^2-a^2)} \qquad \textbf{Eq. 5}$$

$$a^2(L_o + L_i) = \left(a + U_{exposed}\right)^2 L_o + \left(a + U_{jacket}\right)^2 L_i \qquad \textbf{Eq. 6}$$

Solving this system of equations will finally yield the radial displacements for both regions:

$$U_{jacket} = \frac{\pm\sqrt{a^2(L_i^2+L_o^2)+L_iL_o(2a^2-A^2)}-B}{L_i+L_o} \qquad \textbf{Eq. 7}$$

$$U_{exposed} = \frac{\pm\sqrt{a^2(L_i^2+L_o^2)+L_iL_o(2a^2-A^2)}-B}{L_i+L_o} - A \quad \textbf{Eq. 8}$$

$$B \equiv aL_o - AL_o + aL_i \quad \textbf{Eq. 9}$$

$$R = \rho\frac{L}{\pi a^2} \quad \textbf{Eq. 10}$$

From the derived displacements, new inner radii can be determined as a function of pressure. Specifically, the new inner radius of the jacketed region is calculated by adding the displacement of the tube in the jacketed region to the original inner radius to model tube expansion. Similarly, the displacement of the exposed region is subtracted from the original radius to account for tube compression. The electrical resistance is calculated from Eq. 10 using the new radii. As the resistance is the sensed parameter, it was critical to find the sensor dimensions and material properties that maximize the sensitivity of electrical resistance to changes in pressure.

The sensor is designed to be measured with a modified Wheatstone bridge that converts electrical resistance into a voltage signal, which can then be amplified. As depicted in Figure 6.2, the electrode pairs are arranged in order that the exposed region is located in the positive branch of the bridge, and consequently, the jacketed region is in the negative branch. The bridge yields a gauge factor of ½, which is the same as a standard 2-gauge Wheatstone bridge. Just like a 2-gauge bridge, the advantages of this configuration are two-fold. First, the sensor is temperature-compensated. Temperature change has a profound influence on the electrical resistance of fluids due to changes in ion mobility. Second, the sensitivity is increased relative to just one gauge or one region of the sensor in this case. Last, Eq. 11 reveals that the percent change of resistance is what ultimately determines the sensitivity

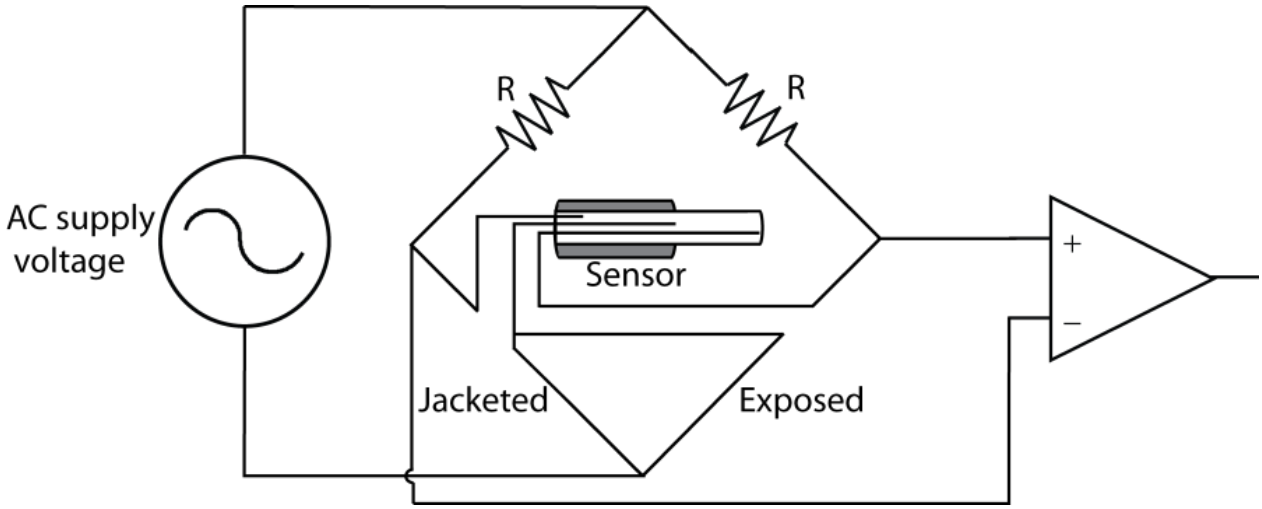

Figure 6.2. Schematic of modified Wheatstone bridge configuration for making voltage measurements with the CRISP sensor. R represents an arbitrary fixed resistor.

6.3 Model Results

The sensor impedance is measured by varying each parameter at a time while holding all other parameters fixed; it is then plotted the displacement of the inner radius of the exposed and elastic tubes as well as the fractional change in resistance as a function of pressure (from 0-300 mmHg), which is the pressure range all blood pressure monitors need to be sensitive [56, 57]. The fixed values of the parameters chosen are listed in Table 6.1.

The values in Table 6.1 for tubing dimensions were based on commercially available silicone tubing (Dow Corning Silastic); the elastic modulus used corresponded to the softest silicone, which has a modulus range from 1.6-7 MPa [58], and the resistivity of 100 mM KCl is used [59]. The tubing lengths were chosen to match prototypes built in the laboratory. Below the implications of each variation of each parameter to the overall system is addressed in turn. The elasticity of the tube is determined by its thickness and material composition and was seen to affect the sensor's sensitivity most compared to other parameters. Plotted in Figure 6.3A are inner and outer tube radius and resistance changes as a function of pressure for different tubing

materials. For reference, soft silicone (E = 1.6 MPa), stiff silicone (E = 7 MPa), stiff synthetic rubber (E = 75 MPa), High density polyethylene (HDPE) (E = 1100 MPa), and Nylon (E = 2000 MPa) [60].

Parameter	Value
Inner radius (bore size)	0.545 mm
Wall thickness	0.123 mm
Elastic modulus	1.6 MPa
Jacketed region length	5 mm
Exposed region length	5 mm
Resistivity	83.3 μΩ-m

Table 6.1. A summary of constants used in the mathematical model.

As expected, a low elastic modulus results in higher sensitivity of the resistance to changes in pressure. Figure 6.3B show the sensitivity to tubing wall thickness, with thin-walled tubes being the most sensitive. The relative lengths of the exposed and jacketed regions affect changes of interior volume that result from applied pressures, which in turn determine the induced inner radius displacements that are measured electrically.

According to Figure 6.3A, the length scale for the tube compression and expansion is on the order of nanometers. It can be concluded that the dimensions of the sealed reference volume do not change much, meaning the air pressure within the reference volume stays fairly constant. Therefore, the expansion of the elastic tube within the jacketed region is ultimately limited by the elasticity of the material since for practical materials; the elastic modulus is greater than any pressure the sensor would experience. Therefore, any dimension change of the elastic tube is dictated by the amount of water flowing between the regions. In either case, the amount of dimension change in one region is driven by the maximum change in the other region. Two situations are presented here: a sensor with a very short jacketed region compared to the exposed region and a sensor with a very long jacketed region relative to the exposed region.

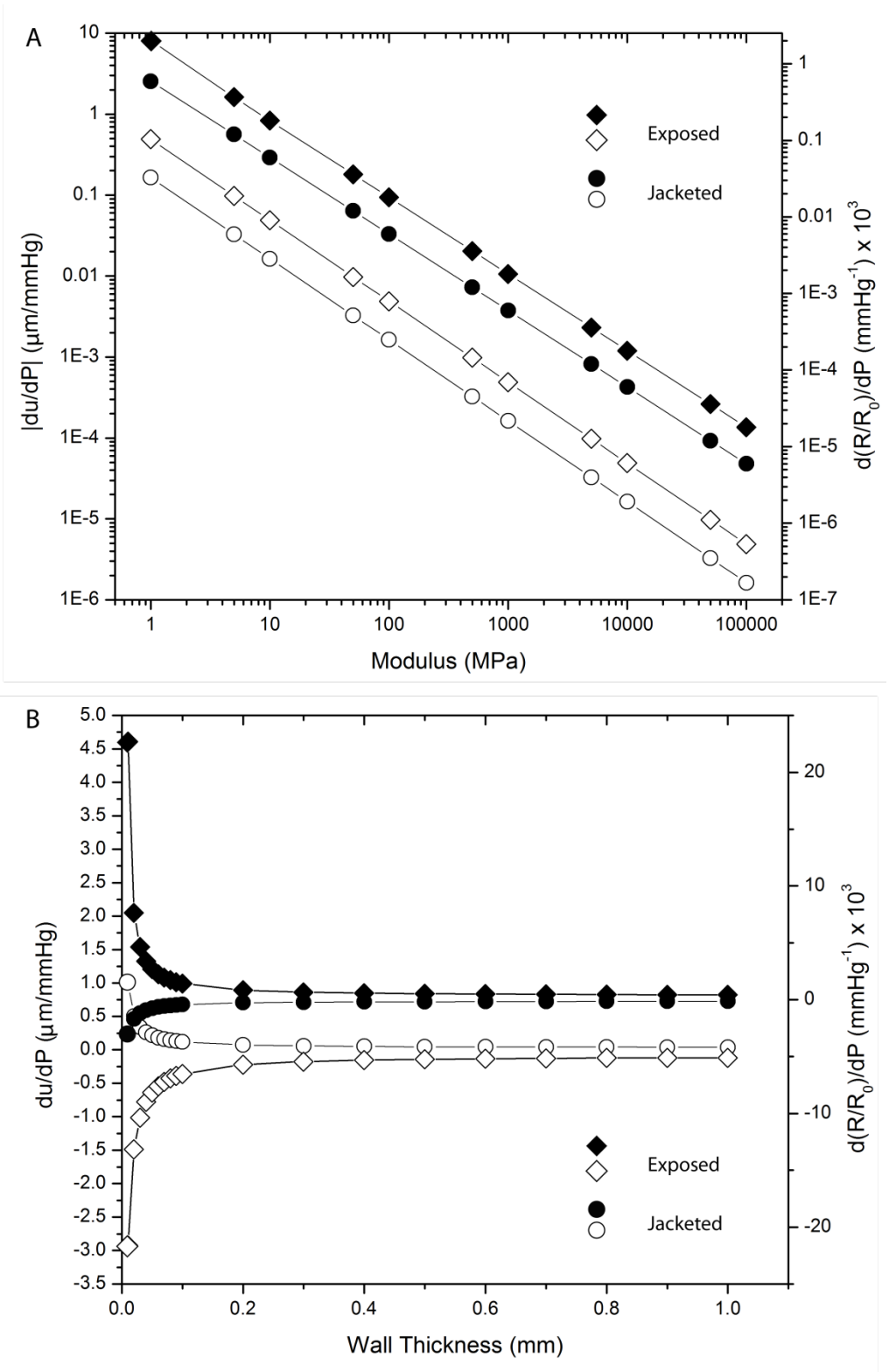

Figure 6.3. A) The pressure sensitivity of the tubing inner radius (empty) and relative resistance (solid) as a function of pressure for a range of materials ranging from rubber (1-10 MPa) to metal (100 GPa). The displacement of the exposed region is negative. B) The pressure sensitivity of the tubing inner radius (empty) and relative resistance (solid) as a function of pressure for tubing thicknesses between .05-1 mm.

When the elastic length of the jacketed region is much larger compared to the exposed region, the expansion of the elastic tube within the jacketed region controls the compression of the outer region. Regardless of the amount of electrolyte solution that is available, the volume of liquid that can flow into jacketed region is constant for any given pressure. Therefore, in order to produce this volume, a short length of the outer tube will result in a greater constriction as compared to a longer length. Since the cross sectional area of the elastic tube has a greater effect on electrical resistance, the effect of constriction plays a larger role in sensitivity than does the length of the tube.

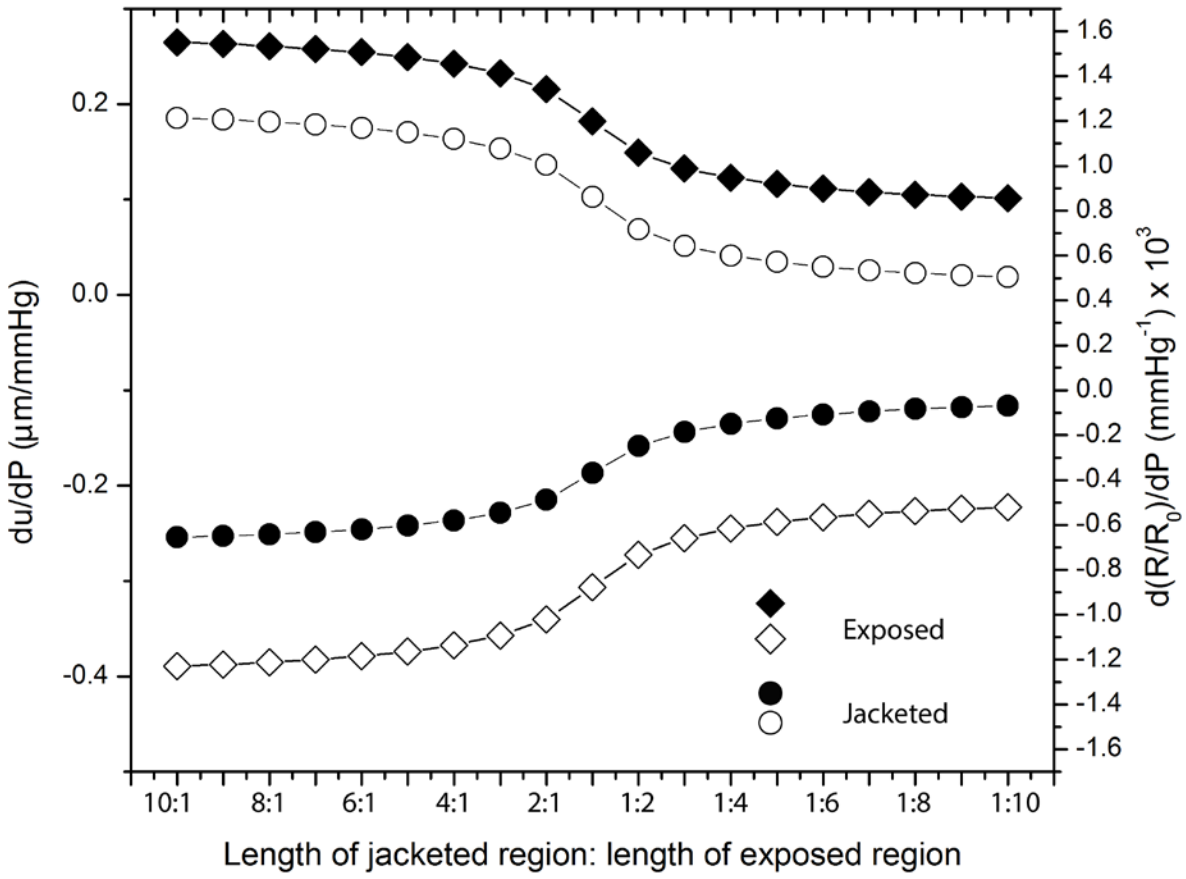

Figure 6.4. The pressure sensitivity of the tubing inner radius (empty) and relative resistance (solid) as a function of pressure for ratios of the inside: outside tube lengths ranging from 10:1 to 1:10.

As shown in Figure 6.4, the expected change in inner radius is greatest when the length of the exposed region is much smaller than that of the jacketed region. The change in diameter upon pressurization falls precipitously as the relative length of the exposed region grows; when the elastic portion of the exposed tubing reaches five times the length of the jacketed region, the change in resistance sensitivity for further increases in the length ratio greatly diminishes. Large bore tubing will experience more compression or expansion as depicted in figure 6.5.

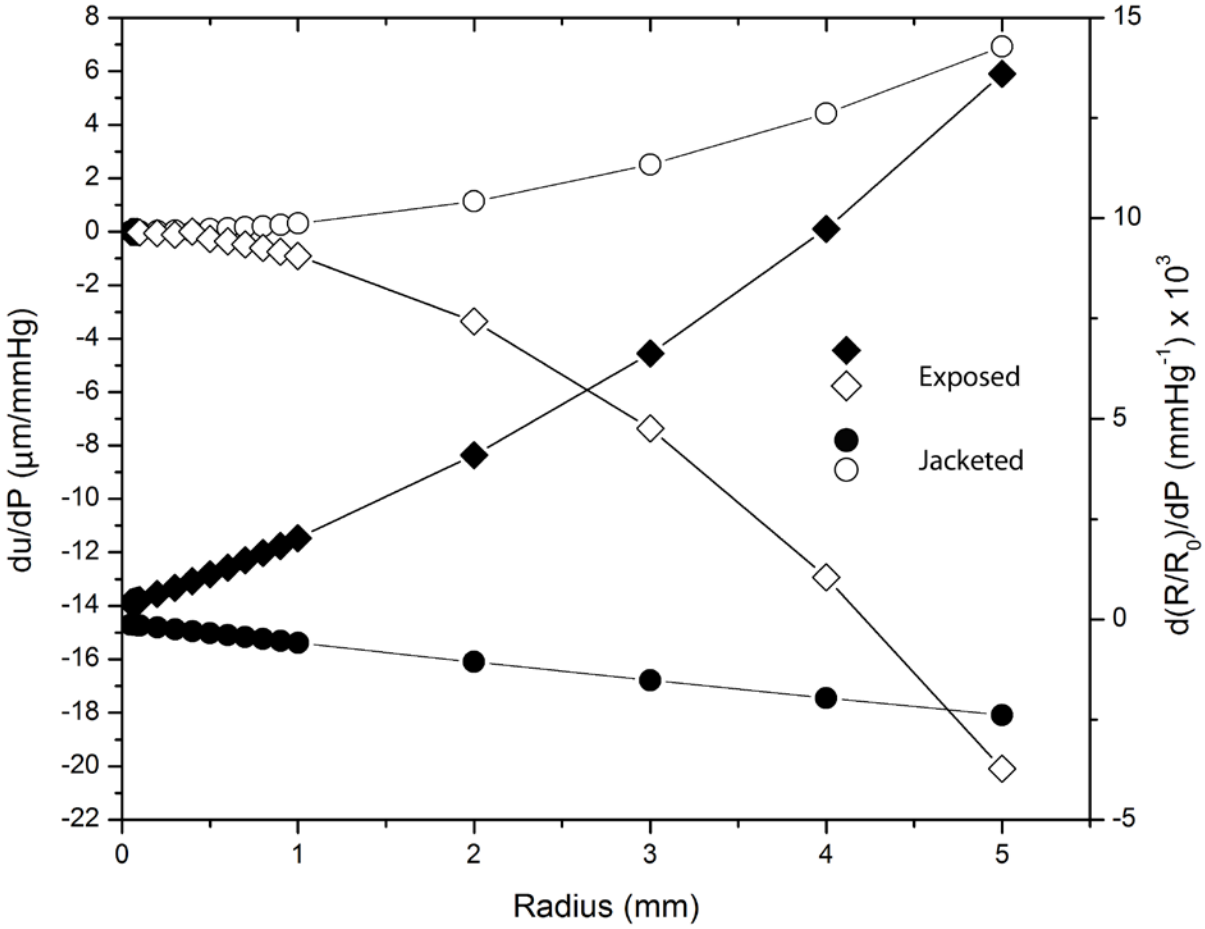

Figure 6.5. The pressure sensitivity of the tubing inner radius (empty) and relative resistance (solid) as a function of inner radius (0.05-5 mm).

This effect is similar to a tube with an increasingly thinner wall: large bore tubing with the same wall thickness as a smaller tube will be more elastic. However, when the total resistance is

calculated, sensors that have use small bore tubing have a larger change in resistance with pressure. On the other hand, as shown in Figure 6.5, the change in resistance as the sensor is pressurized is maximized in sensors with a large bore. This is more favorable for a sensor in a Wheatstone bridge configuration. Last, the concentration of the electrolyte solution used dictates the electrical resistivity of the fluid. Although a high resistivity will result in a larger resistance change for a specific change in cross sectional area, the percentage of change in resistance remains constant, and thus the concentration of the electrolyte is unimportant.

6.4 Model Validation

One of the basic constraints is to use only commercially available materials during this research. It was not completely possible to control each parameter of the tubing to thoroughly test the sensor model. Only silastic tubing (PDMS) is readily available, and tubing made from different materials, such as polyurethane or latex, are available either with large diameters or have to be custom made, which is an expensive option.

Custom tube extrusion in the lab using liquid polymers proved to be a Sisyphean task due to the inability to control wall thickness and demold without destroying the tube. Even with silastic tubing, the wall thickness unfortunately varies with the outer diameter of the tubing. It was not possible to test the effect of only the bore diameter on the pressure sensitivity. One parameter that was controllable, however, was the length of the elastic tubing. The relative pressure sensitivity was tested in a sealed gas pressure chamber by quickly changing the pressure from 0-5 psi (258.6 mmHg). The exact testing set up and protocol is described later in chapter 8. A sensor using silastic tubing measuring 4 mm in the jacketed region and 8 mm in the exposed region was fabricated with an inner diameter of 0.635 mm. The sensor was filled with electrolyte

solution and clamped at the tip of the elastic tubing to temporarily seal it. After each pressure test, the elastic tubing was flushed out with deionized water and dried. The tubing in the exposed region was made rigid incrementally 1 mm at a time for each time using cyanoacrylate glue to effectively shorten the exposed region while keeping the length of the jacketed region constant. The electrical circuit used is described in more detail in section 7.2, but briefly, the sensor electrodes were placed in series with 68 kΩ resistors in a Wheatstone bridge powered by a 1V 1 kHz AC supply, and the voltage drop across the bridge was amplified (G = 100) and measured. The results of the pressure test are summarized in Table 6.2. The behavior of the real sensor tends to follow the model. As the length of the exposed region decreases, the pressure sensitivity generally increases.

Exposed region: jacketed region ratio	**Voltage change (mV)**
1:4	4.446
1:2	56.671
1:1	9.423
3:2	3.901
2:1	<1

Table 6.2. The relative sensitivity difference of the experimental CRISP sensor by changing the length of the exposed region when tested from 0-5 psi (258.6 mmHg). The voltage change in the 2:1 test was on the order of the noise level.

For example, as Table 6.2 shows, even at a modest ratio of 2:1, the sensitivity is so low that it is unperceivable from the background noise. However, when the exposed region was shortened to be half the length of the jacketed region (2 mm), the sensitivity was much higher. One notable deviation from this was when the length of the exposed region was 1 mm (1:4). It is believed that the length of the exposed region was too short to the point that the tube cannot deform. The amount of deformation is related not only to the cross sectional area of the elastic tube, but also the overall length as it is much easier to deform a long tube than a short one. Therefore, there are other considerations aside from the model when fabricating the sensor. Another practical

consideration is the overall length of the sensor. While it may be tempting to fabricate a sensor with a very long jacket and a short, stubby exposed region, this would not be practical in an actual medical deployment since catheters need to be flexible enough to snake through a tortuous pathway for implantation, and the jacket itself is too rigid. Based on these tests, it was concluded that the ideal sensor design would have a jacketed region twice as long as the exposed region and a thin and compliant tube with a diameter that is as large as is practically possible.

Chapter 7 Sensor Fabrication

7.1 Sensor fabrication

The fabrication techniques and materials of the CRISP sensor have changed considerably over time, but the final solution of the sensor is described below. As been described previously [61], three Teflon-insulated platinum wires (A&M Systems) 50-μm thick were modified in such a way that the 5 μm of Teflon was burned off to reveal bare metal at the tip of the wires to create electrodes. Specifically, one wire, which corresponded to the "tip" wire, was exposed 2.5 mm from the tip; the other two wires—the "mid" and "base" wires—were exposed 5 mm from the tip. Platinum metal was chosen for its inertness; the lack of electrochemistry at the electrode surfaces when coupled with an AC excitation signal results in drift-free and stable voltages. The wires were inserted into one end of a silicone (Silastic) tube (Dow Corning), measuring 22.5 mm long and having a 1.19 mm outer diameter and a 0.635 mm inner diameter, and arranged so that the tip wire spanned the entire length of the tubing. The mid wire was inserted 15 mm into the tube, and the base wire was only inserted 5 mm into the tube. Silicone was chosen for its superior elastic properties, wide availability, cost, and its biocompatible nature, which is integral in any implantable medical device.

Polydimethylsiloxane (PDMS) (Nusil Med-4011) is applied to the base of the silicone tubing to affix the wires in place and to act as a sealant of the base of the tube. Med-4011 was the preferred PDMS since its high viscosity limited the amount of material sucked into the tube by capillary forces regardless of how much rubber was added. When using a less viscous PDMS,

too much material applied to the end of the tubing resulted in the shortest wire being completely encapsulated in silicone. Because silicones can only chemically bond onto other silicones, it was found that PDMS was the only appropriate sealant for this application. This was proven when various sealants and adhesives were tested by sealing one end of a silicone tube, which had the same dimensions of the tube used in the sensor. The tube was filled with 1 M KCl and clamped on the other end and submerged in deionized water, which was confirmed to have a conductivity of 0.0 μS/cm using a conductivity meter (Oakton con510). The conductivity of the water bath was measured again 24 hours later for leakage of the hyperosmotic solution out of the silicone tube, and the results are listed in Table 7.1.

Sealant	Final conductivity (μS/cm)
Nusil Med-4011 PDMS	0.5
Loctite 401 cyanoacrylate glue	10.7
E-bond 4-min epoxy	5.0
Parbond 1501 epoxy	7.9
Parbond 905 urethane	6.3

Table 7.1. The final conductivity of deionized water exposed to a sealed silicone tube filled with 1 M KCl.

It is believed that non-compatible sealants will form micro-channels when cured at the interface between adhesive and the silicone tube wall, resulting in a slow leakage of liquid.

A thin coat of Viton (Pelseal PLV2040), a fluoroelastomer (vinylidene fluoride-hexafluoropropylene copolymer) developed by Dupont, is applied to the silicone tube to act as a barrier against evaporation of the electrolyte solution. Dimethyl siloxanes are notorious for their gas permeability; this necessitates the use of a gas impermeable coating to ensure the sensor's functionality during the final sealing step. As an example, the oxygen permeability of siloxane is 6×10^{-8} $cm^2/s \cdot cmHg$ whereas the permeability of Viton is 1.45×10^{-10} $cm^2/s \cdot cmHg$ [62, 63]. Fluorocarbons, fluoroelastomers, and other fluorinated polymers are also well known to be bio-

inert and have been used in dental applications and in implants [64-66], which makes it suitable for *in vivo* use.

Once the Viton has dried, the tube is threaded through a 14-gauge hypodermic needle tube (2.11 mm OD, 1.70-1.83 mm ID) 15 mm long and arranged such that the back edge of the metal jacket tube was flush with the base of the silicone tube. The metal jacket is then sealed to the elastic tube with 4-minute epoxy (E-bond). Epoxy is also applied to the tip of the elastic tube 2.5 mm from the tip. This is done to force the tube to compress in between the electrodes, maximizing sensitivity. The silicone tube is filled with 50 mM KCl solution, and the open end of the tube is sealed with a bead of PDMS, which is allowed to cure in room temperature for nearly 15 hours. Although PDMS cures faster at elevated temperatures, the water evaporates out of the tube faster as well. Also when allowed to cure in a humid environment or even underwater, the final silicone seal often had a pinhole in it. It is believed that the increased vapor pressure within the silicone tube was enough to overcome the viscosity of the liquid PDMS and form a hole to allow vapor to escape. However, such holes did not form when the PDMS was cured in room temperature. Once cured, the sensor is stored underwater to prevent any further evaporation out of the elastic tube for the duration of its lifetime.

7.2 Circuit Design

The circuit used in conjunction with the sensor is depicted in Figure 7.1. Briefly, an AC wave is used to power the Wheatstone bridge that is connected to the sensor. Alternating current was chosen because of the stability of the magnitude of the electrical current in solution. While direct current (DC) power is often used with silver/silver chloride electrodes to measure electrical conductance in solution, in this application, it was found that the expected current was too high, resulting in significant electrode drift. DC power across a galvanic cell results in the

cathode being plated with material while the anode is stripped, resulting in voltage offsets—the rate of formation of which is proportional to the electrical current. Because the polarity of the galvanic cell is reversed at a high frequency when powered by AC, no such offsets formed in an appreciable amount. The frequency and amplitude of the AC potential were arbitrarily chosen. To make things simple, a sine wave with amplitude of 1 V at 1 kHz frequency was supplied by a function generator (Agilent 33120A).

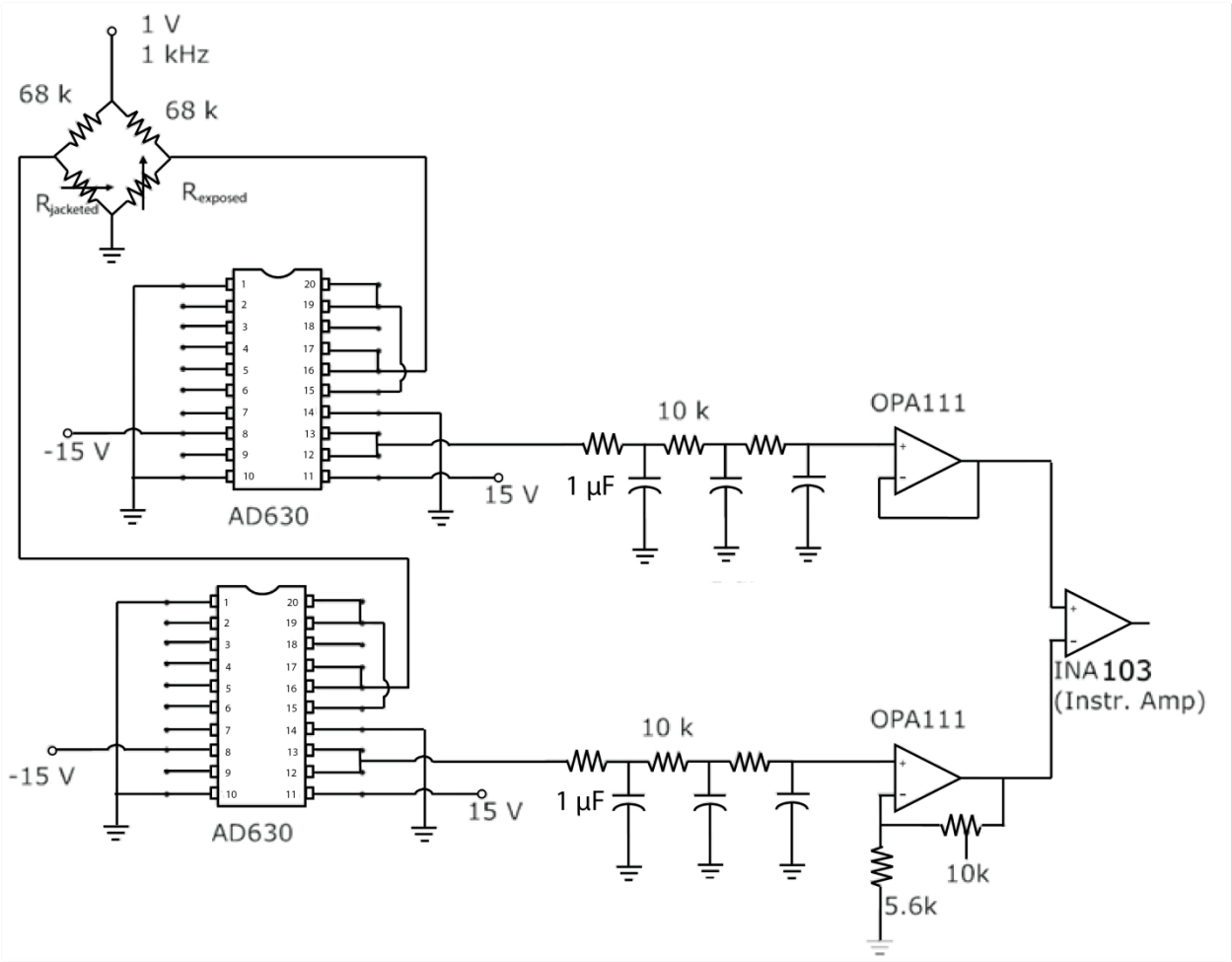

Figure 7.1. A circuit diagram depicting the Wheatstone bridge configuration of the sensor, the demodulation of the carrier wave, and the amplification of the pressure signal.

Each region of the CRISP sensor was placed in a leg of a Wheatstone bridge such that the bridge output was equal to the difference between the voltage drops of the exposed and jacketed

regions. The value of the resistor (68 kΩ) used in each voltage divider circuit was chosen to closely resemble the electrical resistance of each region the closest in most cases. Each section of the AC bridge signal is immediately converted into DC using a demodulator IC (Analog Devices AD630) and a series of three passive low pass filters with a break frequency at ~16 Hz [67]. The signal corresponding to the jacketed region is then amplified with a non-inverting amplifier to match up with the signal of the exposed region since the conductance of the jacketed region has historically been higher than that of the exposed region. In the case that the exposed region is more conductive, the regions are simply reversed and the final data output is inverted. Amplifying the lower resistive region was opted for over adjusting an offset resistor since the temperature sensitivity of both regions would better match if the base resistances were equal. An offset adjustment would not change the temperature sensitivity, which can cause the sensor to drift. Finally, a dual supply instrumentation amplifier (Texas Instruments INA103) with a gain of 100 measures the difference of the two voltages. Although the Analog Devices specification sheet for the AD630 recommends demodulation after amplification for an AC bridge circuit [67], which uses fewer components, it was determined that very few instrumentation and operational amplifiers were able to properly amplify high frequency AC voltages. Therefore, it was decided to convert the AC into DC as quickly as possible to allow a wider variety of IC to use.

7.3 Data acquisition and logging data

The voltage from the sensor amplification circuit was fed into a digital acquisition board (National Instruments PCI-6289) plugged in a desktop PC computer. A custom LabVIEW 8.0 program was developed to read, record, and plot the data from the CRISP sensor as well as from other commercial transducers under the same pressure, including a NIST-calibrated absolute

pressure gauge (Omega PX309-005AV) and a commercial medical pressure transducer (Utah Medical Deltran IV) for comparison purposes. Figure 7.2 depicts the front panel of the program. The front panel features a dual-axis graph of the real-time sensor output and pressure (mmHg) read by the data acquisition board. The filtered numerical values of both are also shown.

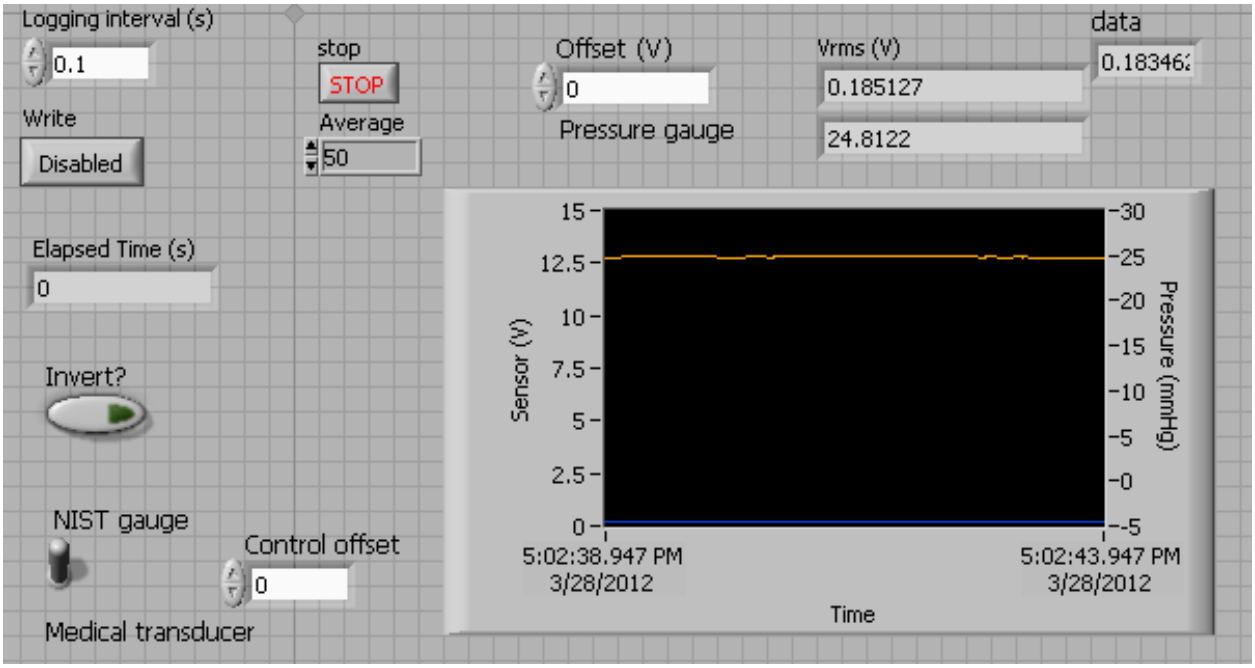

Figure 7.2. The front panel of the LabVIEW program, which reads, plots, and records data from the CRISP sensor and a commercial pressure transducer.

The front panel also controls many other aspects during the experiment, such as the amount of data that is written, a manual write switch, the amount of averaging on the data set, a choice of pressure standard, offset controls for both the sensor and standard, and an option to invert the pressure data.

Figure 7.3 shows the block diagram of the LabVIEW program. Section I contains the code required to acquire data. Two acquisition sub-VIs are used with each reading either the test sensor output or the pressure transducer output. During an iteration of the loop, the data is read serially—the data from the sensor is read first before that of the pressure transducers.

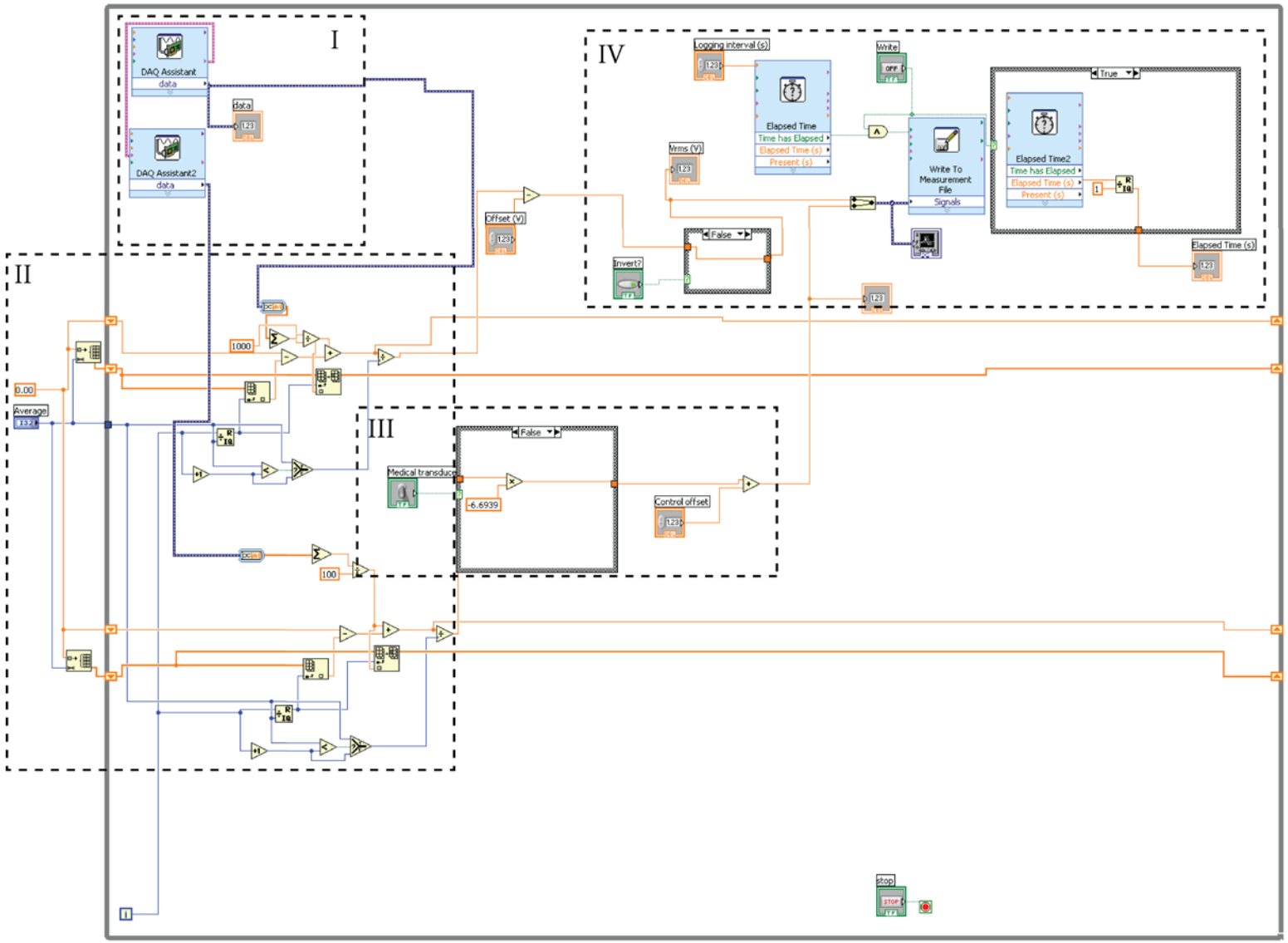

Figure 7.3. The block diagram of the custom LabVIEW program showing the controls used to acquire, smooth and write data, as well as control the pressure standard.

Although there will be some lag between each measurement, and thus it isn't technically a simultaneous measurement, the iteration occurs so fast that the time difference is about 0.01 seconds, which is miniscule relative to the time scale required for physiological use. One advantage of using serial acquisition over parallel acquisition is that different sampling rates can be used for the sensor and reference sensors. When using a parallel process with LabVIEW, it is impossible to specify different acquisition parameters for each data input channel since the parameters are used for all channels within each sub VI. Taking advantage of this, the commercial pressure transducer is read 100 times at a sampling rate of 100 kHz in one loop of the program. On the other hand, the CRISP sensor is sampled at 100 kHz with 1000 samples in each iteration loop. The signal from the sensor is generally noisier than the commercial transducer, so more a higher sampling rate and more data points are required to smooth the signal while still maintaining a good dynamic response and high sensitivity. Therefore, the entire iteration takes nearly $1/100^{th}$ of a second.

Section II of the LabVIEW program filters and smoothes the raw data from the sensor and reference pressure transducer data. Although the data acquisition board has an 18-bit analog-to-digital (ADC) resolution [68], which translates to 70 mV, in practice, the peak to peak voltage of the noise coming from a DC signal is on the order of several hundred microvolts as shown in Figure 7.4. If left unfiltered, the signal to noise ratio for the sensor would be too low, and in order to achieve a resolution of ~1 mmHg, the data needs to be smoothed out. Data smoothing is done in two parts: first, all the measurements within each iteration are averaged together and second, a moving average of the previously averaged points is calculated. As shown in Figure 7.4, merely averaging all the data points acquired in each iteration reduced the noise from hundreds of microvolts to a tenth of the raw data. A 50-point moving average applied to the

previously averaged data reduced it further by another tenth. The amount of points in the moving average is controllable by the user with the front panel, and it ranges from 50 points for static pressure testing and calibration testing to 1 point or effectively no moving average for dynamic pressure and *in vivo* testing. It should be noted, however, that a moving average will attenuate any real frequency information the sensor may pick up, which is undesirable for dynamic pressure studies.

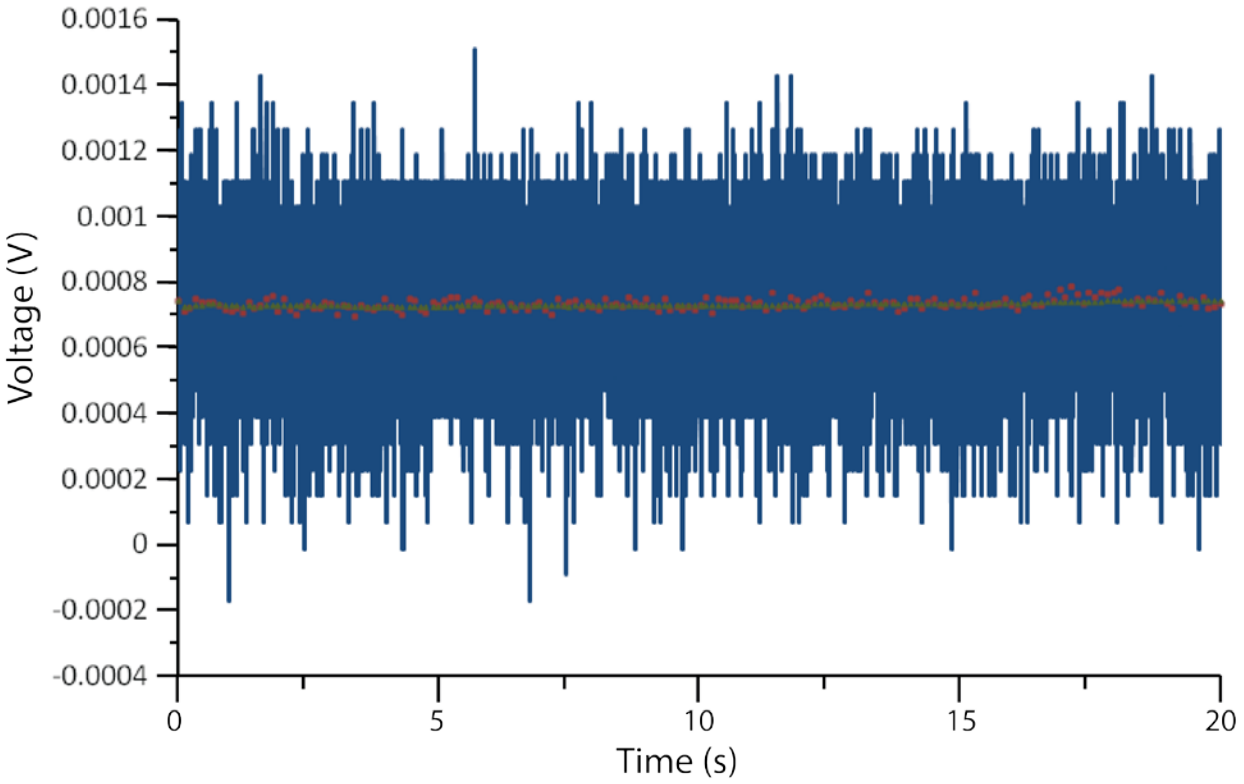

Figure 7.4. Noise comparison between a raw signal (blue), an averaged signal (red), and a signal with a 50-point moving average applied to the averaged signal (green).

Unfortunately, at the range of physiologically relevant heart rates, the attenuation is heavily dependent on frequency. Thankfully, the majority of the smoothing is achieved in the first step, which is not frequency-dependent since each iteration loop occurs much faster than that of a heartbeat. Also, because the amplitude of the pressure wave is fairly large, more noise is

acceptable. In a static test, a clean signal is required to clearly delineate small pressure jumps, the further smoothing is necessary.

Two pressure commercial transducers are used as controls during experiments with the experimental CRISP sensor. The LabVIEW program can read either commercial transducer and convert the data from both into pressure; this is controlled in section III. A simple toggle switch and if-then logic gate determines which conversion to utilize. Section IV allows the operator to specify the rate at which data is logged. If the program was left to write as fast as the computer was able to, the data would be too large, crashing the computer. For static testing, the data was logged at 10 Hz in order to keep the data file small while still fully replicating the pressure profile. Dynamic testing of 1-3 Hz pressure waves required a higher sampling rate to replicate the wave, so 20 Hz was typically used although, as can be seen in section 9.2, 20 Hz was not fully capable of replicating a 3 Hz wave. Therefore, the logging rate was set at 63 Hz, the highest sampling rate the computer would allow, for *in vivo* studies to achieve the highest fidelity of the arterial pressure wave.

Chapter 8 *In Vitro* Testing

Sensors were generally tested and characterized first after assembly by powering up and keeping it in a static environment for some time while checking for drift and unsteadiness in the signal. This *in vitro* test was conducted in a controlled environment. It was a quick method to determine the integrity of the packaging and whether or not evaporation had occurred. Generally, drift and excessive signal noise were the result of leaks in the seals as the electrolyte escapes the elastic tube. Furthermore, the drift and noise were observed over multiple days to ensure the sensor exhibited a stable baseline voltage, meaning no evaporation had occurred and no leaks were present.

8.1 Gas Testing and Temperature Effects

Initial *in vitro* testing of the CRISP sensor focused on looking for any sensitivity to pressure, reversibility, and repeatability. These tests were performed with the sensor placed in a beaker filled with water. This is then placed inside a sealed chamber filled with pure nitrogen or oxygen gas and venting the chamber back to atmospheric pressure. A NIST-calibrated absolute digital pressure gauge (Omega DPG5600B-30A) provided the reference pressure inside the chamber. Early iterations of the CRISP sensor featured only two electrodes—one at the tip of the sensor and one at the base of the sensor. The general belief was the constriction of the exposed tubing contributed more to the overall electrical resistance of the tube than the expansion of the tube inside the jacketed region. Measuring an unamplified sensor in this manner is shown in Figure 8.1. As shown in Figure 8.1A, the sensor has a resolution of 0.5 psi (25.9 mmHg) and range of 0-5 psi (259 mmHg), which is the range necessary for all blood pressure transducers [69].

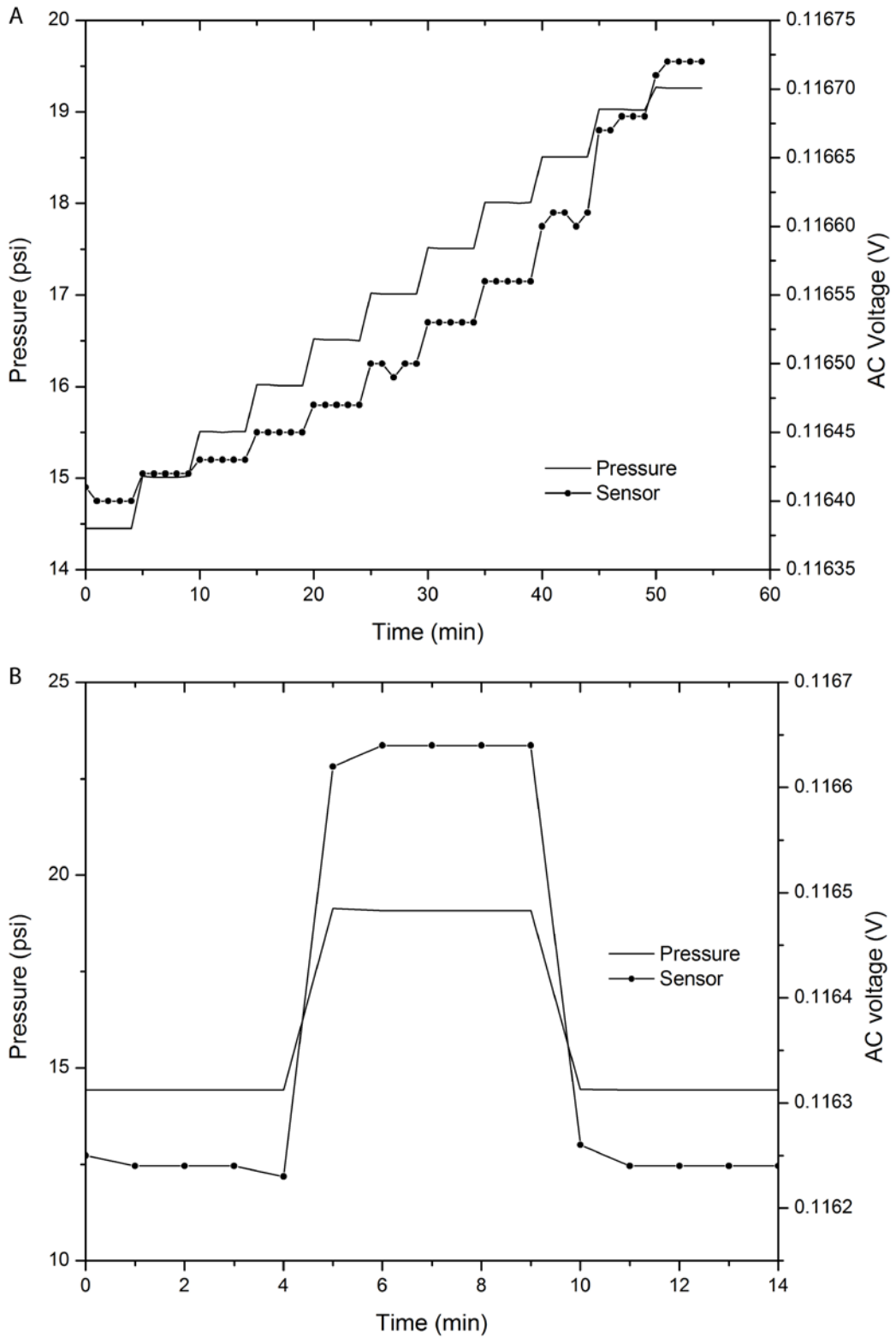

Figure 8.1. A) Sensor voltage as a function of stepwise pressure increases from 14.5-19 psi (25.9 mmHg) with 0.5 psi resolution (259 mmHg) B) A demonstration of the reversibility of the sensor when the pressure is quickly changed from 14.9-19.9 psi back down with little electrode drift.

However, with the resolution less than 100 μV, amplification and more sensitivity was clearly needed since the ultimate goal is to have a resolution of 1 mmHg. Figure 8.1B illustrates the reversibility of the sensor and the lack of drift when held at a constant pressure, validating the use of alternating current and platinum electrodes.

However, in a demonstration of repeatability, the sensor failed to demonstrate repeatability when the pressure inside the chamber was modulated from 0-5 psi in quick repetition. The sensor exhibited a noticeable drift in between sudden pressure increases and venting as depicted in Figure 8.2. When an NTC thermistor was placed in the water bath adjacent to the experimental sensor, it was soon discovered that the temperature inside the water bath changed very slightly during the course of the experiment. It is well known that the temperature affects the electrical conductivity of water dramatically [70], and while the temperature and corresponding electrical resistance change were not large overall, it is significant relative to the resistance change due to pressure differences. Also, as shown in Figure 8.2, the sensor seemed to lose pressure sensitivity although this may have been an additional effect of the temperature change.

Several options were investigated to eliminate the impact of temperature drift. First, the drift could be characterized and mathematically removed if the temperature of the sensing medium was constantly monitored. Another option was to integrate a non-pressure sensitive tube of electrolyte solution that would experience the same temperature changes. When arranged in a Wheatstone bridge, the sensor and temperature compensator would negate the temperature sensitivity. However, these ideas were not practical for multiple reasons. Each sensor would have to integrate another component, which makes the fabrication of each sensor more difficult and

complicated. Also the added components increase the bulk of the device, which needs to be minimized, especially if the sensor is to be scaled down enough to enter a small blood vessel.

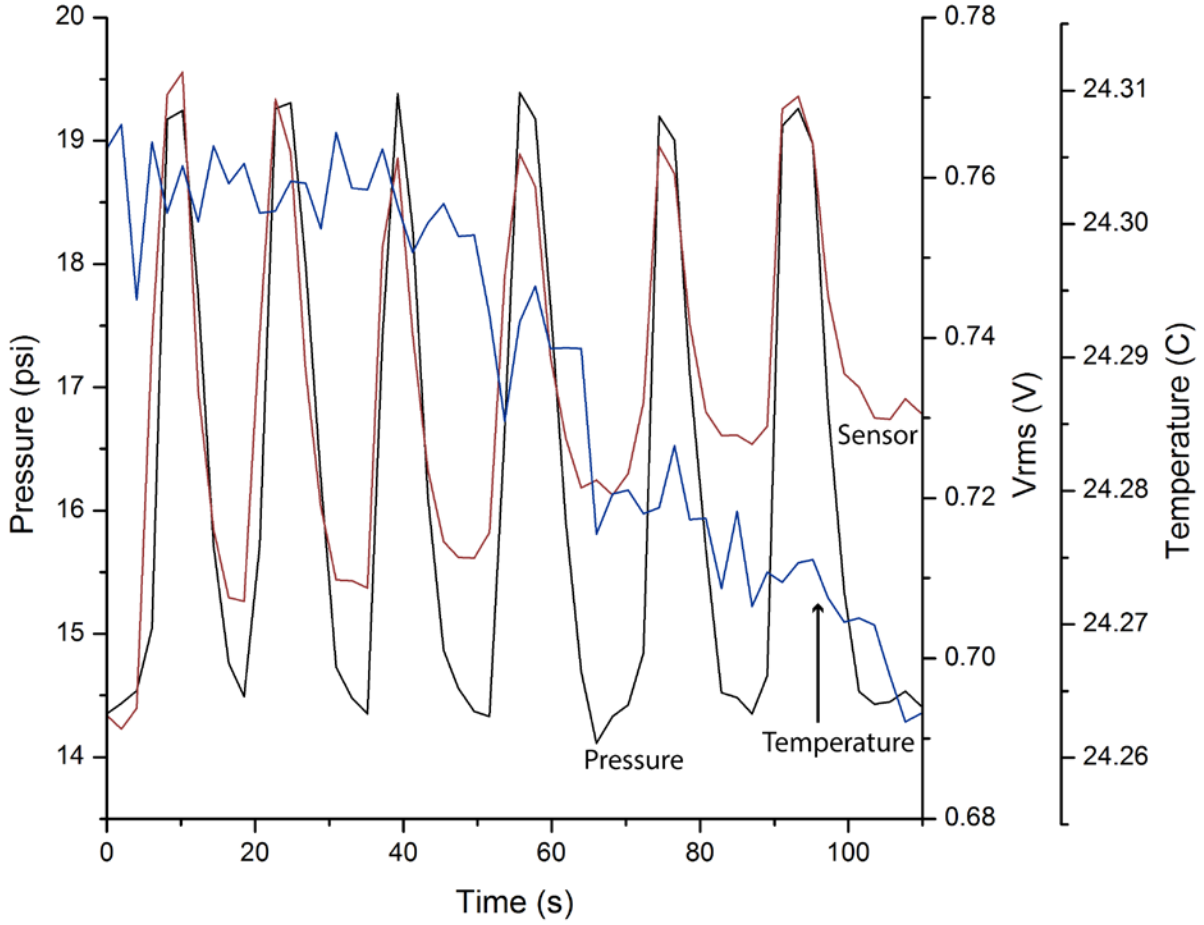

Figure 8.2. The response of a two-lead sensor to pressure and temperature.

In the second case, to make a completely pressure-insensitive tube may also alter the thermal conduction properties of the tube, making the compensator less effective.

Instead, the most ideal solution was the design described previously since it not only negated temperature sensitivity, but also increases pressure sensitivity. The sensor was split into two regions; in one region the elastic tube collapsed and in the other, the elastic tube expanded in response to an increase in pressure. However, both regions were interconnected, and the electrolyte solution freely flowed from one region to another, so any change in temperature that

occurred in the electrolyte solution in one region was quickly transferred into the other region. Therefore, the change in electrical conductance from temperature change was nearly the same for both regions at any given time. Also, the fabrication of the new sensor was not any more complicated than a 2-wired sensor. In addition, the only components required to create this compensator was one extra platinum wire, minimizing any added bulk. As shown in Figure 8.3, the CRISP sensor's temperature drift was minimized, maintaining consistent pressure sensitivity. The gas tests ultimately were vital in determining the correct sensor design. However, there were several problems with gas testing. First, it took a long time for the chamber to pressurize, especially for large pressure increases; second, it was difficult to set the correct pressure quickly and precisely.

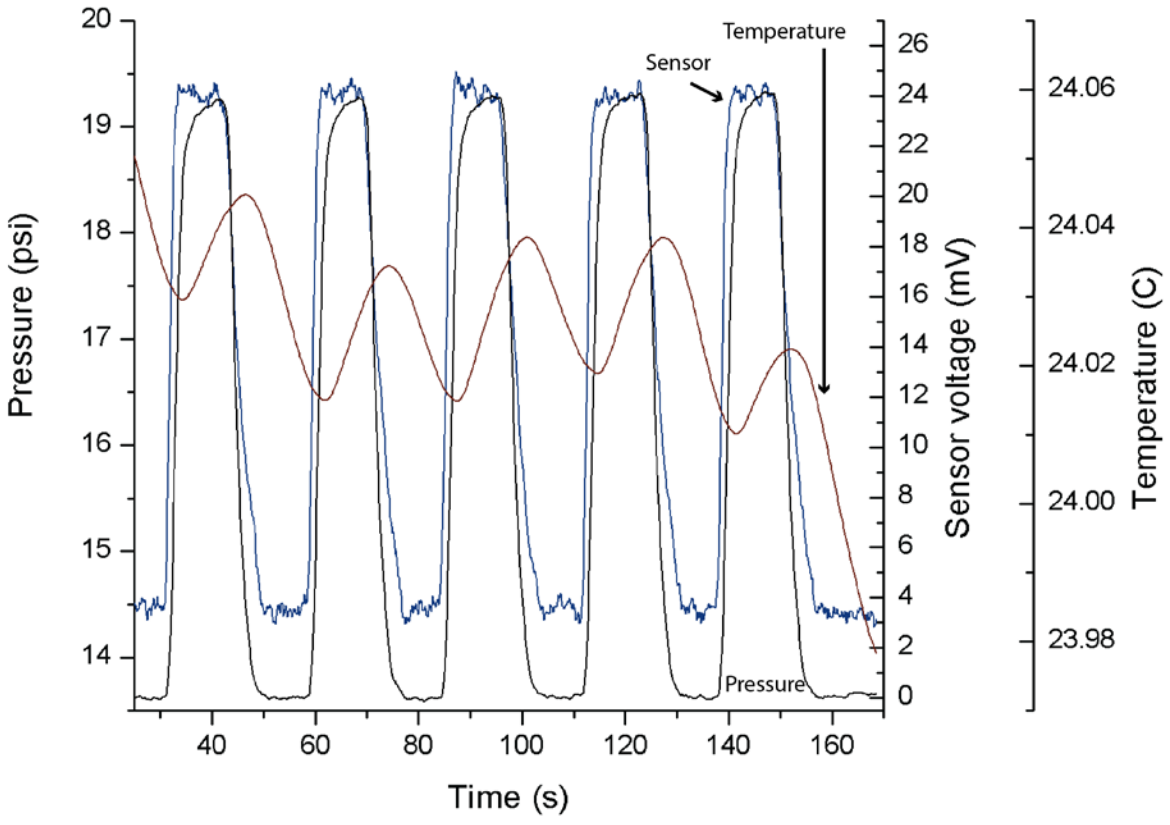

Figure 8.3. The pressure and temperature sensitivity of the temperature-compensated CRISP sensor.

Third, the experiments required venting the chamber to atmospheric which was even slower and less precise than the initial pressurization when testing for reversibility. In addition, the speed at which venting occurred depended on the pressure difference between the chamber and atmospheric—smaller differences vented slower. Therefore, for dynamic studies and for static pressure testing requiring quick and precise small pressure changes, another method was necessary.

8.2 Static pressure testing and calibration

Pressure can be controlled by a column of water since pressure is dependent on air pressure and depth. Also one inch of water corresponds to 1.82 mmHg, so pressure can be changed in small increments very easily provided that the column of water has a fairly small volume. Figure 8.4 depicts a testing chamber designed based on this principle. The Omega PX309-005A gauge was attached to one end of a horizontal tube with the other end capped with a small hole drilled through. The sensor was fed through the hole and sealed off using silicone RTV (Dow Corning 732). A T-junction in the middle of the tube connects a long vertical column. All the components and fittings were made from clear PVC. The vertical column measures only 13 inches high, corresponding to ~24 mmHg. It was reasoned that the static testing of the sensor at a smaller pressure range is a higher standard for satisfactory performance than is encountered in physiological conditions, which is expected to be a periodic pressure wave with amplitude of 40-50 mmHg.

At the start of each test, only the horizontal tube was filled with water. The sensor was left powered for 10 minutes to allow the sensor to stabilize from any drift that occurs from heating when the AC current is applied. It was empirically discovered that sensors that tested

well and consistently stabilized very quickly. Sensors that continued to drift or had unsteady or unstable signals were believed to have had another source for the electrical drift, and it usually was attributed to poor sealing of the silicone tube. These sensors were put aside for later testing since it had also been experimentally discovered that some sensors would eventually produce signals that were steady and drift-free. This effect, if it occurred, took no longer than a week to settle, and if not, the sensor was discarded and remade. Assuming the sensor had passed this checkpoint, static pressure testing ensues. While recording in LabVIEW, with the control being set to the NIST-gauge, a 50-point moving average, and logging at 10 Hz, water was added to the vertical column inch by inch, corresponding to a 1.82 mmHg pressure increase for each step; the pressure was held at each step for 10-15 seconds. The sensor voltage value that was being simultaneously read by LabVIEW was recorded manually. As shown in Figure 8.5, the data was "zeroed out" to remove all offsets that may have been present and effectively forced the sensor to become sensitive to pressure relative to atmostpheric pressure. This adjusted value was then plotted against the pressure to generate a calibration curve. The LabVIEW data was also used to generate a time-dependent plot of the sensor and pressure to check for drift, noise, and any time lag during pressurization steps.

Figure 8.5A depicts the sensor's response with respect to time. Drift was minimal over the course of the experiment, and no appreciable change in voltage signal occurred when the pressure was held constant. The sensor also had a sensitivity of 1.42 mV/V/mmHg. The peak-to-peak voltage of the electronic noise was 681 μV, which corresponds to 0.48 mmHg. Thus, if the resolution limit was defined as twice the noise voltage, that would result in a pressure resolution of <1 mmHg.

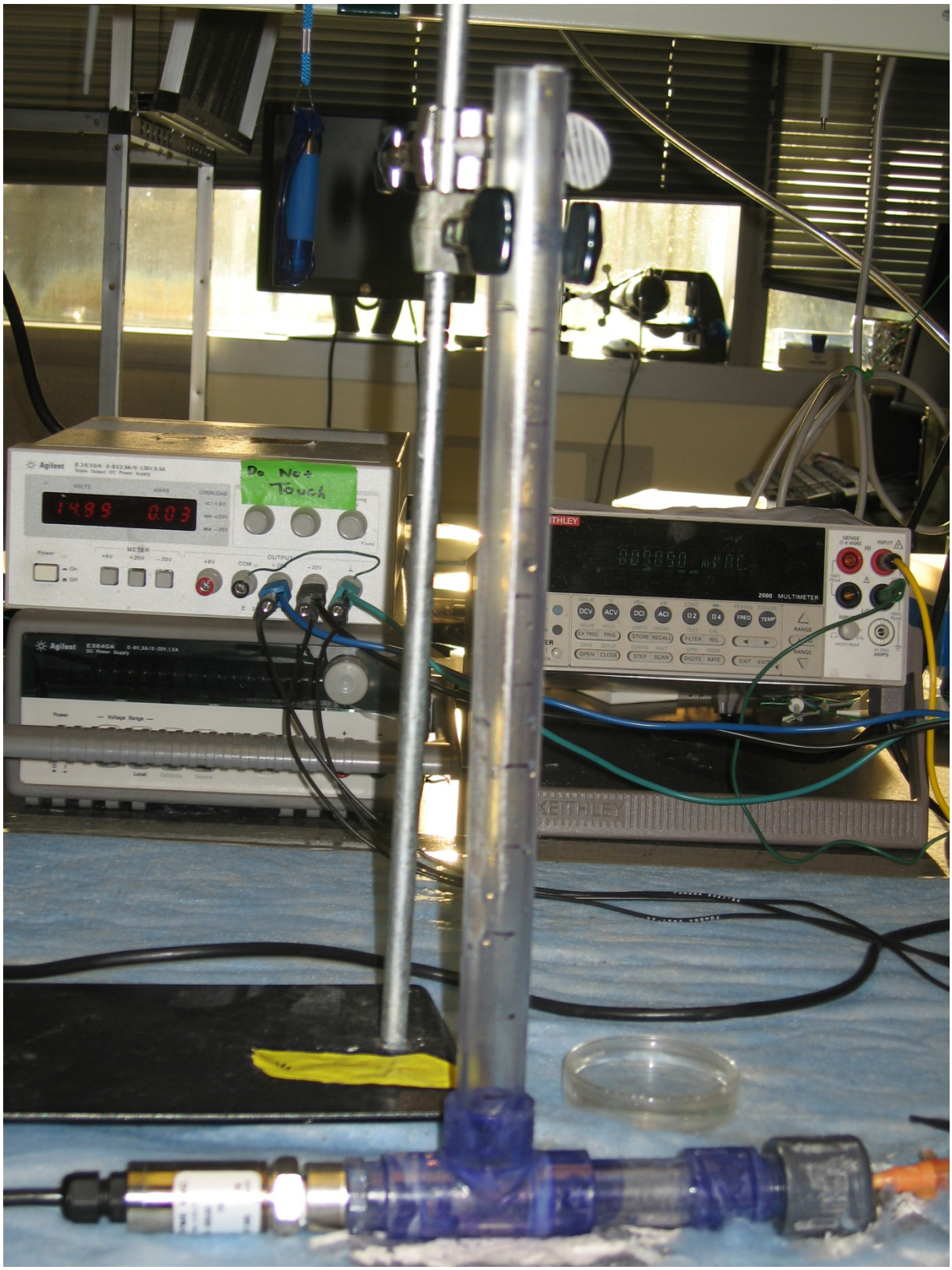

Figure 8.4. The experimental setup for static testing of the pressure sensing using a water column. A catheter port is inserted into the cap where the sensor is normally threaded through.

The sensor, thus, performs comparably to current standard solid state *in situ* blood pressure monitors, such as Millar's catheter. In a clinical setting, the noise level of the Millar catheter was calculated to be nearly 1 mmHg [11].

This test was performed over a course of several days or weeks to test the long-term stability of the sensor without changing the variable gain resistor on the non-inverting amplifier. By plotting the pressure versus sensor voltage data during the test period, the sensitivity of the sensor can be monitored and verified to ensure that any calibration that is used will still be valid for experiments run weeks into the future. To test overall lifetime, a sensor was tested for a period of three weeks; at the end, testing on that sensor ceased since it was believed that the lifetime was adequate. While the baseline voltage at atmospheric pressure does vary day to day and can be zeroed out simply by adjusting the offset in LabVIEW, the sensitivity of the sensor needs to stay consistent. As shown in Figure 8.5B, the slope of the linear regression of the voltage versus pressure data points stayed pretty consistent. Long-term testing is useful for qualifying sensors with good seals since over time, sensors with inferior seals will leak out the salt stored inside the silicone tube by osmosis. In this case, the baseline conductances of both the exposed and jacketed regions would increase over time. Eventually, the Wheatstone bridge would become progressively more unbalanced, the final instrumentation amplifier would saturate, and the sensor would no longer work and required recalibration. For most sensors that displayed stable signals, had good pressure sensitivity, and showed little to no drift over time, the sensitivities remained constant over the course of testing, and so, eventually, testing and evaluation of sensors was reduced to 2-3 days. Many CRISP sensors have been destroyed while inserting or removing the sensor from the test apparatus due to the fragility of the platinum wires and the use of threaded fittings in the testing apparatus.

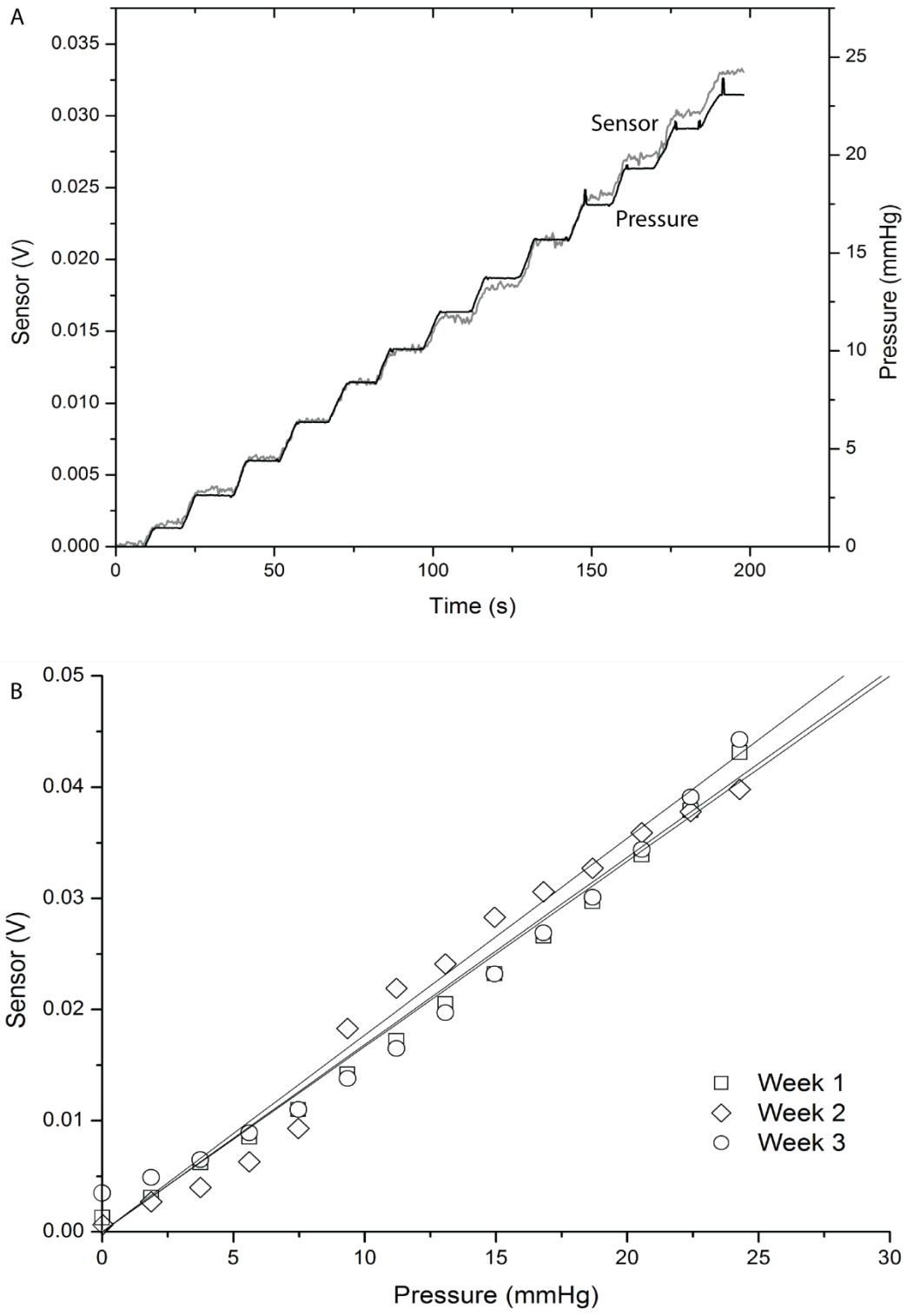

Figure 8.5. A) depicts the time-dependent data of pressure and sensor output for the sensor in its 2nd week of testing. B) Sensor output as a function of pressure of the same sensor over the course of three weeks. The squares represent the calibration curve during the 1st week ($V = 0.0016P$, $R^2 = 0.99$); the diamonds correspond to the 2nd week ($V = 0.0017P$, $R^2 = 0.9769$), and the circles represent the 3rd week ($V = 0.0017P$, $R^2 = 0.9765$).

Therefore, the risk of damaging a well-performing sensor was minimized if the amount of testing of that sensor was limited.

8.3 Dynamic Pressure Testing

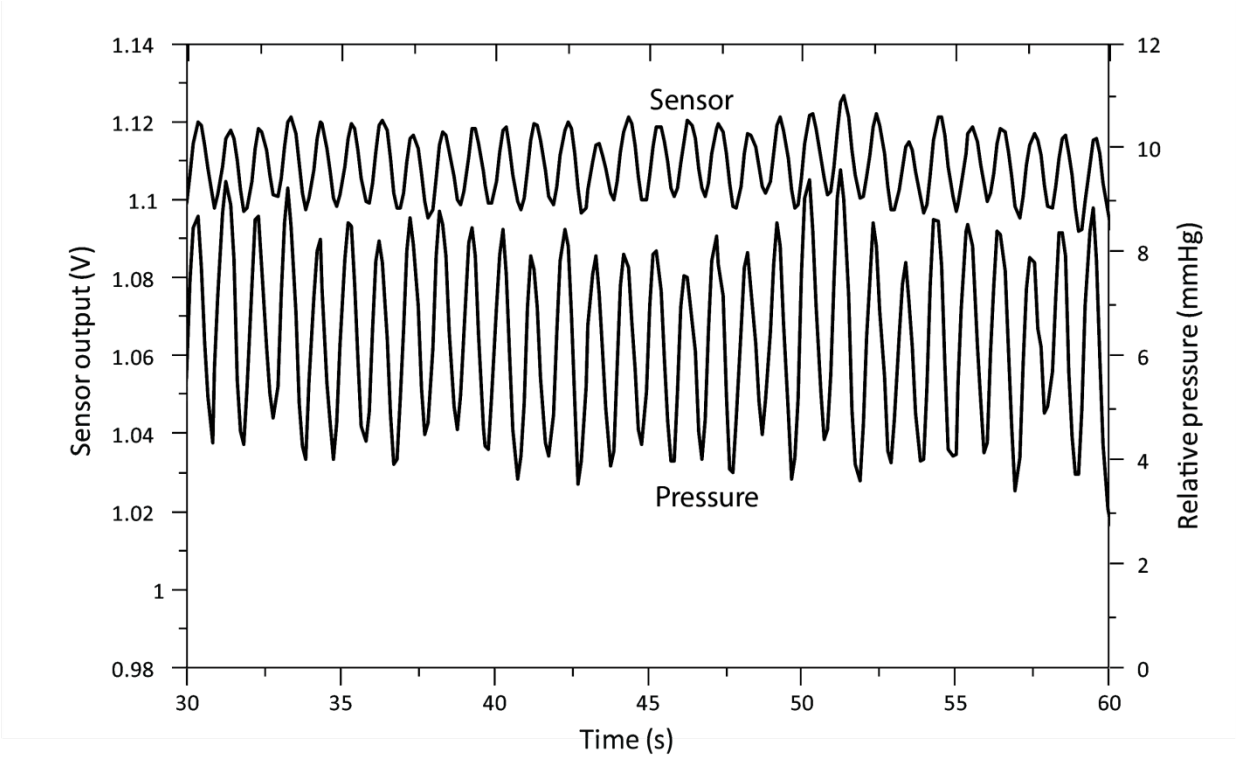

Figure 8.6. A dynamic pressure test using a manually rotated column of water actuated at 1 Hz. The sensor voltage data and pressure data measured from the pressure gauge are taken simultaneously.

Although static testing is useful for determining sensor stability and drift, it does not adequately test for dynamic pressure response, which is critical for arterial blood pressure sensing. This was initially done with another water column setup with a maximum pressure of 25 mmHg using the NIST gauge that was manually rotated from being completely flat to completely vertical. Figure 8.6 represents a typical pressure test performed at 1 Hz. The dynamic response of the CRISP sensor is comparable to the commercial NIST-calibrated gauge, suggesting that the

test sensor would be able to sense arterial blood pressure just as well as a commercial pressure transducer.

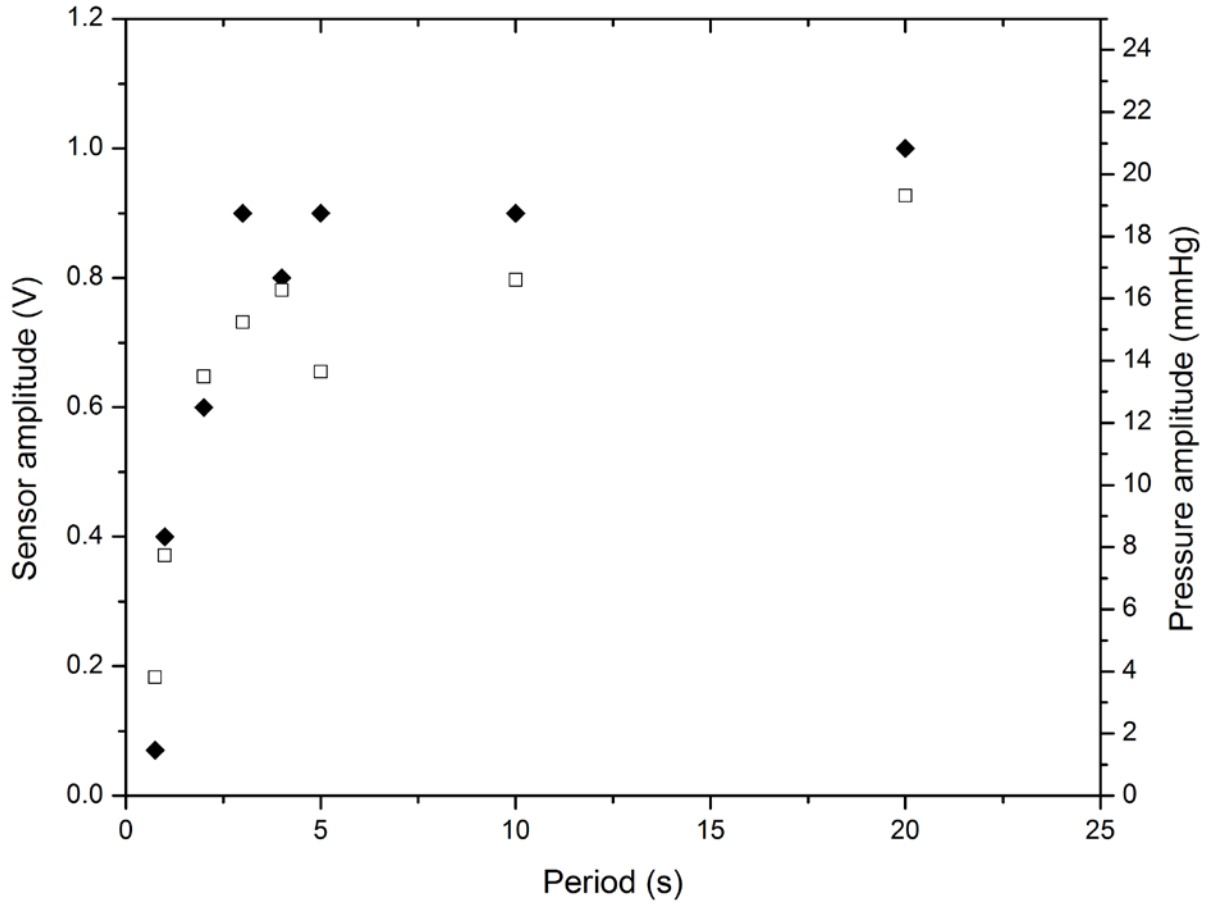

Figure 8.7. The amplitude of the pressure (white square) and voltage (black diamond) waveform from the sensor as the frequency (period) of the pressure waveform is varied.

However, there were several problems from using this setup. For one, being manually powered the frequency and amplitude of the pressure waves couldn't be kept constant. Also, it proved to be very difficult to actuate greater than 1.5 Hz, and at high frequencies, the variation of the frequency and amplitude became worse as it became more difficult to consistently attain the same elevations during each rotation. As shown in Figure 8.6, the median pressure value is not constant as seen in both the sensor and the commercial transducer. This is surely attributable to operator error.

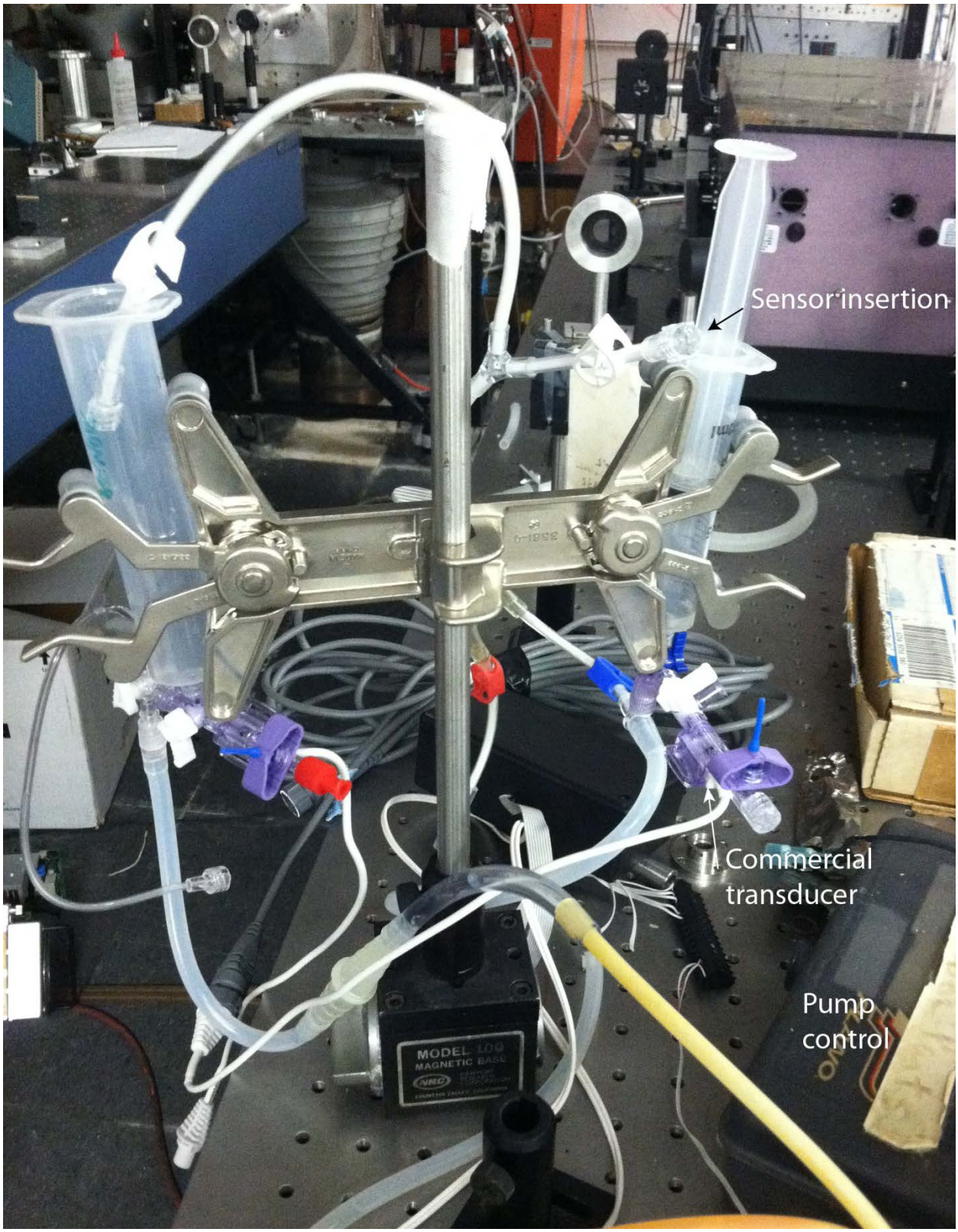

Figure 8.8. The cardiac system simulator in Dr. Peyman Benharash's lab used to simulate dynamic pressure for the CRISP sensor. The pump driving water through the system is off screen. Photo credit: PJ Rezzai.

Furthermore, as the frequency increased, it became necessary to rotate at shorter radial distances, leading to smaller pressure waves as illustrated by Figure 8.7. To ideally mimic blood pressure, a pressure wave needed to be actuated with a frequency of 1-3 Hz (60-180 bpm) and amplitude of 40-70 mmHg. Therefore, with this testing method, it was impossible to correctly replicate an arterial pressure wave. Finally, the placement of the sensor in the water column introduced a lot of stress on the small fragile wires. Many sensors were inadvertently destroyed while using this testing apparatus, so for characterizing sensors destined to go into an animal, this testing method fell out of favor. Therefore, dynamic testing of these sensors required a different approach.

Working with Dr. Peyman Benharash, a physician at the Department of Thoracic and Cardiac Surgery, the sensors were dynamically tested in a simulator designed to replicate the blood pressure anywhere in the cardiac system. The output pressure waveform was controlled by LabVIEW and could be configured for any frequency and amplitude, but typical measurements were conducted at 1 Hz and 75 mmHg. The sensor was placed in an area corresponding to the aorta and secured via a Luer connection. A commercially available medical transducer acted as a control, but unfortunately, it was read and the data was logged on a separate machine, so in order to obtain simultaneous and synchronized measurements, precise timing was required; an easily identifiable change in pressure profile was also helpful to determine the timing differences surrounding between the sensor and commercial transducer.

Chapter 9 *In Vivo* Testing

9.1 Changes in Design and Fabrication for *In Vivo* Use

In vivo use of the CRISP sensor requires the sensor to be packaged differently to be able to successfully implant them. The sensors were always designed to go through a catheter port, which features a one way valve and sheath that is inserted into an artery and into the blood vessel. It is a tortuous path that requires ample protection for the elastic tube and certain stiffness to push through the catheter port into the artery and thin enough to easily slip through the port and artery. The aforementioned CRISP sensors would not be viable for *in vivo* use for several reasons. One, the exposed elastic tubing at the tip of the sensor was floppy and could not pass through the valve. In fact, previous animal studies used this exposed design, and in order to insert the sensor, the valve had to be bypassed with another catheter sheath. As a result, blood gushed out of the port, which is undesirable since copious amounts of blood can have negative effects on the electronics by shorting out connections and even corroding metal, as well as causing unnecessary blood loss. Second, by using liquid adhesives like epoxy or glue as seals, an excessive amount was previously required to ensure good sealing. However, before being fully cured, the adhesives tended to flow and accumulate in certain areas due to gravity depending on how the sensor was oriented during curing. As a result, the seals had a much wider girth than the metal jacket, making the sensor difficult if not impossible to push through a catheter sheath or blood vessel. The obvious solution was to carefully apply the adhesive or even sand down the cured epoxies to size, but often, the seals failed and the sensor was rendered inoperable. Therefore, in order to solve both issues, the rigid jacket and a scaffold for the exposed tip were devised from one piece of hypodermic needle tubing. Two designs, known as the “windowed”

and “brace” jackets, were developed and used as depicted in Figure 9.1. Both featured a large piece of material removed from the area that would be where the exposed tubing lies. The windowed design had a single piece removed on one side, and the brace design had two shallower pieces removed on opposite sides. This allowed the sensor to still access the applied pressure, but maintain rigidity for the catheterization process. Early iterations of the jacket design had a small 2-4 mm window cut out. However, after all the sealants were applied, the inelastic adhesives flowed around the elastic tube until it was completely covered. Needless to say, the sensors were pressure insensitive.

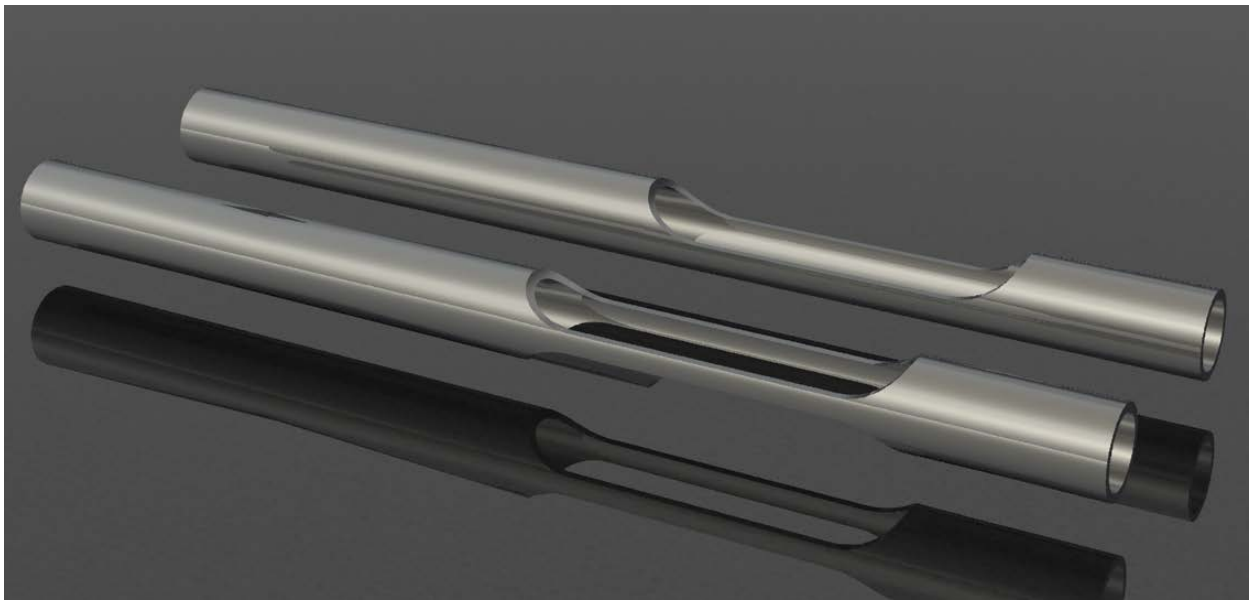

Figure 9.1. The two metal jacket designs. The top design is the “windowed” jacket while the bottom design is the “brace” jacket.

The sensors were also more complicated to fabricate since sealant had to be applied to two different sides of the sensor. Although both jackets yielded functional sensors and were both used, the windowed design was eventually selected. The current version of the windowed design featured a 9 mm window. The larger window, therefore, accounted for excess epoxy. The braced jackets were designed to have a minimalist approach—the metal is only there to give the elastic

tube support. Theoretically, if more of the elastic tubing is exposed to the sensing medium, the pressure would have more effect on the tubing and greater sensitivity. In practice though, the braced jackets had such little material at the tip that the jackets deformed very easily, and there wasn't any noticeable advantage in pressure sensitivity.

The jackets measure 29 mm long—deliberately longer than the elastic tube to give enough head space at the tip of the jacket for the injection of adhesive, which acted as a secondary sealant for the elastic tube as well as secured the tube to the jacket. In order to seal the reference volume, the adhesive was painted or injected onto the elastic tube slowly and forcing it along the sides and underneath the elastic tubing. With time, the adhesive flowed into the tubing to create a solid plug of adhesive with the same diameter as the inner diameter of the jacket. The resulting sensor lacked any globs of sealant that may snag while inserting into the catheter port. There were, however, drawbacks to this sealing method; complete sealing was dependent on the flow of the adhesive to every space between the elastic tube and jacket, but some sensors formed incomplete seals. While the yield of non-functional sensors was higher with this technique, fortunately, enough operable sensors were made to justify the continual use of this method.

The functional component of the sensor is modeled in Figure 9.2. The fabrication of the sensor required a modified technique. The elastic tube (Dow Corning Silastic) used had a smaller radius—0.037 in (0.94 mm) outer diameter and 0.02 in (0.51 mm) inner diameter—to accommodate more clearance for the expansion inside the metal jacket. The 25 mm elastic tubes were also longer than they were previously. The wires were arranged exactly in the same way as the *in vitro*-only sensors: the longest wire is inserted 22.5 mm into the elastic tube to leave a 2.5 mm head space at the tip of the elastic tube, the middle reference electrode is 15 mm long, and

the last wire is inserted 5 mm into the tube. This was designed to have 5 mm spacing between electrode pairs in each region. After the base of the elastic tube was sealed twice with PDMS (Nusil Med-4011) and coated with Viton, a third seal was applied at the base using cyanoacrylate glue (Loctite 401). The high viscosity of Med-4011 was preferable since the amount of PDMS that was wicked into the tube through capillary action was limited, which prevented complete coverage of the base wire. Once all seals were dry, the tube was marked 15 mm from the base to denote the end of the reference electrode and the transition between the jacketed and exposed regions, as well as the last 5 mm of the tip of the tube to denote the head space and the exposed metal of the tip wire, which corresponded to the base of the electrode in the exposed region to the tip. These marks indicated where inelastic adhesives should be applied to ensure proper sealing and to guarantee that the compression of the exposed region occurred in between the electrodes for maximum sensitivity.

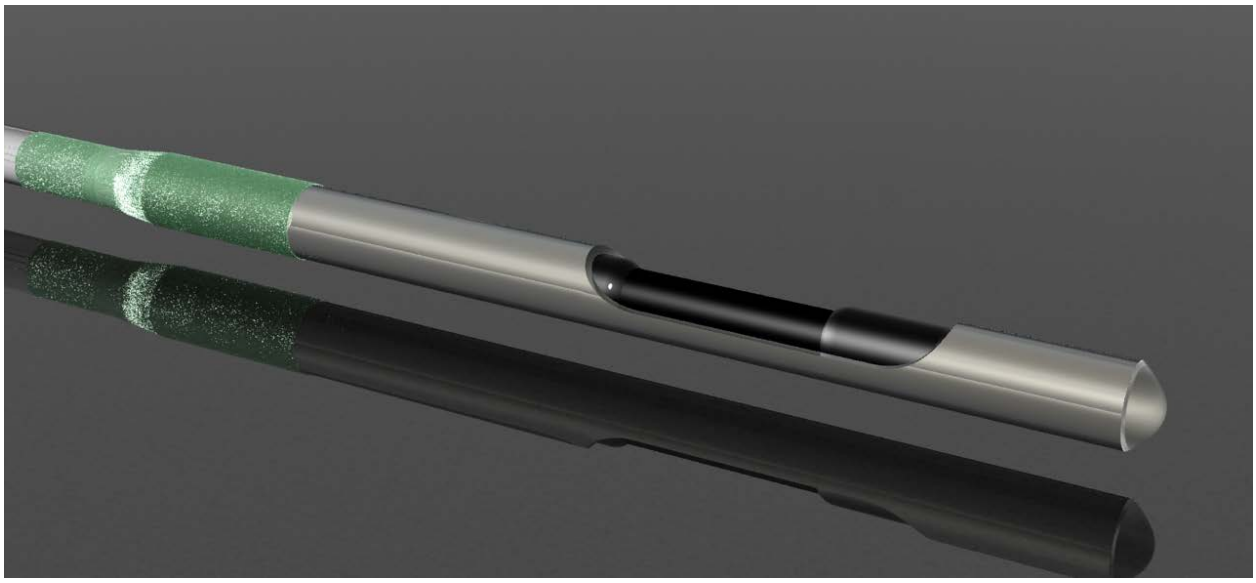

Figure 9.2. A model of the fully assembled CRISP sensor. Medical shrink tubing is shown connecting the base of the sensor to a sheath for the platinum wires.

The elastic tube was filled with 50 mM KCl; immediately, the last 2.5 mm of the tube was filled with liquid PDMS (Dow Corning Sylgard 184). The Sylgard 184 PDMS is less

viscous than the Med-4011 used to seal the base of the silicone tube, which allowed the Sylgard 184 PDMS to be injected through the requisite small bore needle (27-30 ga.) very easily. The conductance of each sensor was tested at this stage to verify the tubes were properly filled. Any sensor that had an open connection in either of the electrodes was refilled, resealed, and retested. If the sensor still was nonconductive in both electrodes, the sensor was discarded based on the assumption that the problem was unfixable without complete disassembly of the sensor.

The remaining working sensors are then inserted into the one piece jackets. 4-minute epoxy (E-bond) is injected into the tip of the jacket to the opening of the cut out portion. The filled elastic tube was pushed all the way into the epoxy until the 15 mm mark was exposed through the window and the elastic tube was flushed with the base of the jacket. This ensured that the window cut into the metal jacket corresponded perfectly with the exposed region. The epoxy displacing from the tip assures the tip of the elastic tube is encased in solid material when the epoxy cures. A small amount of epoxy was applied to the base of the jacket just enough to plug the jacket. Epoxy was finally applied to any marked areas on the elastic tube. It was important to allow the epoxy to coat the underside of the tubing to seal the jacket. The high viscosity of the epoxy will only increase as it cures, so gravity-driven flow of the epoxy around the silicone tube could not be expected. Finally, cyanoacrylate glue was applied to the tip and base of the jacket as a triple redundant seal. The sensors were stored in 50 mM KCl solution for a day as the silicone finished curing to prevent evaporation during this step. Because the sensor was submerged in water quickly after filling the elastic tube, the yield of conducting sensors was generally about 75%, which was a drastic improvement over the previous *in vitro* only iterations. However, because the sealing of the reference volume depended on epoxy flow to completely

plug the jacket, the number of fully functional sensors was just a fraction of that. Despite that, the yield of fully functional sensors was still much improved.

The last modification of the sensor for *in vivo* use was the protection of the fragile platinum wires. For sensors that were strictly used for *in vitro* testing, the wires were unprotected, but this obviously was not viable for use in an animal. Initially, the platinum wires were threaded into a silicone tube similar to the elastic tube used in the sensor. However, the silicone tube coupled with very thin platinum wires had been aptly described as a "wet noodle," namely that threading the sensor through a catheter port would be nearly impossible. A thin guide wire either made of nitinol or high tension steel piano wire was inserted into the silicone sheath to provide some rigidity. While this was effective, it was less than ideal since the guide wire could electrically short the wire connections out if contacted. Also the guide wire made the entire sensor unwieldy, causing some to break. The last solution was to use a semi-rigid sheath. Several materials were looked at, namely polyethylene and Teflon tubing, but ultimately polyethylene was chosen due to its being rigid enough to pass through the valve and thread down the catheter sheath, but soft enough to overcome its inherent memory when necessary without too much force. Teflon, on the other hand, was too stiff—the tubing took the shape of the spool it was stored on, so the sensor stayed coiled—making insertion through a catheter difficult. Because *in vitro* testing and characterization of each sensor required the use of a twist cap, having the polyethylene sheath on the wires imparted a lot of stress on those wires, causing them to break during testing. Therefore, sensor characterization was performed with naked wires and the polyethylene sheath was threaded on after the sensor passed the calibration testing and was ready for dynamic testing and implantation.

However, even when testing the sensors without the protective polyethylene sheaths, wires, especially older reused wires, sometimes broke during multi-day testing or during packaging preparation. For sensors that exhibited good sensitivity, stability, and drift properties, a broken wire was particularly devastating. Fortunately, depending on where the wire broke, the sensor can be repaired. Wires that broke near the end of the wire, which was usually soldered to the conditioning circuit can easily be re-soldered without losing too much overall length. On the other hand, wires that broke at the base of the metal jacket could not be salvaged. Wires that broke somewhere in the middle could not be trimmed down and re-soldered since the overall sensor would be too short to be effectively implanted. The obvious solution was to splice on another wire. However, the material properties of platinum precluded using a solder joint. Normal lead/tin solder does not wet very well to platinum, meaning that a high-contact angle solder ball would form if used on platinum wire. The size of this ball would make it impossible to thread through the polyethylene sheath.

To remedy this, several well-known splice knots were investigated in connecting two wires together. A well-cinched knot would have great contact between the platinum strands and be thin enough to easily thread through a protective sheath. However, being a single solid core of thin metal meant that tying the knot would be very difficult since the wires had memory, kinked very easily, were fragile and required tweezers to manipulate them. There were several considerations in choosing which knot was ideal, such as the amount of wire required, the complexity of the knot or the dexterity required, the force required to cinch the knot down, and the knot strength. The knots that were tested included the half hitch: a simple overhand knot tied around the other wire, a double uni knot, a “Bob Sands” knot, and a modified Albright knot. The advantages and disadvantages of each knot are described below in Table 9.1:

Knot Name	Disadvantages	Advantages
Half hitch	Slips very easily	Simple and does not require a lot of wire
Double uni knot	Requires a lot of wire to tie and a lot of dexterity	Strong
"Bob Sands"	Difficult to tie and requires a lot of wire	Very strong
Modified Albright	Requires a fair amount of wire	Very strong

Table 9.1. The advantages and disadvantages of knots considered in tying two pieces of platinum wire together.

The preferred knot was the modified Albright knot, which when tied with 4 wraps, was strong enough to hold without slipping, yet did not generate enough friction when cinching down to break the wire. As illustrated in Figure 9.3, the knot was tied by first forming a loop in the broken wire that was already in the sensor. A spool of fresh wire was threaded through the loop (step 1) and wrapped twice around the loop (step 2). The wire was wrapped back towards the loop twice (step 3). Next, the fresh wire was passed back through the loop in the same direction that the wire first entered, and the knot was cinched down by pulling both the main wires and their tag ends (step 4). At this step, the wire insulation was completely removed and the knot was fully cinched down by pulling just the main wires (step 5). The knot was complete when the wire was completely cinched down tight and the tag ends trimmed (step 6). A blown up photograph of a spliced wire in a test sensor is shown in Figure 9.4. When that sensor was eventually discarded and the parts salvaged, the electrical resistance of the knot was measured to be around 8 Ω, proving a good contact can be formed when splicing wires in this manner. As shown in Figure 9.4, the Teflon insulation around the wires was not completely removed before cinched down, so a more thorough removal of the insulation can potentially result in a much tighter knot and even better electrical contact.

Once a sensor has demonstrated good functionality by holding its sensitivity for at least two days, it was set aside to be fully packaged.

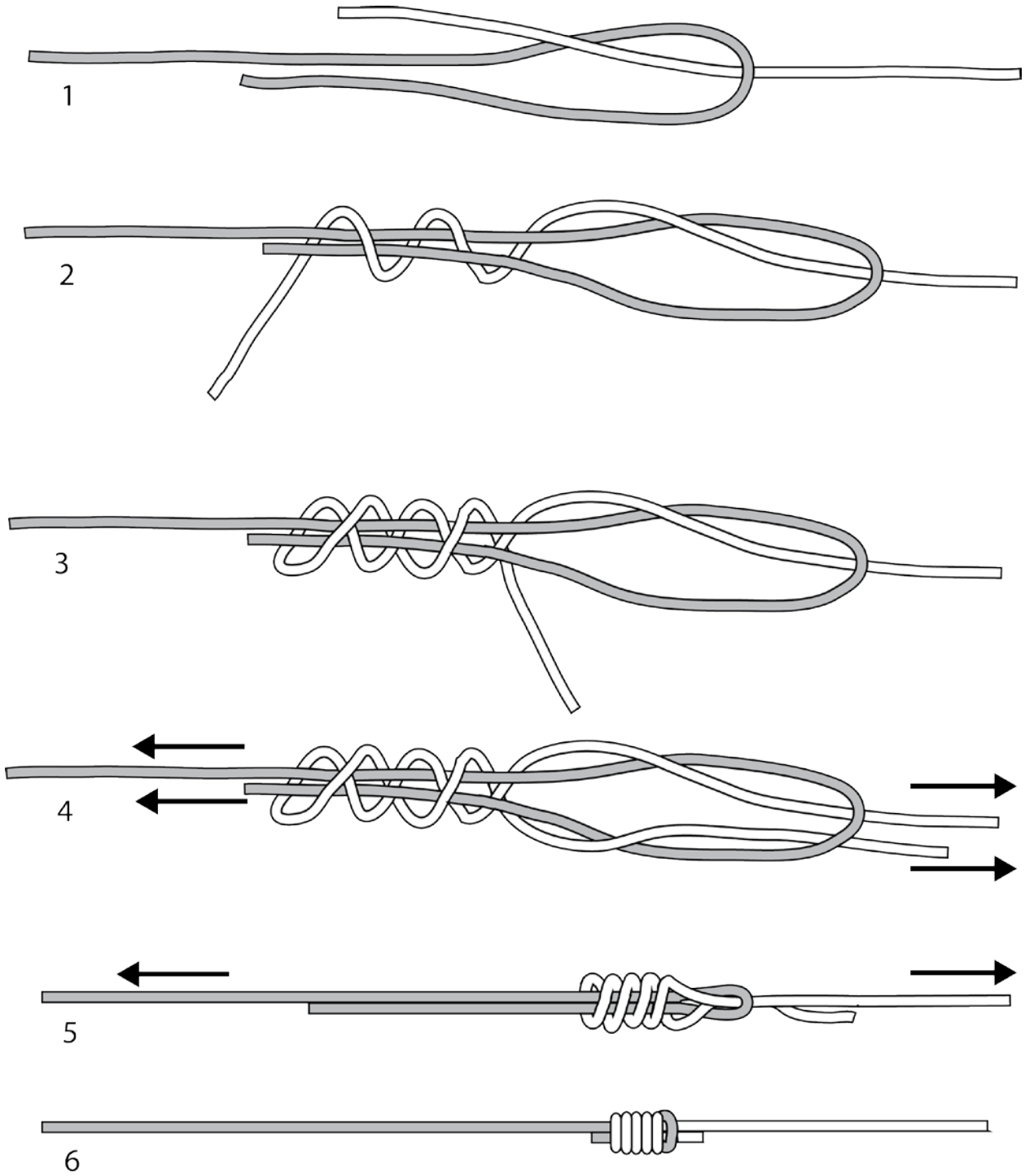

Figure 9.3. A step-by-step illustration on how to tie a 4-turn modified Albright knot to splice two platinum wires

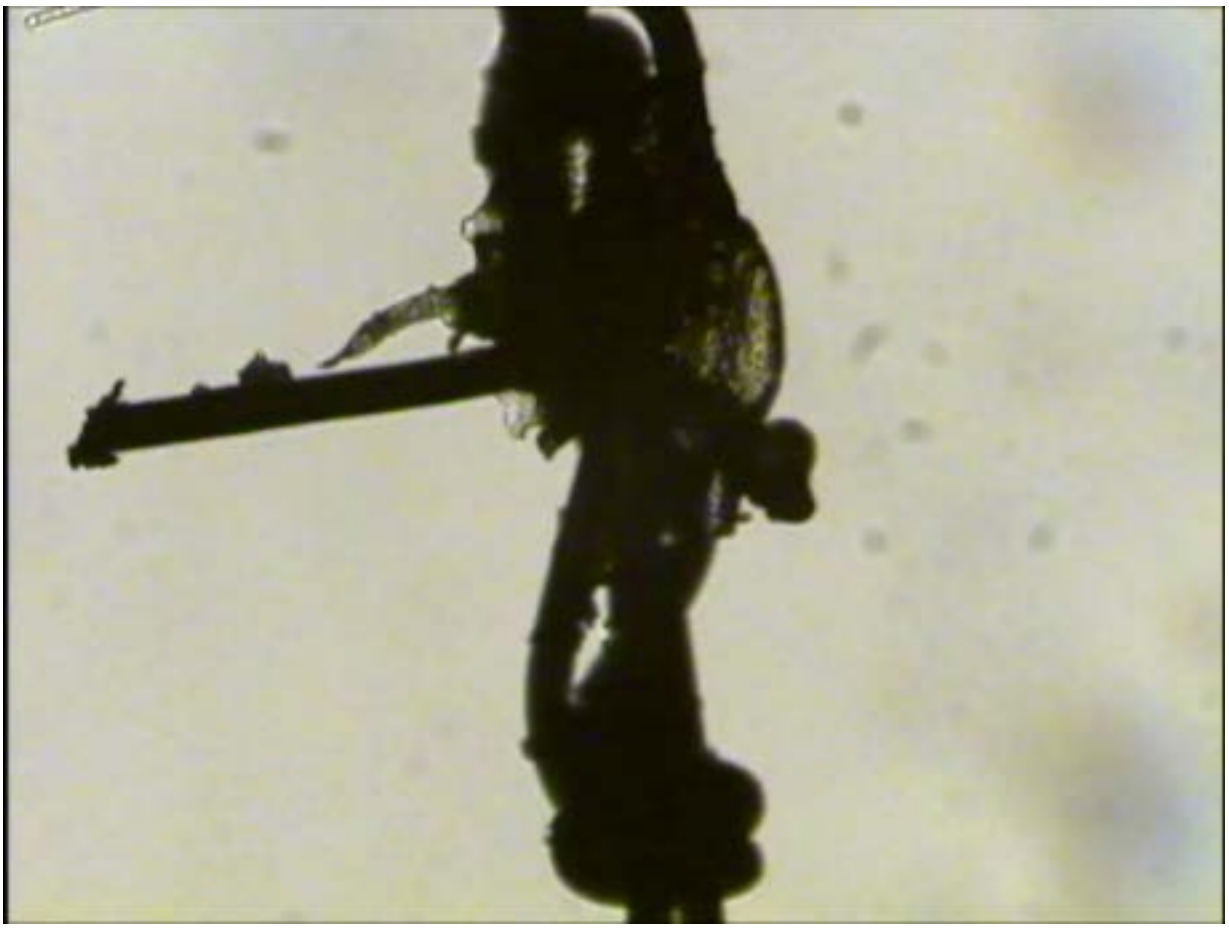

Figure 9.4. A magnified view of a modified Albright knot splicing two platinum wires together. The magnification is 100x.

The sensor was inspected for any excess glue that may be on the jacket, especially at the base of the jacket, where excess epoxy may have accumulated when sealing the jacket. These spots were problematic when the finished product is threaded through the port, so they needed to be removed by gently grinding them down with a 60-grit sanding bit on a rotary tool (Dremel 3000). The polyethylene sheath was threaded on, and silicone oil (Nusil Med-420) was injected into the sheath. Based on prior experience with this oil and water evaporation, it effectively acted as a barrier for evaporative water loss through the base of the sensor. The polyethylene sheath was then attached to the sensor by first applying 4-minute epoxy to the wires and base of the jacket and keeping the polyethylene tube flush against the jacket. Care was required to ensure

that there were no kinks in the junction between the jacket and sheath while the epoxy cured. Excess epoxy was removed to prevent any droplets of epoxy from forming on the outside of the polyethylene sheath. This epoxy joint was typically very weak and could be broken easily as had been shown in previous animal implantations, so it was strengthened by slipping a small half inch piece of medical shrink tubing (Vention Medical) made of polyethylene terephthalate with a nominal inner diameter of 0.083" (14 gauge) and a wall thickness of 0.001" over the base of the metal jacket. The shrink tubing was shrunk around the joint, and a thin layer of cyanoacrylate glue was applied over the shrink tubing and polyethylene sheath to prevent the shrink tubing from slipping off the jacket during extraction of the sensor from the catheter port. At the other end of the sensors, the wires were soldered into a connector using crimp contacts mounted onto a piece of printed circuit board (PCB). 4-min epoxy was applied over the entirety of the wires, crimp contacts, and PCB to protect the connections from intermittent blood contact. From the crimp contact were pins that slipped into a custom made connector attached to 8 feet of cable made of thin braided wire, which was then connected to the conditioning circuit. This way, sensors can easily be swapped even if the recording computer was far away.

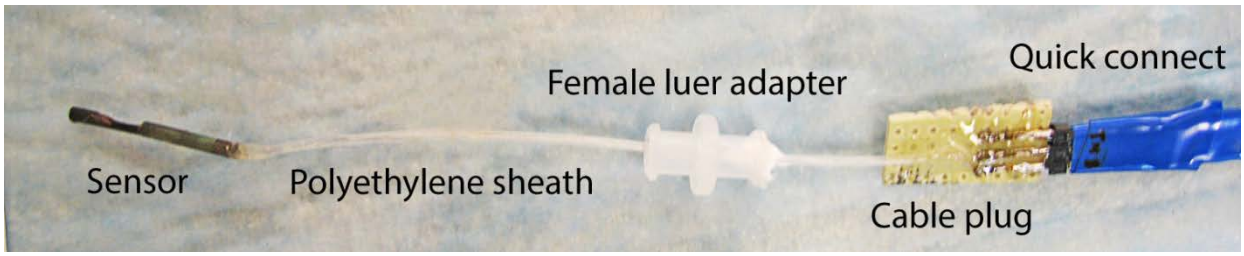

Figure 9.5. The fully assembled sensor featuring a protective polyethylene sheath and blood-proof wire connector. The sensor is connected to an 8-foot cable that connects to the conditioning circuit. It also has a female Luer adapter for use in the cardiac simulator.

The cable was limp, so it would not pull the sensor out of the catheter port trying to relax into a coil like was typical when using solid core wire. Figure 9.5 shows a fully packaged sensor albeit a particularly short one.

9.2 Sensor Characterization

Once fabricated, sensors were characterized for sensitivity, drift, signal stability, and whether or not the calibration remains unchanged. The voltages from each arm of the Wheatstone bridge were monitored and compared from day to day to check for any slow leaks that may alter the conductivity of the electrolyte solution within the sensor. Assuming each signal measured directly from the bridge did not drift and did not exhibit any noise, the entire amplified signal was read through LabVIEW. If the signal exhibited a noise amplitude <1 mV, then static pressure testing ensued as described in Chapter 8. After a successful initial pressure test of a sensor, the variable resistor used on the non-inverting amplifier of the jacketed electrode was set aside and reserved for use only on that particular sensor. When the new packaging and sensor designs were first implemented, the long-term performance of the sensor needed to be tested to ensure that altering the fabrication techniques did not effect reduced sensor performance. Therefore, the sensor was observed for more than a month and tested nearly once a week (Figure 9.6). The sensor behaved brilliantly, yielding a resolution of <1 mmHg. Unfortunately, this particular sensor was made before the use of a secondary sealing step at the base of the jacket. After a month of submergence in water, the epoxy had lost its grip on the Teflon-coated platinum wire, and the electrode in the jacketed region pulled out of the sensor—rendering it useless and unsalvageable.

While the aforementioned sensor performed very well, because fabricating functional sensors was inherently difficult and the sensor was generally meant to be a proof of concept, the requirements for sensor performance were relaxed. A sensor passed the characterization step if it had a resolution of < 5 mmHg.

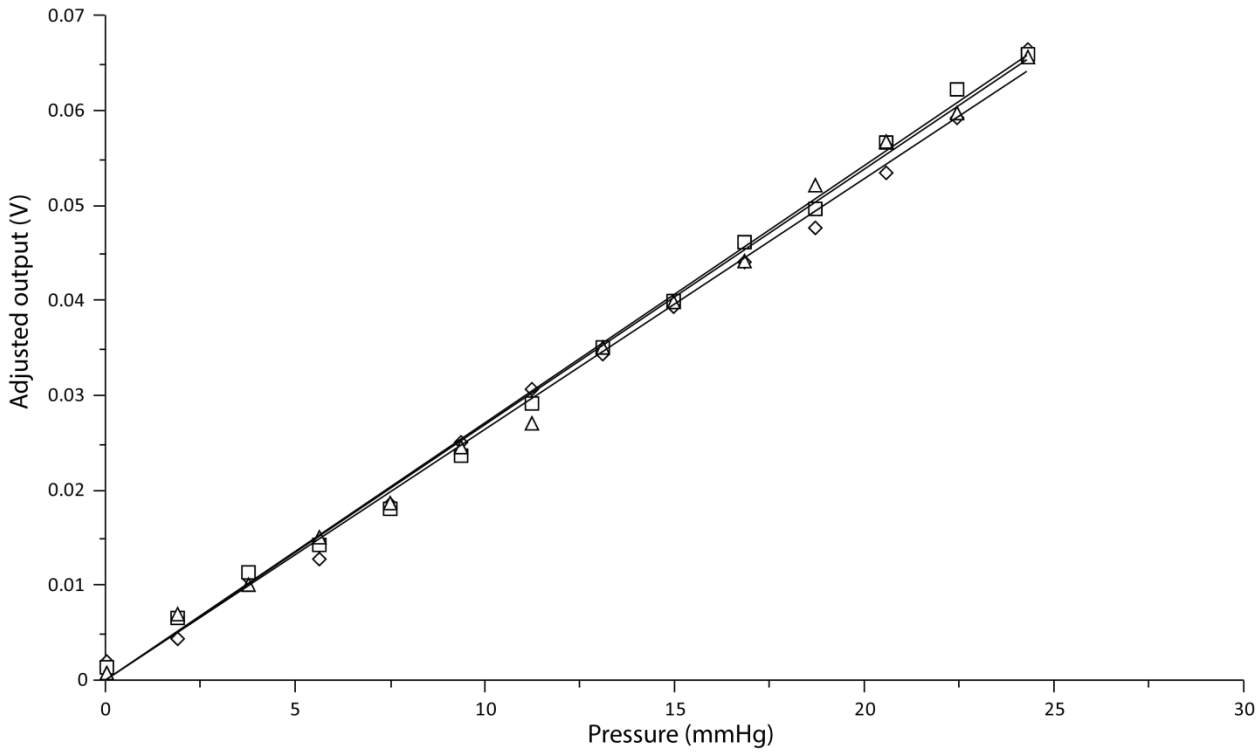

Figure 9.6. A series of calibration curves of a fully packaged sensor designed for *in vivo* use. The last 3 weeks of testing are represented here: the slopes of the linear regressions: day 21 (diamond): 0.0026 (R^2 = 0.9963), day 25 (square): 0.0027 (R^2 = 0.9959), day 32 (triangle): 0.0027 (R^2 = 0.9965)

Also, the long-term study of sensitivity was generally not required for each sensor, and since a sensor that experienced a change in sensitivity over time had never been observed, testing was restricted for 2-7 days to lessen the risk of breaking the platinum wires during testing. A total of 5 sensors were fabricated that met this metric before moving onto *in vivo* testing.

One particular sensor, which was tested a day apart, had a sensitivity of 23.9 mV/mmHg. The sensor experienced a slight change in sensitivity between each day. Specifically, the slope of the linear regression changed from 0.0228 (R^2 = 0.9982) to 0.0249 (R^2 = 0.9992) after one day, resulting in a 9% change in sensitivity. For a typical arterial waveform of 40 mmHg, this would result in a 4.5 mmHg resolution. It should also be noted that this test was conducted soon after fabrication—a time when the greatest variability in sensor performance occurs. Furthermore, the sensor exhibited very stable and drift-free signals. This is mostly due to the high sensitivity of

the sensors. The least sensitive of the five sensors had a sensitivity of 12 mV/mmHg, with a SNR of 6. Sensors that weren't as sensitive, although clearly showing incremental pressure increases, were marred by having unstable baselines or very noticeable signal drifting and were generally rejected. Overall, the accepted sensors exceeded the minimum sensitivity requirements, which was defined by the sensing limit of the PCI-6289 Digital Acquisition (DAQ) card used in the test. Since the *in vivo* sensors were to be used without data smoothing, the sensitivity had to be greater than 3 mV/mmHg to satisfy a SNR of 2.

Two sensors were set aside for nearly three weeks before testing them dynamically in Dr. Benharash's cardiac simulator, which was earlier described in Chapter 8. Both sensors demonstrated a good dynamic response and had even better response than the commercial transducer since the CRISP sensor did not output any digitization steps, which could be subject to misinterpretation if one assumed that the increments were real pressure steps. One sensor was tested at three frequencies: 1 Hz (Figure 9.8A), 2 Hz (Figure 9.8B), and 3 Hz (Figure 9.8C), which is equivalent to a heart rate of 60 bpm, 120 bpm, and 180 bpm, respectively and 70 mmHg amplitude. Moreover, the amplitude of the sensor output decreased proportionally with the corresponding decrease in the pressure waveform. Because the pressure from the commercial transducer and the test sensor output were read by different computers, it was difficult to perfectly synchronize the sensor to the transducer. However, by using frequency changes as landmarks, the two readings were realigned. The sensor demonstrated a very clean signal with very little noise and little drift. It should be noted that because the transducer and sensor were placed in different areas of the simulator and because the simulator relied on fluid flow, there was a frequency-dependent time lag between the sensor and transducer signals, which was why at higher frequencies, the signals became out of synchronization again.

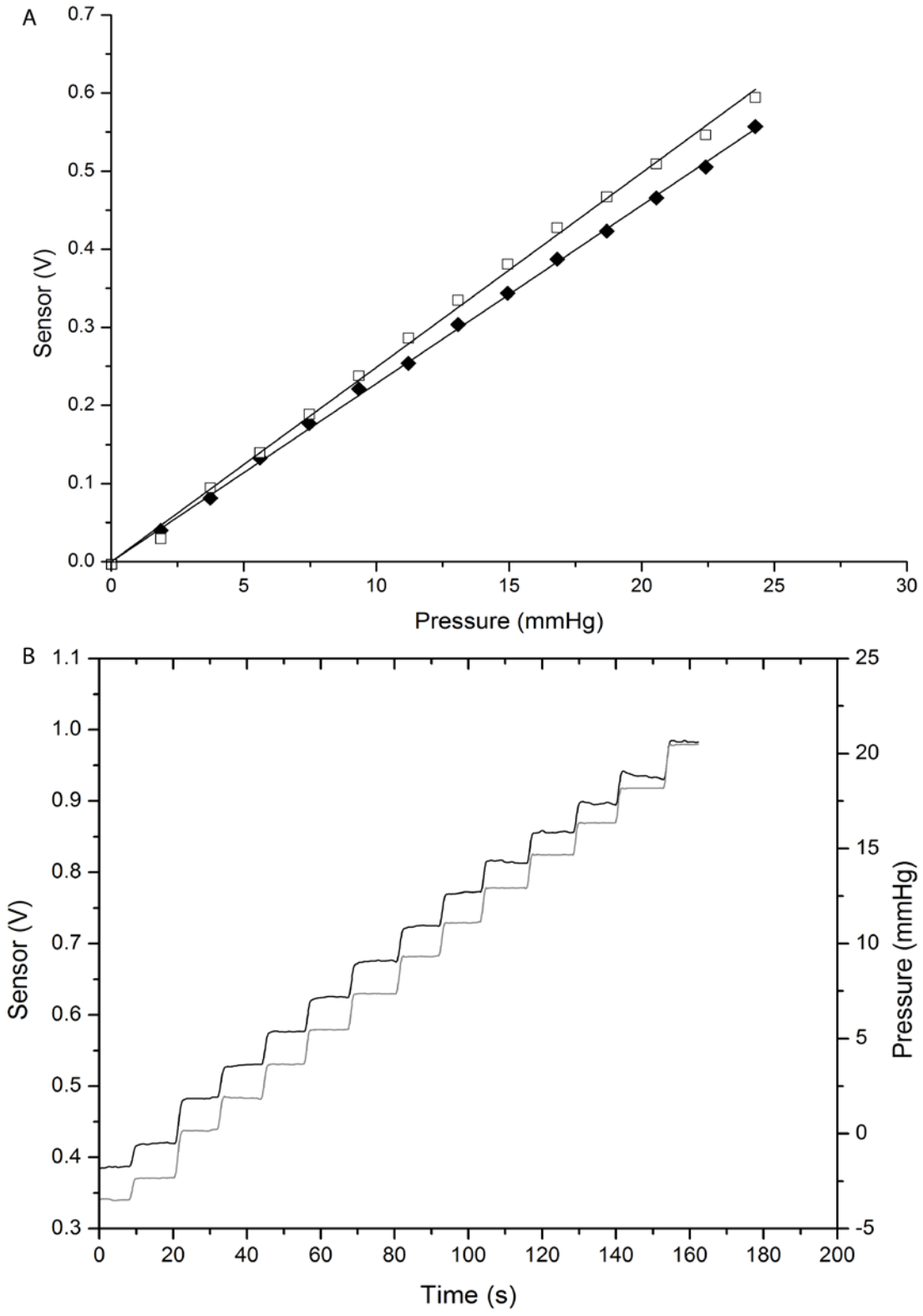

Figure 9.7. The results of static pressure testing of an implantable sensor. Testing occurred over two days and shows the A) sensitivity over those days and B) a characteristic time-dependent plot of the sensor output (black) and simultaneous pressure measurements (gray).

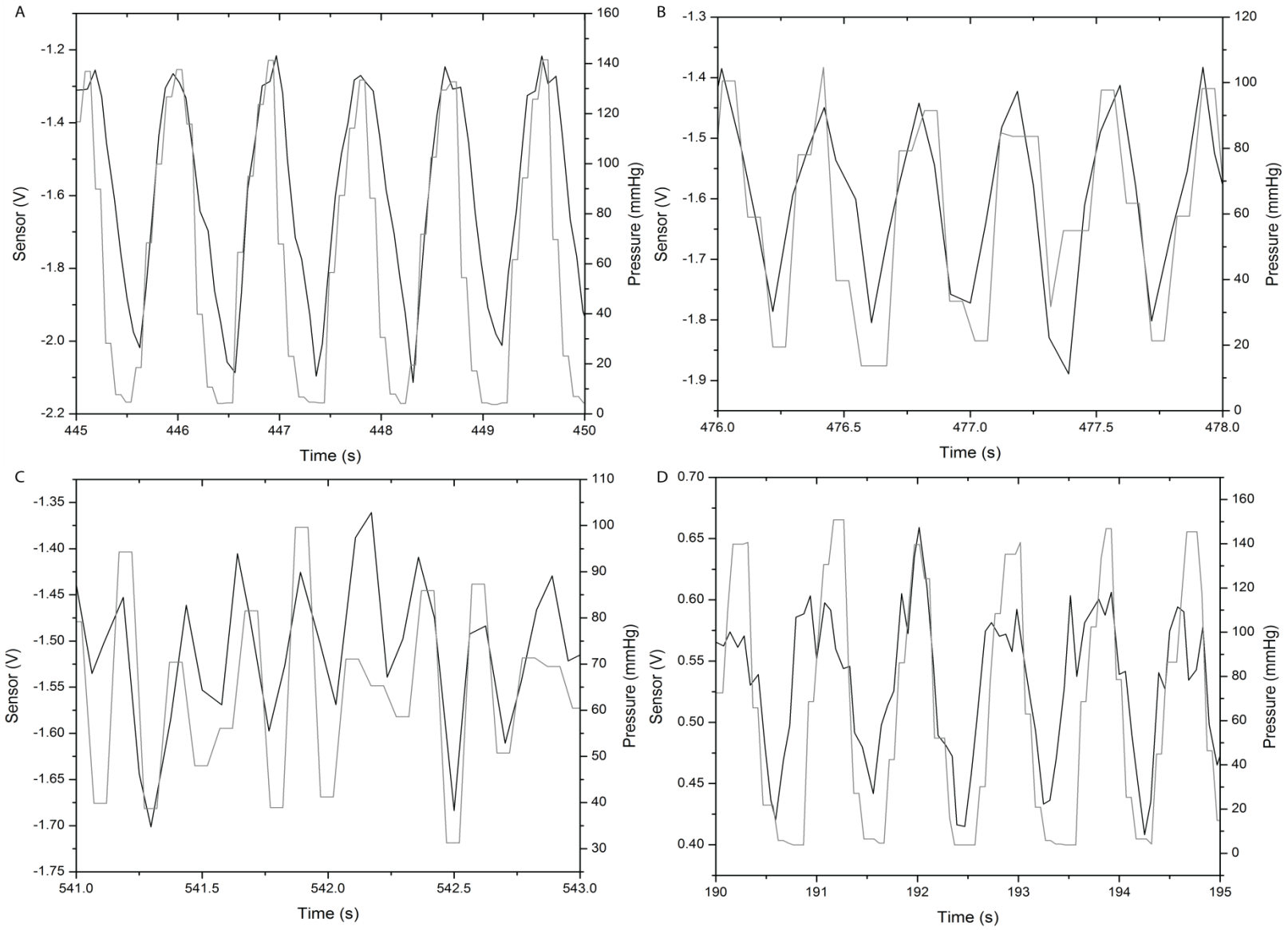

Figure 9.8. Dynamic pressure testing of two sensors with the black trace representing the sensor and gray trace is the pressure gauge. One sensor was tested at three different frequencies: A) 1 Hz (60 bpm), B) 2 Hz (120 bpm), and C) 3 Hz (180 bpm). The other was only tested at D) 1 Hz (60 bpm).

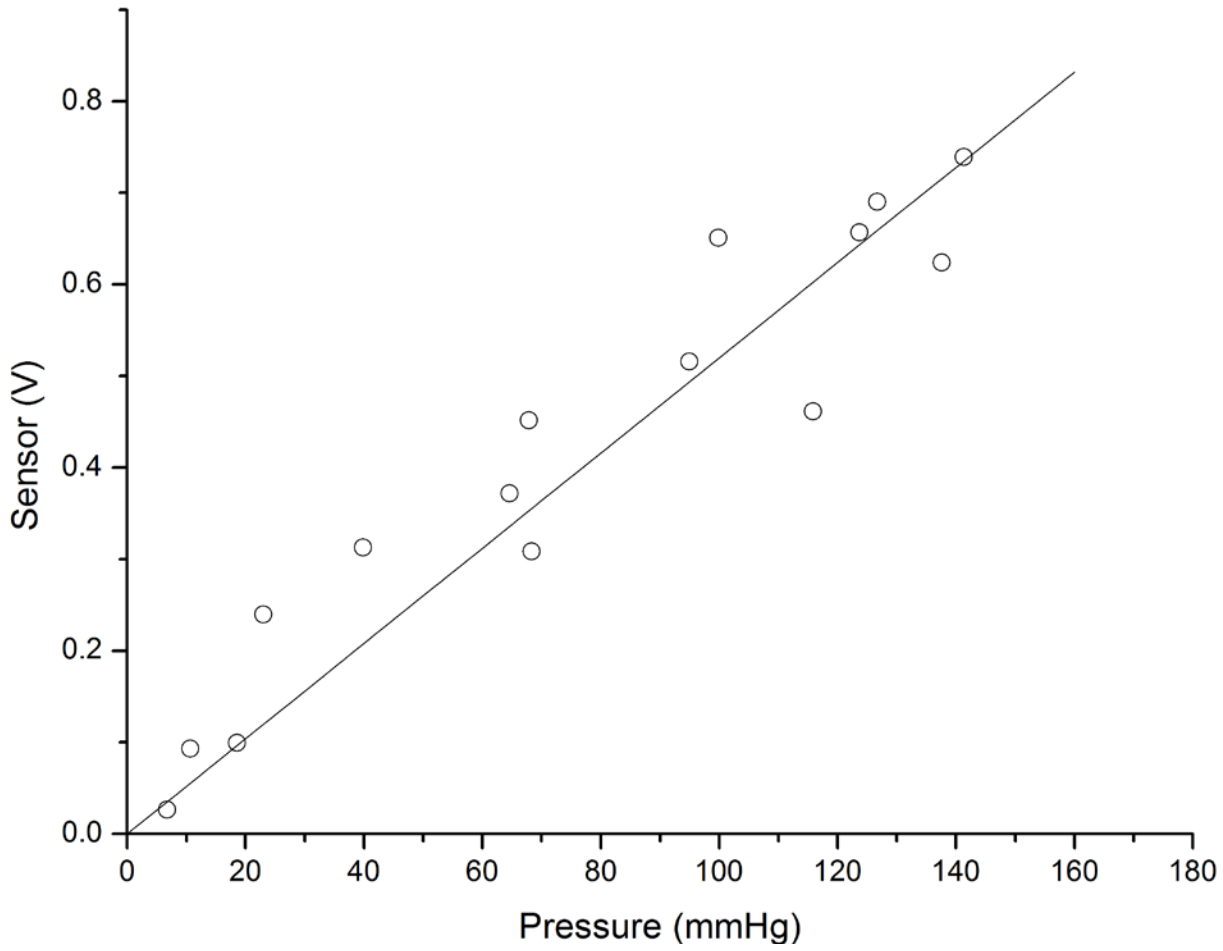

Figure 9.9. The linear regression of the CRISP sensor voltage and pressure taken during a 1 Hz dynamic pressure test ($V = 0.0052P$, $R^2 = 0.8897$).

Although the amplitude of the pressure wave was reduced as the frequency is increased, the median pressure of the sensor stayed the same regardless of frequency. According to Dr. Benharash, this indicated proper functionality. The second sensor was only tested at 1 Hz (Figure 9.8D) or 60 bpm. It unfortunately had a noisier signal, but it was not enough to obscure the pressure waveform. Both sensors functioned properly at 70 mmHg, an amplitude that was higher than expected in a human or animal model, which was a testament to its ruggedness in testing large pressure differences in a dynamic environment.

Both sensors displayed their sensitivities close to the expected sensitivities as predicted by the static tests with slight differences. A linear correlation between actual pressure and sensor output voltage was calculated using the data set at 1 Hz (Figure 9.9). As seen in Figure 9.8, the data from 2 Hz and 3 Hz did not yield clean waveforms for the commercial pressure transducer. Therefore, the data correlated very poorly. The linear regression of the CRISP sensor tested at 1 Hz was $V = 0.0052P$ ($R^2 = 0.8897$), which was very close to the linear regression of the same sensor in the static test ($V = 0.0051P$). This underscored the belief that the static testing should not be used for calibration per se, but rather comparing the amplitudes of the waveforms in dynamic testing to the amplitudes during *in vivo* testing would be a more appropriate check of calibration. Static testing, on the other hand, really was only useful as an initial checkpoint for qualifying the operable sensors and to characterize the long-term stability of the sensor.

9.3 *In Vivo* Testing

A female porcine model was catheterized in the femoral artery with a 7 French catheter sheath. The pig had undergone open heart surgery earlier to test and characterize different heart socks for electrophysiological studies. The sensor was inserted through the sheath, and the transducer was attached to the catheter port. However, due to the extreme angle of the sheath with respect to the femoral artery, the sheath was occluded and no pressure was transmitted to either the sensor or the transducer. Clearing the catheter to force it open proved futile. Another catheter was introduced into the femoral vein; although that catheter was not occluded, the sensor and transducer both did not yield any pressure waveforms. This was mostly expected since venous walls are highly elastic and lack musculature.

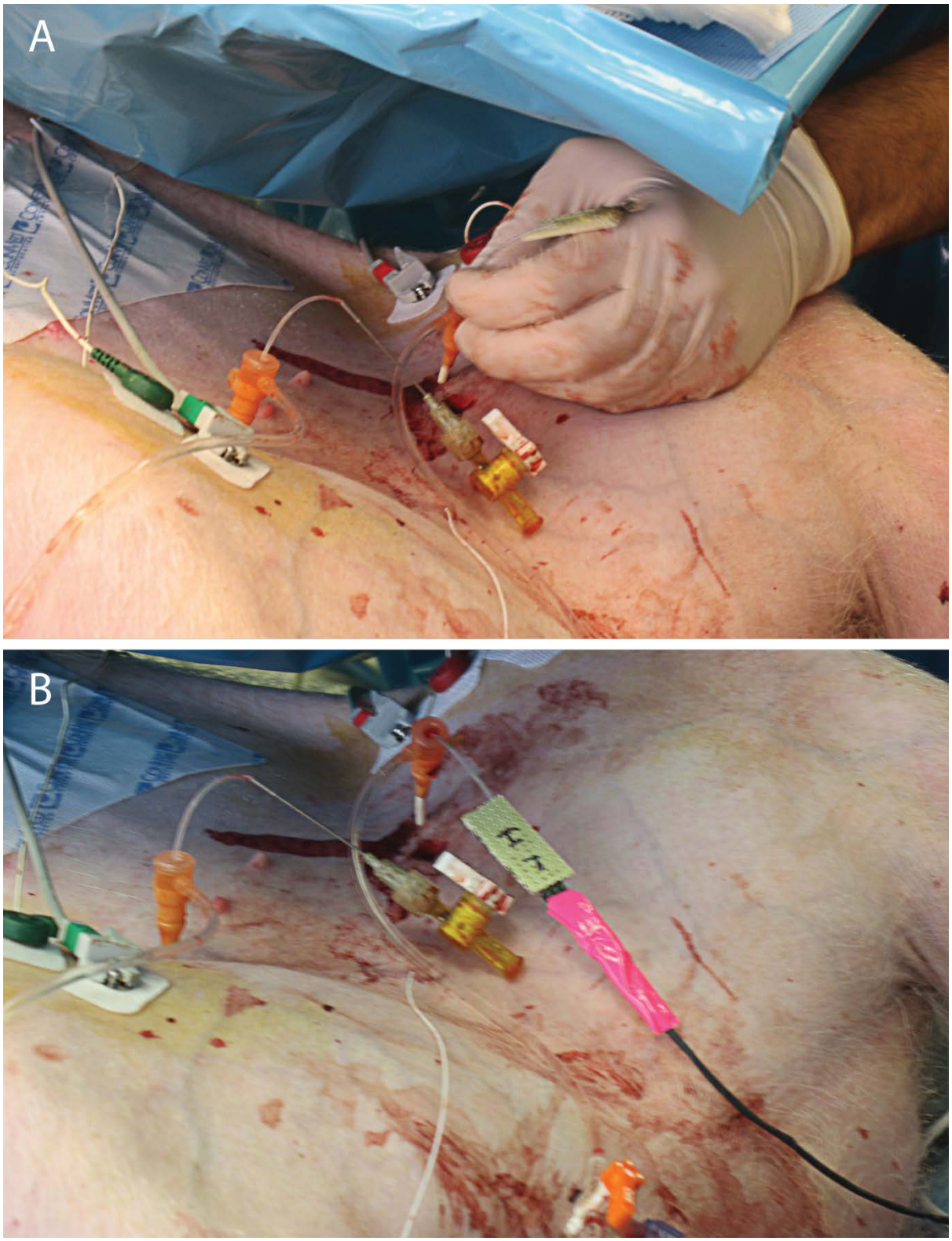

Figure 9.10. A) The implantation of the catheter mounted CRISP sensor through a 7 French port and B) the functional sensor after insertion. Note the pressure transducer used as a reference at the bottom of the picture. Photo credit: Carl Salazar.

Therefore, venous pressure usually ranges 5-8 mmHg with an irregular waveform [71], which is difficult to identify to the untrained eye. At last, a third attempt at catheterization into the femoral artery occurred, which proved successful. Insertion of the sensor was performed simply by threading it through the catheter port valve into the sheath. Insertion of the catheter is shown in Figure 9.10A. Once inserted, the sensor is connected to the conditioning circuit via a quick connect system (Figure 9.10B). The limp wires used in the quick connect allow the catheter to remain in place without pulling out and without the use of tape. Only one sensor was implanted at a time.

In previous experiments using catheter ports in both animals and in a laboratory setting, a common mode of failure was the sensor separating from the polyethylene sheath. As more force was applied to pull the sensor out, the platinum wires would often pull out of the sensor. This not only destroyed the sensor, but also left a foreign object in the catheter, which would need to be replaced, or even worse, inside the body. Throughout the most recent experiment, multiple sensors were inserted and removed many times by multiple people and in all cases, each sensor remained intact. In fact, every sensor was able to pass through the catheter sheath easily although the sheath was a little snug for some sensors. All sensors were able to pass through the port valve while being removed multiple times without packaging failure. Another weakness of the packaged sensor that has been noticed in the past has been the solder joints connecting the platinum wires to the conditioning circuit. The stiffness of the polyethylene sheath, the fragility of the wires, and the hard solder joints all cause wire breakage. However, during this experiment, the wires and a portion of the polyethylene tube were completely encased in epoxy. As a result, no wire breakages occurred.

One thing that was not completely anticipated was the amount of bleeding that occurred. Since only the sensor itself at the tip of the catheter was intended to be in constant direct contact with blood, it was the only portion that was robustly packaged. The polyethylene sheath, cable plug at the end of the platinum wires, and quick connector were all designed for incidental blood contact.

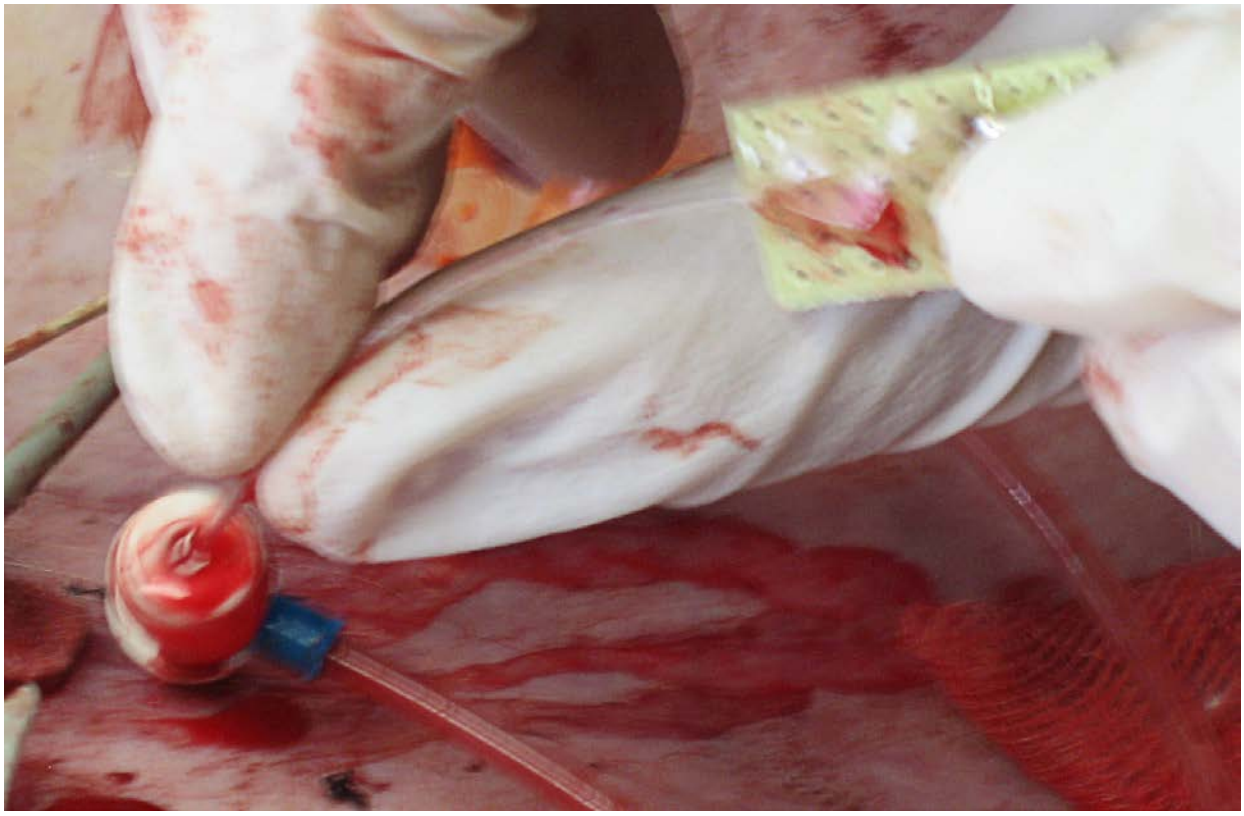

Figure 9.11. The sensor upon extraction out of a catheter port. Note the blood underneath the protective epoxy layer on the cable plug. Photo credit: Carl Salazar.

Even though the cable plug had all metal pieces covered in epoxy, blood was able to permeate the epoxy in all sensors as shown in Figure 9.11, which was taken upon extraction of a sensor. In fact, in one sensor, blood was found in the joint between the sensor and the polyethylene tube underneath the medical shrink tubing and coating of cyanoacrylate glue. After the procedure was done, all the sensors were cleaned in an ethanol solution and inspected. The blood that had been trapped in the epoxy was easily removed in the alcohol bath, suggesting that there were voids in

the epoxy that had formed a pathway for liquids to reach the wires and crimp contacts used in the plug. Visual inspection of the sensors confirmed this suspicion. Regardless, pressure data was still obtained and the arterial waveform was clearly discerned in three of the four sensors tested that day. The detected heart rate of the test subject throughout the entire study was about 60 bpm.

Because of the permeation of blood into the cable plug and quick connector, short circuits may have formed between the electrodes, which affected the signal noise and altered the baseline conduction levels between electrodes. Therefore, in all sensors, the preset values of the potentiometers that determined the gains of one of the electrodes were rendered useless, which disallowed any comparison of sensitivities and calibration between multiple days. The signal noise for each sensor was also much higher compared to all *in vitro* tests, including the dynamic pressure studies. This suggests that the noise issues were completely unique to the use in an animal.

The first sensor inserted stayed in the animal for nearly five minutes. The sensor displayed a clear pressure waveform throughout the entire experiment, but for the purposes of this discussion, only two short windows (Figures 9.12 and 9.14) were used to clearly show the waveforms. The first window (Figures 9.12A and 9.14A) was chosen for its consistent frequency and interesting secondary pressure peaks. It was also highly representative of the entire data set. The second window, which occurred near the end of the experiment, indicated a highly irregular pressure profile as evidenced by a relatively low heart rate and inconsistent amplitude. It should be noted, however, that at the time of these readings, as well as all the pressure readings, that the test subject was undergoing multiple procedures, including a coronary bypass surgery and the insertion of another catheter into the femoral artery. The peaks and troughs of the waveforms

clearly match up with those shown on the commercial pressure transducer acting as a reference. Also, the amplitudes of each wave were consistent, which is to be expected when analyzed in such a small time frame. However, it's clear that the raw data (Figure 9.12) is extremely noisy, which sometimes obscures shorter secondary pressure peaks that were clearly evident in the real-time pressure trace. Furthermore, large negative voltage spikes occurred seemingly randomly. Both these phenomena and the noisiness (15 Hz) are attributable to the blood fouling of electrical components found on the cable plug and quick connector.

To remove the noise resulting from blood contamination, the data was filtered with a 10^{th} order, 12-Hz low pass Butterworth filter. When tested against a 15-Hz sine function with the same sampling frequency as that used in the *in vivo* study, this filter fully removed the sine function, yet filters with higher corner frequencies did not. The filtered *in vivo* data from the three remaining sensors still had harmonic waves present as seen in Figure 9.13B. This could be attributed to either resonant pressure waves or ringing artifacts from the filter used. System damping or resonance is dependent on a variety of factors, such as tubing compliance, tubing length, the presence of air bubbles, tubing kinks, and blood clots. An underdamped system features additional harmonic waves; the systolic and diastolic levels are often exaggerated, leading to an overestimation of blood pressure. On the other hand, an overdamped system result in an underestimation of blood pressure since wave energy is absorbed by tubing or clots, and the systolic and diastolic peaks are reduced [72]. This is surprising since the sensors never exhibited any resonance artifacts during any *in vitro* testing even when tested at higher pressure wave frequencies than that observed in the animal. In addition, because silicone was used, which is highly compliant and vapor permeable, there was a general belief that the sensor would potentially be overdamped.

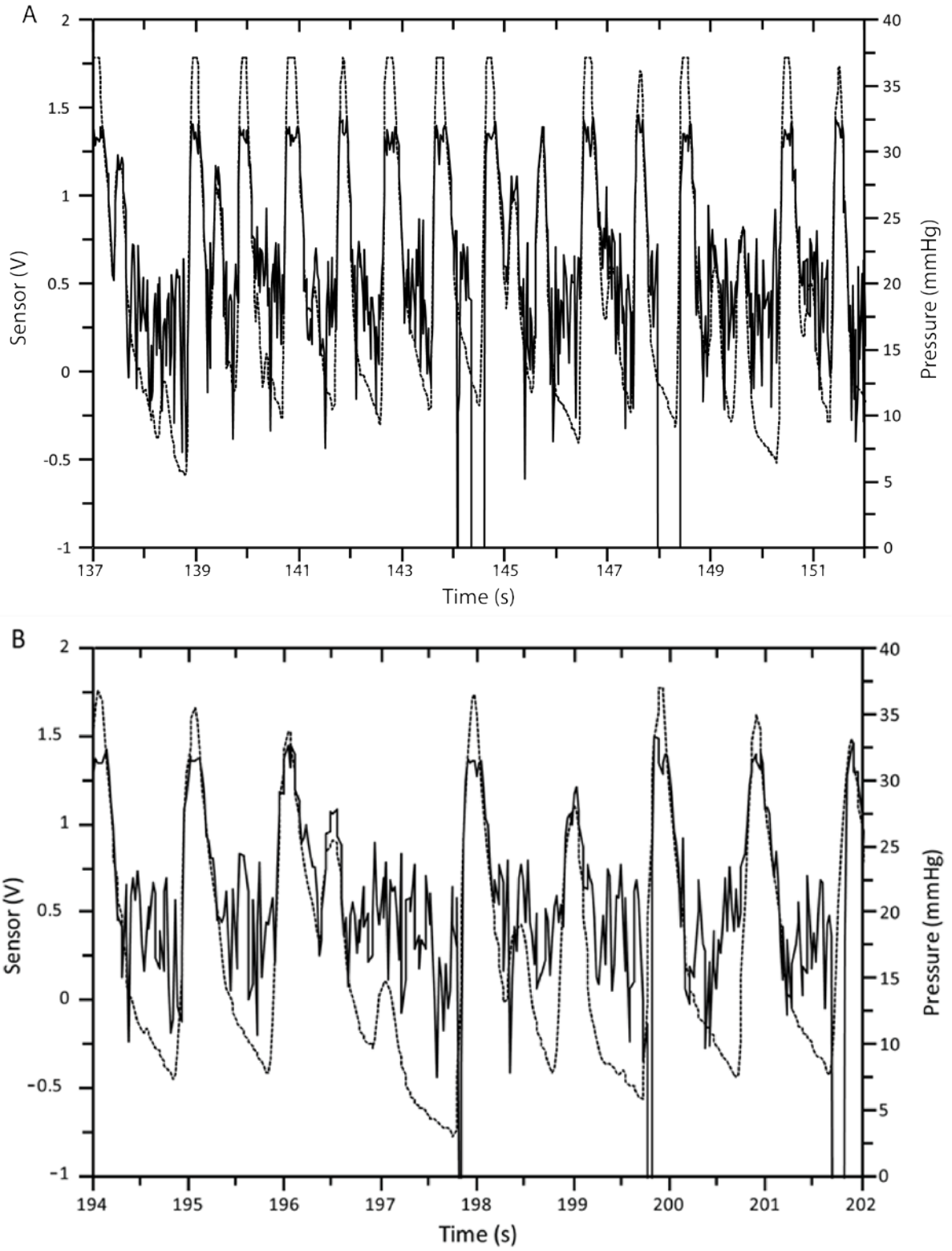

Figure 9.12. Select windows of raw data from a sensor implanted in the femoral artery of a porcine model. The data from the sensor is represented by the solid trace; dotted is the pressure.

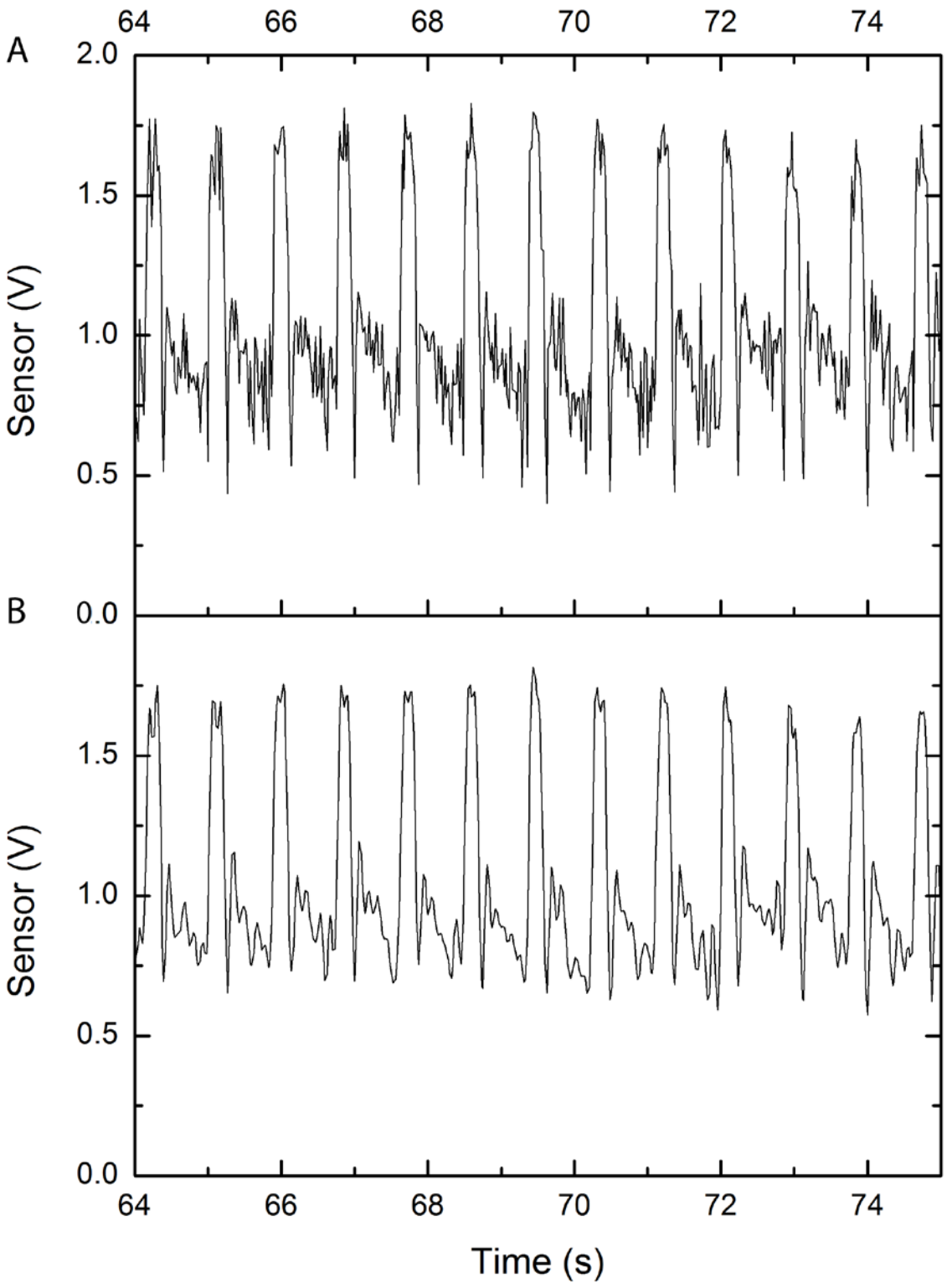

Figure 9.13. A comparison of A) the raw data, B) the data filtered with a 10th order Butterworth filter (f_c = 12 Hz) and of a sensor used in the *in vivo* study.

Therefore, it can only be concluded that any reflected pressure waves the sensor detected must have resulted from variables introduced during the animal study or from the filter used. A simple model using the same filter on a 15-Hz wave superimposed onto the data from the pressure transducer, which would best replicate the pressure wave sensed by the CRISP sensor, did not replicate the oscillations seen in the experimental sensor data. However, this model is limited since it is unclear how well the model replicated the waveform seen in the CRISP sensor data. It is also possible that the oscillations are a combination of an underdamped system and filtering artifacts, and further study is required to isolate the exact source of these harmonic waves. This also stresses the need to fully insulate all electronic components from blood fouling in order to avoid any filtering.

The data was then subjected to a low pass 10^{th} order Butterworth filter with a corner frequency of 5 Hz. It's immediately evident that the noise has been cleared out, and many of the resonance artifacts have been removed. The amplitudes of the pressure waves have also been slightly reduced as well, but this is a minor issue since the sensor can easily be calibrated after filtering for future use. Two data sets of the first implanted sensor are shown in Figures 9.12 (raw) and 9.14 (filtered at 5 Hz). The number of large negative voltage spikes seen in the raw data has been reduced. Once the data has been filtered, the data displayed many more secondary peaks that were completely obscured in the raw data. This is particularly interesting since many of the peaks are present only in the sensor data, but not in the reference pressure trace recorded by the commercial pressure transducer. This is especially evident when comparing Figures 9.12B and 9.14B. It must be remembered, however, that although the commercial pressure transducer was connected to the same catheter port that the CRISP sensor was inserted into, the catheter-based sensor measures blood pressure *in situ*.

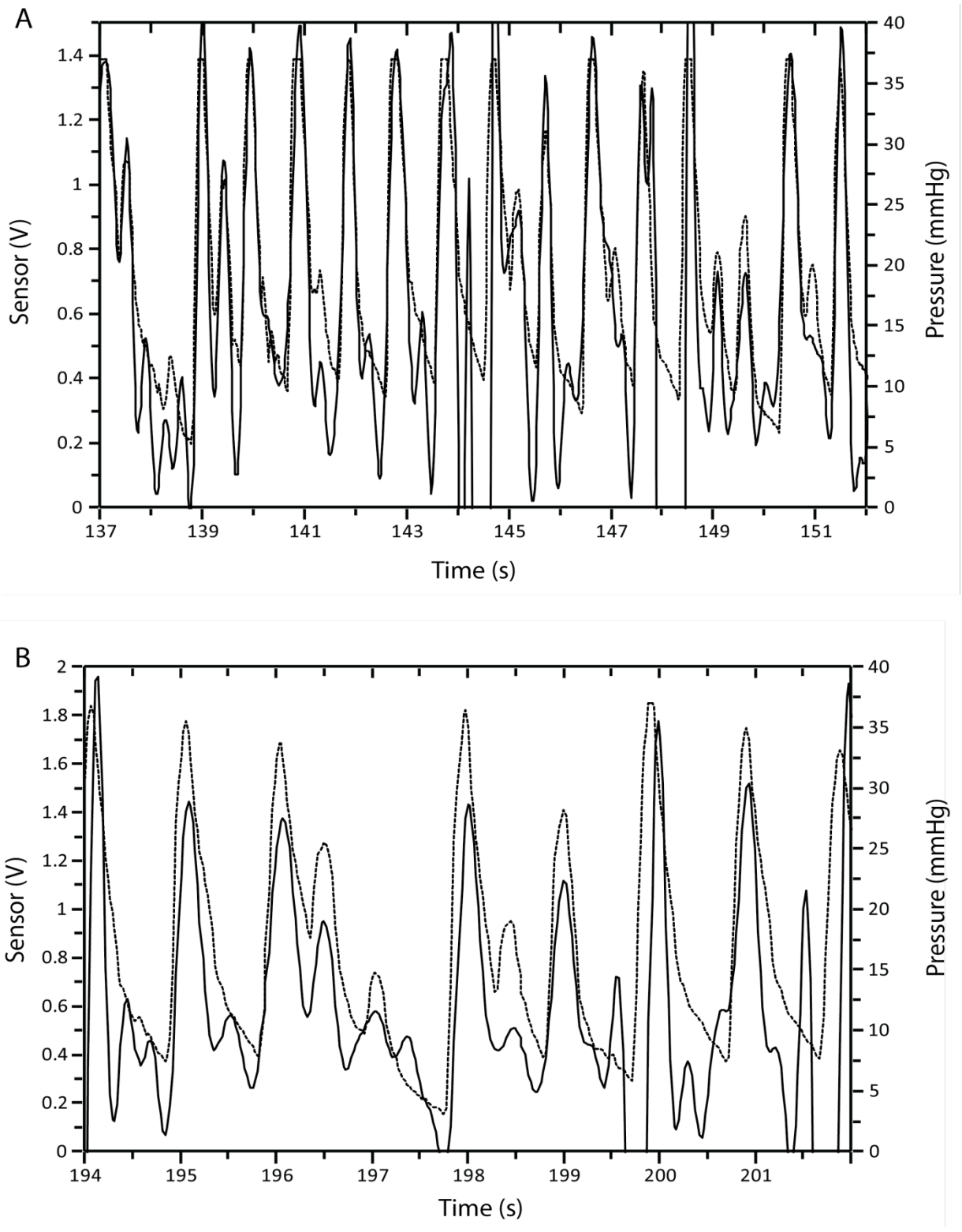

Figure 9.14. The filtered data previously shown in Figure 9.12. The filter is a 10th order low pass Butterworth filter (f_c = 5 Hz). Solid represents the sensor data and dotted is the pressure.

It is entirely possible there were some nuances to the pressure profile that were not completely transmitted to the commercial pressure transducer through the arterial line, yet were picked up by the CRISP sensor. If that is the case, then these two traces already demonstrate the superiority of a catheter-based sensor over the traditional method of measuring pressure through an *ex vivo* pressure transducer connected to an arterial line. The mere presence of secondary pressure peaks that were detected by both sensors tends to support the belief all the secondary peaks are real regardless of whether or not they were sensed by the commercial transducer. It is reasonable to assume that these secondary peaks were prevalent during this experiment. Moreover, looking at Figure 9.14B, the period between secondary peaks remains consistent at a little under 0.45 seconds, or a frequency of 2.2 Hz; this further supports the hypothesis that these peaks are real. The heart rate as detected by the commercial transducer would be 60 bpm. The secondary peaks in the CRISP sensor, if counted as heart beats, would boost the heart rate to 120 bpm. There would be little reason why the test subject would be temporarily tachycardic and return to its normal heart rate without intervention. It is entirely possible that these secondary peaks are actually dicrotic waves, which are small momentary increases in pressure as the arotic valve closes at the start of diastole. Dicrotic notches are more evident in peripheral arteries readings, including the femoral artery than in the aorta [73-76]. In fact, in Figure 9.14A at 140-144 seconds, the dicrotic notch is quite noticeable in the CRISP sensor data, but is muted in the commercial transducer. The dicrotic notch as sensed by the CRISP sensor is shown in more detail in Figure 9.15.

Two other sensors that were implanted also yielded pressure data although the pressure data tended to be more stable. Both sensors were not as noisy as the first sensor shown above, which was expected since the first sensor was used the most during the entirety of the animal

experiment, and thus, accumulated the most amount of blood. The second sensor implanted during the study did not have a typical waveform profile as indicated by the raw data in Figure 9.16A.

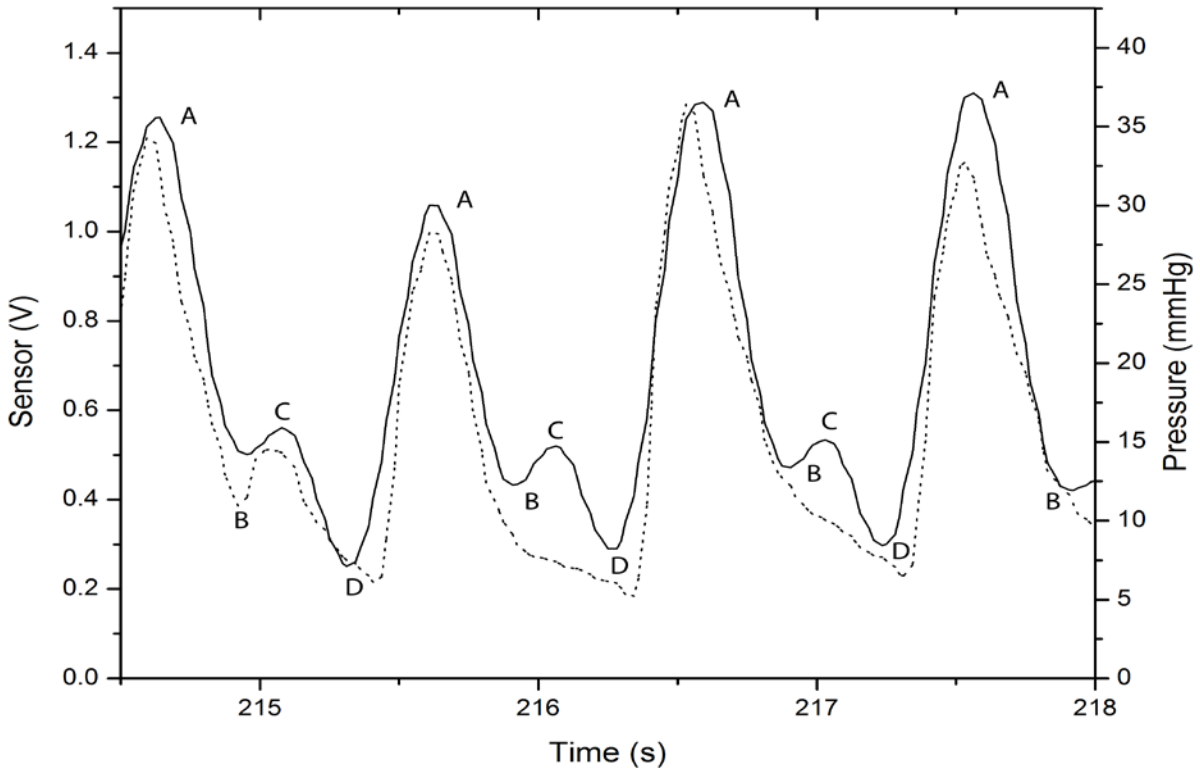

Figure 9.15. A detailed plot of the femoral pressure wave as detected by the CRISP sensor (solid) compared to a commercial arterial line pressure transducer (dotted). A) the systolic pressure, B) the dicrotic notch, C) the dicrotic wave, and D) the diastolic pressure.

The trough of the wave as detected by the CRISP sensor seemingly occurred earlier than in the commercial transducer. However, by looking at the filtered data (Figure 9.16B), it's pretty evident that there were small secondary peaks immediately succeeding the large primary peak for each wave. This small peak was not detected by the commercial transducer. These peaks may actually be ringing artifacts as a result of the use of a high-order Butterworth filter.

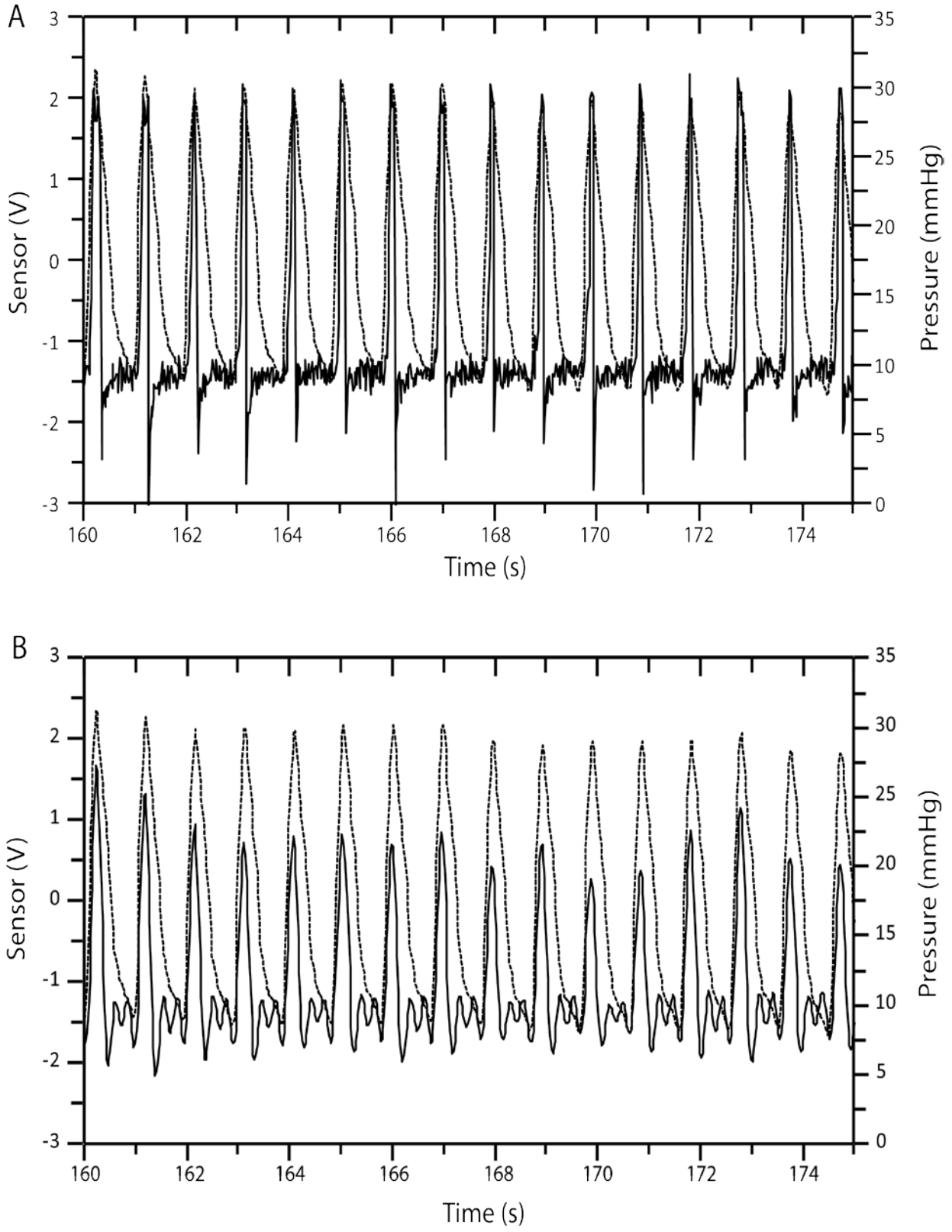

Figure 9.16. A 15-second window of the a) raw data and b) filtered data using a 10^{th} order low pass Butterworth filter (f_c = 5 Hz) for a second sensor implanted into the femoral artery of a porcine model.

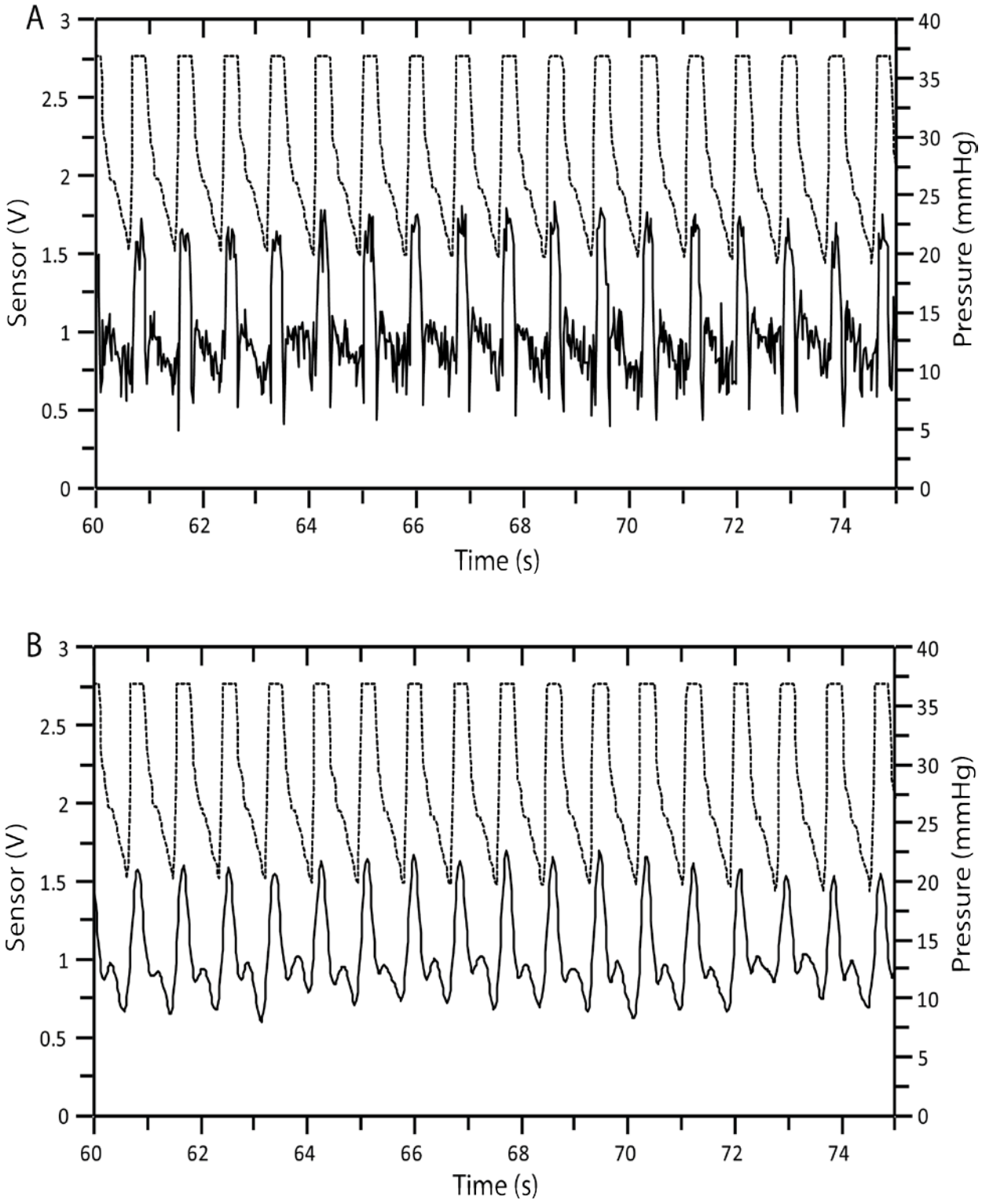

Figure 9.17. A 15-second window for a third CRISP sensor showing a) the raw data and b) the filtered data using a 10^{th} order low pass Butterworth filter (f_c = 5 Hz) implanted into the femoral artery of a porcine model.

The third operable CRISP sensor implanted into the porcine model had arguably the best performance since the waveforms matched that of the commercial transducer almost exactly (Figure 9.17). It was not as noisy as the first implanted sensor. Also there weren't any secondary peaks in either the commercial transducer or in the CRISP sensor as the sensor may have been recording pressure at a relatively stable time. Unfortunately, however, the commercial transducer was amplified with a gain of 100, which in the end was too high. The pressure as measured in the porcine model was too high and the amplifier saturated yielding a truncated wave. One more pressure transducer, which had undergone static testing the same day as the animal experiment, was also implanted, but it yielded no pressure waveforms. That particular sensor did have a large amount of blood accumulation on the electrical components, so it's possible that the sensor was entirely short circuited.

It was generally assumed that the commercial transducer was the gold standard that the experimental CRISP sensor had to meet. However, after this animal experiment, it's clear that may not be the case because many small pressure peaks were picked up by the CRISP sensor, but were not detected by the commercial transducer. Furthermore, details in the pressure wave itself, such as the dicrotic notch was only prominent in the CRISP sensor. Moreover, the difference between the systolic and diastolic peaks was only 22-30 mmHg as detected in the commercial sensor, which is lower than expected. The difference between the CRISP sensor being an *in situ* sensor and the commercial transducer being an *ex vivo* sensor may ultimately be the reason behind the different pressure traces. The blood needs to travel out of the artery, through the catheter sheath, into silicone tubing, and finally to the sensor. The transducer was connected on the other end to a syringe, which was used to 1) seal the system off from blood loss and 2) draw blood past the pressure sensitive die in the transducer. Therefore, there was air in the system in

contact with a piston, and due to the lack of a flushing system, the blood in the arterial line was stagnant, which can lead to clots. Both of these effects may act as dampeners and reduce many small amplitude pressure waves.

While the setup for the transducer may be incorrect for accurately measuring hemodynamic pressure, the complexity alone of fluid-filled catheter systems proves the advantage of *in situ* systems. Furthermore, the mere presence of long compliant tubing and Luer connections, such as stopcocks, and the lack of a flush bag all lead to overdamped systems, which lead to erroneous readings in fluid-filled catheters [74]. The steps required to prevent this are all an indictment against the traditional arterial hemodynamic monitoring methods.

Chapter 10 Conclusion

A novel *in situ* arterial pressure sensor discussed in this research was created by utilizing the fluidic conductance of normal saline solution housed in an elastic tube. By using strictly commercially available components, the material costs were kept to a minimum. The most expensive component was the platinum wire electrodes, but platinum may not be certainly necessary for the sensor to properly function. MEMS sensors have been touted to be highly economical due to their low price. However, in order to keep micromachined sensors unit cost low, it has to manufacture in large quantity, and incur a high setup charge due to the need to customize photolithography masks or molds. Moreover, the cost of assembly and packaging are typically not included. For these reasons nearly all *in situ* pressure sensors found in the market, were made by hand, driving the cost very high. The previously described CRISP sensor, while also hand-made, is simple to assemble and only takes a few man-hours for each device. At industrial scale production, the fabrication can only get more efficient by automating certain fabrication steps in an assembly line.

MEMS sensors are also plagued with packaging problems to protect the fragile connections, especially during implantation. The MEMS-based bladder pressure sensor required the pressure die to be electrically connected to the rest of the circuit with wirebonds, which can easily be lifted off. Additionally, the die needed to be protected from the harsh environment found within the test subject. Likewise, the test subject needed to be protected from any potentially toxic, thrombogenic, or bioactive materials used in the sensor fabrication. All the packaging adds to the bulk of the sensor, making it impractical for implantation. The experimental blood pressure sensor ingeniously utilized the packaging as the main components of the sensor, and hence minimizes the physical size. By combining the sensor design with the

cost of components, it's possible to scale the sensor down easily and economically. It is feasible to economically produce 1-2 French catheter-mounted pressure sensors which are implantable into small animals or even in small peripheral arteries in neonates. The idea is to produce low cost sensors, which can then be considered as one of the standard tools in patient monitoring and care. This would increase the number of prospective patients using these blood pressure sensors and providing physicians with a wealth of information, which will hopefully make the diagnosis of diseases easier and quicker.

The experimental blood pressure sensor performed at least on par, if not slightly better than a standard commercial pressure transducer used with a standard fluid-filled arterial line. In all *in vitro* tests, the CRISP sensor was able to replicate the same response as any commercial pressure gauge used in this experiment. *In vivo* testing showed the CRISP sensor detecting small details that were diminished in the commercial pressure transducer's trace although the transducer was potentially overdamped due to improper setup. At the very least, the simplicity of deployment of the CRISP sensor gives it an edge over the standard transducer. Proper diagnosis of medical condition sometimes relies on the analysis of arterial pressure wave by looking at the characteristics like the steepness of the systolic upstroke curve and the position and magnitude of the dicrotic notch and wave. From this experiment, it is clear that the reliance on the standard arterial line for patient monitoring requires draconian procedures to ensure proper functionality and that any deviation from these procedures can lead to misinterpretation of the data. A pressure sensor, like CRISP sensor, mounted on a catheter measures blood pressure directly, circumventing many of these issues.

10.1 Design Improvement

The CRISP sensor was successfully deployed in an animal through a 7 French catheter port. With any implantable sensor, there is always a concern with the integrity of the packaging and whether or not it would survive the implantation procedure, as well as continue to function inside a body. After several failed animal tests and *in vitro* dynamic studies, the sensor was packaged with a technique that was believed to be able to survive the catheterization with high confidence. However, the packaging of the connection between the small micro-sized platinum wires and the signal conditioning circuit was an afterthought since it was assumed that the cable plug and quick connector would come into contact with very little blood. The incidental contact of blood was not foreseen, and it ultimately proved to be the biggest problem. Although that area was protected, it clearly was not adequate since blood easily permeated the epoxy layers. It is not believed, however, that the epoxy itself is permeable to liquid, but rather, an incomplete coating led to pinholes in the coating that formed a pathway for the blood to reach the wires. The packaging on the cable plug can be improved simply by using an excess amount of epoxy to ensure complete coverage of the electronic components. The quick connector was constructed using a female plug and duct tape for protection. A commercial 3-contact plug would be more than suffice.

When the animal study was performed, a large, mostly outdated desktop computer and all its accessories were carted across campus to the operating room along with the conditioning circuit, LabVIEW Block, and the AC and DC power supplies. The circuit was laid out on a solderless breadboard; during transport, circuit elements were prone to jarring loose. While fixing that is easy, a lot of time was required to identify which component had come loose. While temporary solutions, such as providing a cushion for the circuit or softening the ride of the cart, exist, a more permanent solution would be to integrate all the electronic components onto a

single printed circuit board. The advantage is twofold: not only will the circuit be more physically durable during transportation, but the size of the circuit is scaled down, which is necessary if the sensor is to be commercialized.

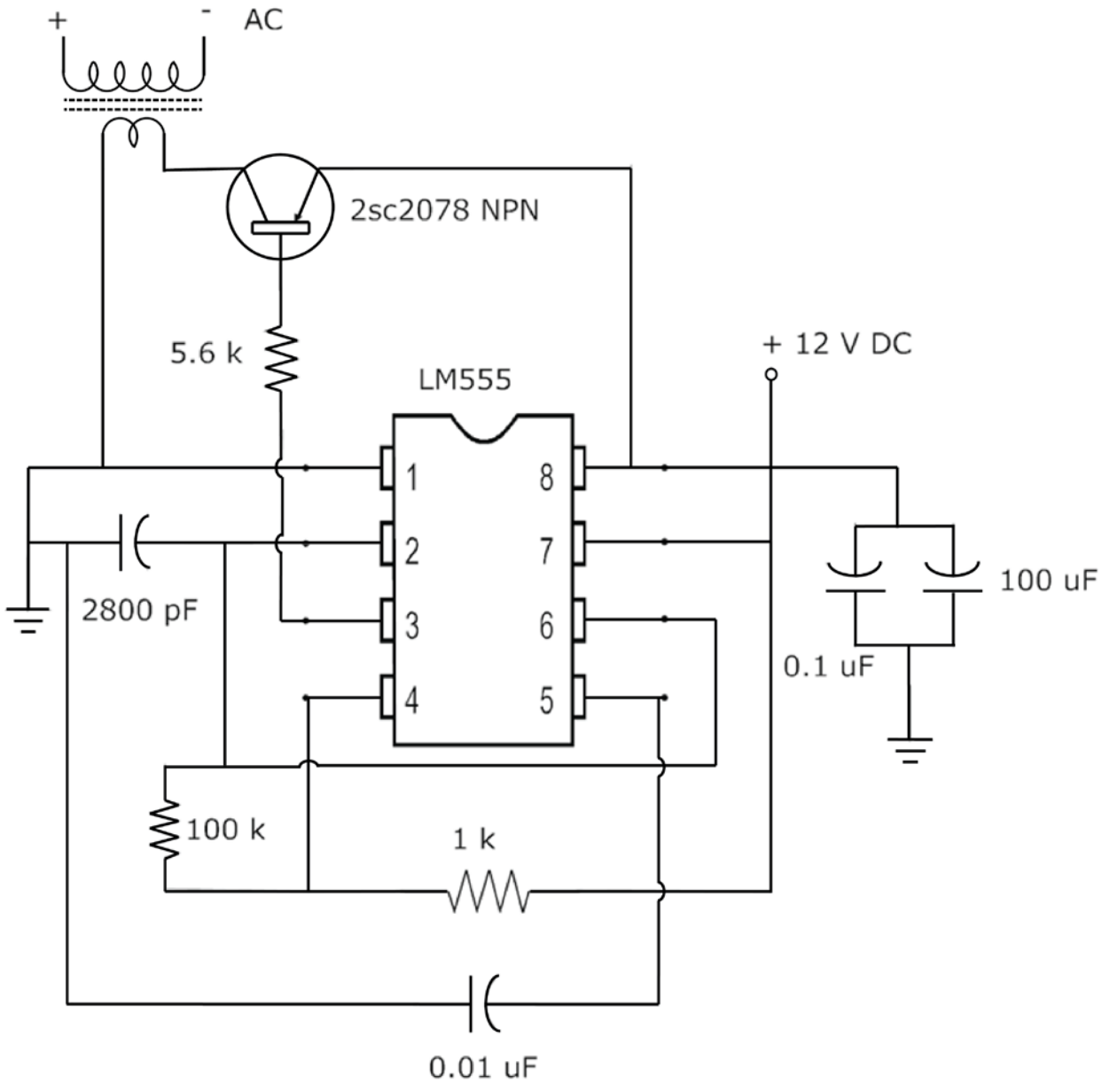

Figure 10.1. A sample power inverter circuit diagram. Circuit copied from Wyatt [77, 78].

The bulkiness required to operate the sensor can be further reduced by eliminating the function generator that powers the AC bridge. This can be accomplished by either using

LabVIEW to generate the wave or integrating a power inverter circuit (Figure 10.1), which converts a DC supply to an AC signal. This option is absolutely necessary if wireless transmission is implemented since all power needs to be supplied by a miniature battery. The algorithm that reads and records the data from the CRISP sensor can also be optimized. It currently utilizes a moving average to smooth out the noise in the data; however, in dynamic environments, this has an adverse effect on the sensitivity and is frequency-sensitive. The animal study clearly showed that noise is still a problem even if *in vitro* tests showed otherwise. Since software filtering with a low pass Butterworth filter was effective, real-time filtering of the data may be useful. In order to do so, the algorithm can be modified by creating a temporary buffer file that can store enough data to be filtered effectively, yet small enough that the filtered data can be plotted without a time delay or lag.

Another useful modification would be an early warning system embedded into the LabVIEW program. If a fully embedded sensor network were deployed in a hospital, physicians would be unable to monitor every patient's vital signs at the same time. Therefore, by having the LabVIEW program automatically monitor the pressure waveform for any specific characteristics that are indicative of life threatening conditions, the physician can divert his/her attention elsewhere until an alarm sounds. A simple peak detector triggered with amplitude that passes a certain threshold can help diagnose many conditions. For example, by using a timer, heart rate can be determined and conditions like bradycardia and tachycardia can be detected. Furthermore, by monitoring the absolute pressure values of the systolic peak relative to the diastolic level, an alarm can be triggered if the difference between the systole and diastole falls too short as can occur with shock. Moreover, the lack of a discernible systolic peak can indicate ventricular fibrillation, and long-term patient monitoring may require an alert to be sent to a physician if the

mean blood pressure exceeds a certain level. Last, an extension of an automatic patient monitoring system is to have the program automatically send an alert wirelessly to a phone, tablet computer, pager, or computer would speed up the diagnostic process and reduce the patient risk.

Further analysis of the arterial pressure waveform can be performed by software to monitor other critical vital signs. By integrating the area under systolic phase of the arterial pressure wave, the cardiac output can be measured continuously using pulse contour methods developed by Wesseling in 1983 [2, 79]. By knowing the age and weight of the patient, the vascular resistance and cardiac output can be calculated from the arterial pressure. Also, since the arterial waveform needs to be accurately portrayed, *in situ* pressure sensors have an advantage over standard arterial line pressure sensors for calculating cardiac output. Continuous monitoring of cardiac output has always been desired, but there were previously no practical ways of doing it. The traditional method, using pulmonary arterial catheters, only gives discrete measurements using thermodilution techniques.

10.2 Future Work

As with any implantable device, biocompatibility tests are required despite the use of FDA-approved materials. There are standard testing protocols for biocompatibility testing to study toxicity, immune response, and inflammatory response. These tests can be broken down to cytotoxicity, thrombogenecity, hemolysis, protein and platelet adhesion, and pyrogenicity [80]. Since the catheter is designed to be a short-term implant, hemocompatibility is the highest priority. Specifically, both the assembled product and the individual components would be subjected to a flowing solution of radiolabeled fibrinogen and albumin for a few days [81].

Afterwards, the device and its components would be inspected by both light and SEM microscopy for any bioadhesion. A similar test involving blood serum can also be conducted as a more thorough study on hemocompatibility of the CRISP sensor. Last, after catheter insertion for a prolonged period, the sensor would be extracted and imaged. Histology would need to be performed at the implant site after the test subject is sacrificed to study scar tissue formation and immune response to the sensor.

One feature of the sensor design is its ability to be scaled down easily. While the catheter only needs to be about 3 French for radial artery catheterization [82], catheters as small as 1 French can be used in a variety of specialized locations, such as neonatal arteries and the spinal column to measure central spinal fluid for hydrocephalus. One specific condition that can be tested but hasn't been looked into is compartment syndrome. Compartment syndrome arises when massive trauma forces the tissue to become so edematous that the fluid pressure occludes local blood supply. The tissue becomes ischemic and will eventually die if unchecked. Compartment syndrome typically arises after bone fractures, soft tissue injury, burns, hemorrhage, iatrogenic causes, bites, muscle overexertion, pancreatic and bowel obstructions, and surgery [83-85]. Mortality rates are high in some cases—up to 60% for abdominal cases [86]. Diagnosis often relies on qualitative descriptions of symptoms: intense and increasing pain and paresthesia. The condition is often misdiagnosed until too late when a physician notes swelling, paralysis, and a lack of pulse in the affected area. At this point, it is a race against time, and a fasciotomy becomes necessary to save the patient's life and limbs. Current monitoring of compartment syndrome requires discrete pressure measurements in the affected area every few hours. A small catheter-based sensor can easily be inserted into the afflicted area as a precaution for patients at higher risk for compartment syndrome, such as those who have suffered massive

trauma or have undergone surgery. This would provide physicians with an ability to detect compartment syndrome should it arise earlier, apply treatment correspondingly and avoid needless fasciotomies or more drastic treatments.

As of this point, the catheter was developed only to house a pressure sensor; by adding different sensing modalities onto the catheter, a true vital signs monitoring platform can be developed. Potentially, a wealth of patient data can be provided to a physician with the implantation of one catheter. Patients will no longer be forced to be tethered to a variety of bedside patient monitors, increasing their comfort. Sensing modalities like temperature can easily be added by simply attaching a thermocouple to the catheter. A simple galvanic cell using platinum and silver/silver-chloride electrodes can be used to measure pO_2.

Many vital signs, such as blood chemistry, previously were limited to discrete measurements only. For example, the blood pH value is an important parameter to track in acidodic or alkalotic patients. However, the blood pH level currently can only be measured by using a glass electrode that houses a galvanic cell with platinum and silver/silver-chloride electrodes and a buffered solution or by using an ion-selective field effect transistor. Both require the use of a reference electrode, which preclude them from being shrunk down for implantation. This is especially important if a pH sensor is to be coupled to other sensing modalities. An innovative new field is the use of pH-sensitive conductive polymers, such as polyaniline, as the sensor since the design is simple and the polymer is nontoxic [87]. By depositing a thin film [88] onto to the outside of a catheter and making electrical contact with it, a pH sensor can easily be integrated into the CRISP sensor developed in this research. To take it one step further, integrating the polyaniline film with a hydrogel laden with bicarbonate can convert it into a

pCO_2 sensor. Alternatively, using glucose oxidase with the polyaniline sensor can potentially create a glucose sensor for diabetes monitoring. By measuring pH and pCO_2 levels along with pressure, compartment syndrome can be more easily detected and tracked by measuring ischemic tissue directly. Last, a variety of different salts and enzymes can be used in conjunction with polyaniline to detect different parameters that traditionally have required laboratory work to quantify. Figure 10.2 depicts a rendition of the layout of multiple sensor modalities on the catheter.

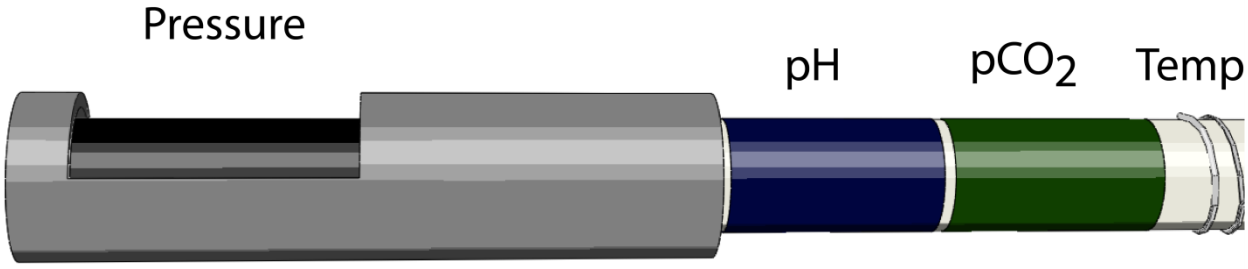

Figure 10.2. An artist's rendition of the layout of different sensing modalities on the pressure sensitive catheter.

To take the project full circle, the sensor developed in the latter half of the project can be paired with wireless capabilities of the fully implantable sensor covered earlier. For hospital use, the transmitter and signal conditioning circuit can be kept *ex vivo*. Wireless communication would allow the patient to be free from the patient monitor and fully ambulatory to allow for more accuracy and patient comfort. By implementing a better wireless protocol and utilizing the proposed software upgrades mentioned before, a true hospital sensor network can be established, allowing for greater efficiency in patient care and diagnoses. On the flip side, a fully implantable sensor can be revisited for patients with chronic illnesses. However, several upgrades need to be completed before a viable platform can be created. First, the battery must be rechargeable inside the body. This can be performed either through radio induction similar to that used by other

implantable sensors or through kinetic energy harvesting, a technique akin to that used in some wristwatches. A rechargeable battery also allows the overall size of the implant to be reduced. Second, the device receiving the signal from the implanted sensor must be able to alert the patient or the patient's physician if a serious condition arises. Fortunately, with recent developments in mobile phones and tablet PCs, this is quickly becoming a fast-growing field. Third, the privacy of patient data is of utmost importance. Data encryption needs to be implemented with a unique encryption key for each patient, which can be challenging to implement and deploy.

10.3 Final thoughts

The biggest problem in diagnosis that physicians face is an incomplete amount of data required to accurately identify specific diseases and conditions. Diagnosis was often based on qualitative descriptions or observations; due to the conservative nature of the medical community, quantitative data was often obtained through using the relatively ancient but proven techniques and technology while advancements in sensor technology were spurned. In fact, for certain measurements, like blood pressure, traditionally require a trained operator to infer when systole and diastole occurred. Last, many quantitative measurements were done discretely due to practical and technological limitations. However, as technology advances, medical sensors and the computing power required to run them become more readily available and more economical. By integrating wireless communication with real-time sensing, the potential to create a medical care facility fully networked with a litany of sensors exists. Suddenly, medical care personnel would have access to a wealth of information containing real-time information on a variety of vital signs to paint a more accurate picture of the physiology of the patient. Misdiagnoses and treatment errors would be reduced and health care would be more efficient. Building on this,

soon, based on the information from a variety of embedded sensors, computers could easily diagnose diseases and conditions automatically and recommend treatment options to physicians. Another aspect of wireless communication is patient comfort. The ability to wear the sensor without being tethered to bulky patient monitors and bedside transducers frees patients to be able to walk and move around without compromising the integrity of the data. Quality of life is oftentimes considered to be more important than actual treatment. Building from what currently has been done and what is presented here, it is not farfetched to imagine a world where people are kept alive and functional by embedded, implanted, or wearable sensors/transducers a la Darth Vader in *Star Wars*.

Finally, C4ISR, which stands for command, control, computers, communications, intelligence, surveillance, and reconnaissance, is a concept used by the United States military to describe the ability to direct fighting forces and supporting logistics and methods of observing the enemy and their area of operations. Although medical care hopes to accomplish a vastly different task, the concepts of fighting a disease and fighting an opposing army are similar. To defeat the "fog of war," medical staffs need to determine an accurate picture of a patient's physiology. Continuous, real-time vital signs monitors can help accomplish this task to give physicians an upper hand in fighting disease. However, while the military brass has been quick to adopt technology in warfighting, medicine has been slow to follow suit. As technology developments advance at breakneck speed, the need to revolutionize healthcare becomes increasingly clear. It is up to physicians to adopt and embrace technology and make this happen.

References

[1] L. Kohn, J. Corrigan, and M. Donaldson, *To Err is Human: Building a Safer Health System*. Washington DC: National Aacademy Press, 2000.

[2] G. D. Rocca, M. Cecconi, and M. G. Costa, "Mini invasive hemodynamic monitoring: from arterial pressure to cardiac output," *Signa Vitae*, vol. 3, pp. S7-9, 2008.

[3] P. L. Marino, *The ICU Book*. Baltimore: Lippincott Williams & Wilkins, 1998.

[4] A. Reisner, P. Shaltis, D. McCombie, and H. Asada, "A Critical Appraisal of Opportunities for Wearable Medical Sensors," presented at the 26th Annual International Conference on the IEEE EMBS, San Francisco, CA, 2004.

[5] C. K. Yeung, "Continuous Real-Time Ambulatory Urodynamic Monitoring in Infants and Young Children Using Infrared Telemetry," *British Journal of Urology*, vol. 81, pp. 76-80, 1998.

[6] J. G. Clement, P. Mills, and B. Brockway, "Use of telemetry to record body temperature and activity in mice," *J Pharmacol Methods*, vol. 21, pp. 129-140, 1989.

[7] K. Kramer, H. P. Voss, J. A. Grimbergen, P. A. Mills, D. Huetteman, L. Zwiers, and B. Brockway, "Telemetric monitoring of blood pressure in freely moving mice: a preliminary study," *Lab Anim.*, vol. 34, pp. 272-280, 2000.

[8] G. T. Livezey, J. M. Miller, and W. H. Vogel, "Plasma norepinephrine, epinephrine and corticosterone stress responses to restraint in individual male and female rats and their correlations," *Neurosci Lett*, vol. 62, pp. 51-56, 1985.

[9] M. J. Field and J. Grigsby, "Telemedicine and remote patient monitoring," *Jama*, vol. 288, pp. 423-5, Jul 24-31 2002.

[10] R. A. Chaer, S. Trocciola, B. DeRubertis, R. Hynecek, Q. Xu, R. Lam, K. C. Kent, and P. L. Faries, "Evaluation of the accuracy of a wireless pressure sensor in a canine model of retrograde-collateral (type II) endoleak and correlation with histologic analysis," *Journal of Vascular Surgery*, vol. 44, pp. 1306-1313, Dec 2006.

[11] N. Najafi and A. Ludomirsky, "Initial animal studies of a wireless, batteryless, MEMS implant for cardiovascular applications," *Biomed Microdevices*, vol. 6, pp. 61-65, Mar 2004.

[12] J. A. Potkay, "Long term, implantable blood pressure monitoring systems," *Biomed Microdevices*, vol. 10, pp. 379-92, Jun 2008.

[13] R. Schlierf, U. Horst, M. Ruhl, T. Schmitz-Rode, W. Mokwa, and U. Schnakenberg, "A fast telemetric pressure and temperature sensor system for medical applications," *Journal of Micromechanics and Microengineering*, vol. 17, pp. S98-S102, Jul 2007.

[14] U. Schnakenberg, C. Krüger, J.-G. Pfeffer, W. Mokwa, G. v. Bögel, R. Günther, and T. Schmitz-Rode, "Intravascular pressure monitoring system," *Sensors and Actuators A: Physical*, vol. 110, pp. 61-67, April 20, 2003 2003.

[15] A. S. Walton and H. Krum, "The Heartpod implantable heart failure therapy system," *Heart Lung Circ*, vol. 14 Suppl 2, pp. S31-3, 2005.

[16] B. Ziaie, T.-W. Wu, N. Kocaman, K. Najafi, and D. J. Anderson, "An implantable pressure sensor cuff for tonometric blood pressure measurement," *Biomed Microdevices*, vol. 3, pp. 285-292, December, 2001 2001.

[17] C.-C. Chiang, C.-C. K. Lin, and M.-S. Ju, "An implantable capacitive pressure sensor for biomedical applications," *Sensors and Actuators a-Physical*, vol. 134, pp. 382-388, June 6, 2006 2007.
[18] T. Eggers, J. Draeger, K. Hille, C. Marschner, P. Stegmaier, J. Binder, and R. Laur, " Wireless intra-ocular pressure monitoring system integrated into an artificial lens," presented at the Microtechnologies in Medicine and Biology, 1st Annual International, Conference On. 2000, Lyon, France, 2000.
[19] M. Leonardi, P. Leuenberger, D. Bertrand, A. Bertsch, and P. Renaud, " A soft contact lens with a MEMS strain gage embedded for intraocular pressure monitoring," presented at the TRANSDUCERS, Solid-State Sensors, Actuators and Microsystems, 12th International Conference on, 2003, 2003.
[20] A. Meir, D. S. McNally, J. C. Fairbank, D. Jones, and J. P. Urban, "The internal pressure and stress environment of the scoliotic intervertebral disc - a review," *Proceedings of the Institution of Mechanical Engineers Part H-Journal of Engineering in Medicine*, vol. 222, pp. 209-219, Feb 2008.
[21] M. R. Tofighi, U. Kawoos, A. Rosen, and S. Neff, "Wireless intracranial pressure monitoring through scalp at microwave frequencies," *Electronics Letters*, vol. 42, pp. 148-150, Feb 2 2006.
[22] P. Walter, U. Schnakenberg, G. vom Bogel, P. Ruokonen, C. Kruger, S. Dinslage, H. C. L. Handjery, H. Richter, W. Mokwa, M. Diestelhorst, and G. K. Krieglstein, "Development of a completely encapsulated intraocular pressure sensor," *Ophthalmic Research*, vol. 32, pp. 278-284, Nov-Dec 2000.
[23] H. J. Yoon, J. M. Jung, J. S. Jeong, and S. S. Yang, "Micro devices for a cerebrospinal fluid (CSF) shunt system," *Sensors and Actuators a-Physical*, vol. 110, pp. 68-76, Feb 1 2004.
[24] J. Coosemans and R. Puers, "An autonomous bladder pressure monitoring system," *Sensors and Actuators a-Physical*, vol. 123-24, pp. 155-161, Sep 23 2005.
[25] E. Siwapornsathain, A. Lal, and J. Binard, "A telemetry and sensor platform for ambulatory urodynamics," presented at the 2nd Annual International IEEE-EMBS Special Topic Conference on Microtechnologies in Medicine & Biology, Madison, Wisconsin, USA, 2002.
[26] CardioMEMS. (2007, July 2, 2008). *Endosure AAA Sensor*. Available: http://www.cardiomems.com/content.asp?display=medical+mb&expand=ess
[27] E. Bell, "Obstruction of the Urinary Tract-Hydronephrosis," *Renal Diseases*, pp. 113-139, 1946.
[28] J. Koh, M. Wong, M. Li, and K. Foo, "Idiopathic Retroperitoneal Fibrosis with Bilateral Lower Ureteric Obstruction - A Case Report with Literature Review," *Singapore Medical Journal*, vol. 39, pp. 416-417, 1998.
[29] R. B. Jaffe and A. W. Middleton, "Whitaker Test: Differentiation of Obstructive From Nonobstructive Uropathy," *American Journal of Roentgenology*, vol. 134, pp. 9-15, 1980.
[30] N. J. Hellenthal, S. A. Thomas, and R. K. Low, "Rapid onset renal deterioration in an adult with silent ureteropelvic junction obstruction," *Indian J Urol*, vol. 25, pp. 132-133, 2009.
[31] R. Whitaker, "The Whitaker Test," *Urol Clin North Am*, vol. 6, pp. 529-539, 1979.
[32] "Intracranial Pressure Monitoring Technology," *Pediatric Critical Care Medicine*, vol. 4, pp. S28-S30, 2003.

[33] J. Ellis, R. Campo, M. Marx, R. Cohan, J. Platt, L. Sonda, G. Faerber, and D. Kim, "Positional variation in the Whitaker test," *Radiology*, vol. 197, pp. 253-255, 1995.
[34] P. C. Walsh, A. B. Retik, and T. A. Stamey, *Campbell's Urology*, 8 ed. Philadelphia, PA: Saunders Title, 2002.
[35] L. P. Lawler, T. W. Jarret, F. M. Corl, and E. K. Fishman, "Adult Ureteropelvic Junction Obstruction: Insights with Three-dimensional Multi-Detector Row CT," *Radiographics*, vol. 25, pp. 121-134, 2005.
[36] R. Tan, T. McClure, C. K. Lin, D. Jea, F. Dabiri, T. Massey, M. Sarrafzadeh, M. Srivastava, C. Montemagno, P. Schulam, and J. Schmidt, "Development of a fully implantable wireless pressure monitoring system," *Biomed Microdevices*, vol. 11, pp. 259-264, 2009.
[37] R. Tan, T. McClure, P. Schulam, and J. J. Schmidt, "Development of a Minimally Invasive Implantable Wireless Vital Signs Sensor Platform," in *Medicine Meets Virtual Reality 17*, Long Beach, CA, 2009, pp. 380-385.
[38] Nusil. (2008, July 10). *Med-4011 Product Profile*. Available: http://www.nusil.com/library/products/MED-4011P.pdf
[39] C. K. Lin, "The development of an implantable sensor network system for continuous measurement of obstructed renal pressures," Thesis Ph D --UCLA 2007, UCLA, 2007.
[40] C. K. Lin, D. Jea, F. Dabiri, T. Massey, R. Tan, M. Sarrafzadeh, M. Srivastava, P. Schulam, J. Schmidt, and C. Montemagno, "The Development of an In-Vivo Active Pressure Monitoring System," presented at the 4th International Workshop on Wearable and Implantable Body Sensor Networks (BSN 2007), Aachen University, Germany, 2007.
[41] F. Dabiri, T. Massey, H. Noshadi, H. Hagopian, C. K. Lin, R. Tan, J. J. Schmidt, and M. Sarrafzadeh, "A Telehealth Architecture for Networked Embedded Systems: A Case Study in *In Vivo* Health Monitoring," *IEEE Transactions on Information Technology in Biomedicine*, vol. 13, pp. 351-359, 2009.
[42] N. Najafi and A. Ludomirsky, "Initial animal studies of a wireless, batteryless, MEMS implant for cardiovascular applications," *Biomedical Microdevices*, vol. 6, pp. 61-65, Mar 2004.
[43] R. Tan, T. McClure, C. K. Lin, D. Jea, F. Dabiri, T. Massey, M. Sarrafzadeh, M. Srivastava, C. Montemagno, P. Schulam, and J. Schmidt, "Development of a fully implantable wireless pressure monitoring system," *Biomed Microdevices*, 2008.
[44] B. D. Hoit, N. Ball, and R. A. Walsh, "Invasive hemodynamics and force frequency relationships in open- versus closed-chest mice," *AJP-Heart*, vol. 273, pp. H2528-H2533, 1997.
[45] A. Nair, B. D. Kuban, E. M. Tuzcu, P. Schoenhagen, S. E. Nissen, and G. Vince, "Coronary plaque classification with intravascular ultrasound radiofrequency data analysis," *Circulation*, vol. 106, pp. 2200-2206, 2002.
[46] X. Wang, J. Xu, Y. Zhu, B. Yu, M. Han, K. L. Cooper, G. R. Pickrell, and A. Wang, "An Optical Fiber Tip Pressure Sensor for Medical Applications," presented at the Quantum Electronics and Laser Science Conference (QELS), Baltimore, Maryland, 2005.
[47] T. Cuisset, C. Beauloye, N. Melikian, M. Hamilos, J. Sarma, G. Sarno, M. Naslund, L. Smith, F. Van de Vosse, N. H. Pijls, and B. De Bruyne, "In Vitro and In Vivo Studies on Thermistor-Based Intracoronary Temperature Measurements," *Catheterization and Cardiovascular Interventions*, vol. 73, pp. 224-230, 2009.

[48] K. Totsu, Y. Haga, and M. Esashi, "Ultra-miniature fiber-optic pressure sensor using white light interferometry," *J. Micromech. Microeng.*, vol. 15, pp. 71-75, 2005.
[49] C.-Y. Wu, W.-H. Liao, and Y.-C. Tung, "Integrated ionic liquid-based electrofluidic circuits for pressure sensing within polydimethylsiloxane microfluidic systems," *Lab on a Chip*, vol. 11, pp. 1740-1746, 2011.
[50] D. Zhao, Y. Liao, and Z. Zhang, "Toxicity of Ionic Liquids," *Clean*, vol. 35, pp. 42-48, 2007.
[51] E. J. Hearn, *Mechanics of Materials 1*, 3 ed. Oxford: Butterworth-Heinemann, 1997.
[52] R. W. Ogden, *Non-linear elastic deformations*. Mineola: Dover, 1997.
[53] T. J. Chung, *General Continuum Mechanics*, 2 ed. Cambridge: Cambridge University Press, 2007.
[54] A. C. Ugural and S. K. Fenster, *Advanced Strength and Applied Elasticity*, 4 ed.: Prentice-Hall, 2003.
[55] E. A. Wilder, S. Guo, S. Lin-Gibson, M. J. Fasolka, and C. M. Stafford, "Measuring the modulus of soft polymer networks via a buckling-based metrology," *Macromolecules*, vol. 39, pp. 4138-4143, 2006.
[56] I. E. Commission, *IEC 60601-2-34 Ed. 2.0 b:2005, Medical electrical equipment - Part 2-34: Particular requirements for the safety, including essential performance, of invasive blood pressure monitoring equipment*, 2 ed.: American National Standards Institute, 2000.
[57] A. f. t. A. o. M. Instrumentation, *ANSI/AAMI BP22:1994 Blood Pressure Transducers*: American National Standards Institute, 2006.
[58] J. G. Kohl and R. N. Bolstes, "A study on the elastic modulus of silicone duplex or bi-layer coatings using micro-indentation " *Progress in Organic Coatings*, vol. 41, pp. 135-141, 2001.
[59] R. A. Horne and R. P. Young, "Electrical conductivity of aqueous 0.03 to 4.0M potassium chloride solutions under hydrostatic pressure," *J. Phys.Chem.*, vol. 71, pp. 3824-3832, 1967.
[60] W. A. Kaplan, *Modern Plastics Encyclopedia '99* vol. 75. New York: McGraw-Hill, 1999.
[61] R. Tan, P. Schulam, and J. J. Schmidt, "Conductometric Catheter-Mounted Pressure Sensor," in *Medicine Meets Virtual Reality 19*, Newport Beach, CA, 2012, pp. 512-514.
[62] L. K. Massey, *Permeability Properties of Plastics and Elastomers: a Guide to Packaging and Barrier Materials, 2nd Edition*. Norwich, NY: William Andrew Publishing, 2003.
[63] W. L. Robb, "Thin Silicone Membranes--Their Permeation Properties and Some Applications," *Annals of the New York Society of Sciences*, vol. 146, pp. 119-137, 1968.
[64] L. Gettleman, "Polypohosphazene Fluoroelastomer for Denture Liners and Facial Prosthetics," *Phosphorus, Sulfur, and Silicon and the Related Elements*, vol. 144, pp. 205-208, 1999.
[65] S. Guruvenket, G. R. S. Iyer, L. Shestakova, P. Morgen, N. B. Larsen, and G. M. Rao, "Fluorination of polymethylmethaacrylate with tetrafluoroethane using DC glow discharge plasma," *Applied Surface Science*, vol. 254, pp. 5722-5726, 2008.
[66] H. L. Milligan, W. T. Cleminshaw, and K. W. Edmark, "Some Observations on the Dielectric Properties of Cardiovascular Implant Materials," *Journal of Biomedical Materials Research*, vol. 7, pp. 445-470, 1973.

[67] A. Devices, "Balanced Modulator/Demodulator AD630 Rev. E," ed. Norwood, MA, 2004, p. 12.
[68] N. Instruments. (2008, 04/01). *High-Accuracy M Series Multifunction DAQ - 18-Bit, up to 625 kS/s, up to 32 Analog Inputs*. Available: http://sine.ni.com/ds/app/doc/p/id/ds-25/lang/en
[69] AAMI, *Blood Pressure Transducers*, 2 ed. vol. BP22:1994, 2006.
[70] T. S. Light, S. Licht, A. C. Bevilacqua, and K. R. Morash, "The Fundamental Conductivity and Resistivity of Water," *Electrochemical and Solid State Letters*, vol. 8, pp. E16-E19, 2005.
[71] A. C. Guyton and J. E. Hall, *Textbook of Medical Physiology, Eleventh Edition*, 11th ed. Philadelphia: Elsevier, 2006.
[72] P. A. Iaizzo, *Handbook of Cardiac Anatomy, Physiology, and Devices (Current Clinical Oncology)*, 2nd ed. New York, NY: Springer Science, 2009.
[73] R. D. Miller, L. I. Eriksson, L. A. Fleisher, J. P. Wiener-Kronish, and W. L. Young, *Miller's Anesthesia*: Churchill Livingstone/Elsevier, 2009.
[74] B. H. McGhee and E. J. Bridges, "Monitoring Arterial Blood Pressure: What You May Not Know," *Critical Care Nurse*, vol. 22, pp. 60-79, 2002.
[75] S. Munir, B. Jiang, A. Guilcher, S. Brett, S. Redwood, M. Marber, and P. Chowienczyk, "Exercise reduces arterial pressure augmentation through vasodilation of muscular arteries in humans," *AJP-Heart*, vol. 294, pp. H1645-H1650, 2008.
[76] P. Shi, S. Hu, Y. Zhu, J. Zheng, Y. Qiu, and P. Y. S. Cheang, "Insight into the dicrotic notch in photoplethysmographic pulses from the finger tip of young adults," *Journal of Medical Engineering & Technology*, vol. 33, pp. 628-633, 2009.
[77] T. Instruments, "LM555 Timer," ed: National Semiconductor Corporation, 2006, pp. 1-14.
[78] J. D. Wyatt. (2007, May 18). *Low-power inverter using LM555 Timer IC For Electroluminescent (EL) backlights and Fluorescent tubes*. Available: http://joshua.raleigh.nc.us/LM555-inverter/LM555-inverter.pdf
[79] J. Jansen, K. Wesseling, J. Settels, and J. Schreuder, "Continuous cardiac output monitoring by pulse contour during cardiac surgery," *European Heart Journal*, vol. 11, pp. 26-32, 1990.
[80] J. O. Hollinger, *An Introduction to Biomaterials*, 2 ed. Boca Raton, FL: CRC Press, 2012.
[81] P. Yang, N. Huang, Y. Leng, J. Chen, H. Sun, J. Wang, F. Chen, and P. Chu, "In vivo study of Ti-O thin film fabricated PIII," *Surface and Coatings Technology*, vol. 156, pp. 284-288, 2002.
[82] J. Fitzgerald, H. Andrew, B. Conway, S. Hackett, and N. Chalmers, "Outpatient angiography: a prospective study of 3 French catheters in unselected patients," *The British Journal of Radiology*, vol. 71, pp. 484-486, 1998.
[83] W. Köstler, P. C. Strohm, and N. P. Südkamp, "Acute compartment syndrome of the limb," *Injury*, vol. 36, pp. 992-998, 2005.
[84] M. M. McQueen, P. Gaston, and C. M. Court-Brown, "Acute compartment syndrome. Who is at risk?," *J Bone Joint Surg Br.*, vol. 82, pp. 200-203, 2000.
[85] C. K. Norton, P. I. Linenfelser, K. E. Cyron, and K. A. Casey, "Trauma and intraabdominal hypertension. To prevent potentially lethal effects, monitor intraabdominal pressure.," *Am J Nurs.*, vol. 106, pp. 51-55, 2006.

[86] A. Schachtrupp, M. Jansen, P. Bertram, R. Kuhlen, and V. Schumpelick, "Abdominal compartment syndrome: significance, diagnosis, and treatment," *Anaesthesist*, vol. 55, pp. 660-667, 2006.

[87] J. Huang, S. Virji, B. H. Weiller, and R. B. Kaner, "Nanostructured Polyaniline Sensors," *Chem. Eur. J.*, vol. 10, pp. 1314-1319, 2004.

[88] J. M. D'arcy, H. D. Tran, V. C. Tung, A. K. Tucker-Schwartz, R. P. Wong, Y. Yang, and R. B. Kaner, "Versatile solution for growing thin films of conducting polymers," *PNAS*, vol. 10, pp. 19673-19678, 2010.